TABLE OF CONTENTS

Page

LIST OF TABLES

Page

LIST OF FIGURES

LIST OF ABREVIATIONS

AWGN	Additive White Gaussian Noise
BER	Bit Error Rate
BPSK	Binary Phase Shift Keying
BS	Base Station
CDF	Cumulative Density Function
CDMA	Code Division Multiple-Access
CIM	Code Index Modulation
CM	Channel Model
CMOS	Complementary Metal–Oxide–Semiconductor
CP	Cyclic Prefix
CS	Code Shifted
CSD	Chaotic Symbolic Dynamic
CSI	Channel State Information
DBR	Data Energy to Bit Energy Ratio
DCSK	Differential Chaos Shift Keying
DF	Decode and Forward
ESIM	Enhanced Subcarrier Index Modulation
ETS	École de Technologie Supérieure
FBMC	Filter Bank Multicarrier

FFT	Fast Fourier Transform
FH	Frequency Hopping
FIM	Frequency Index Modulation
FM	Frequency Modulation
FPGA	Field-Programmable Gate Array
IAS	Inter-Antenna Synchronization
ICI-CSK	Initial Condition-Index Chaotic Shift Keying
ICT	Information and Communication Technology
IEEE	Institute of Electrical and Electronics Engineers
IM	Index Modulation
IoT	Internet of Things
ISM	Industrial Scientific and Medical
LED	Light Emitting Diode
LLR	Log-Likelihood Ratio
LPI	Low Probability of Interception
MA	Multiple-Access
MEMS	Micro Electro Mechanical Systems
MFSK	Multiple Frequency-Shift Keying
MIMO	Multiple-Input Multiple-Output
MISO	Multiple-Input Single-Output

ML	Maximum Likelihood
MMSE	Minimum Mean Square Error
MQAM	$M-$ary Quadrature Amplitude Modulation
Msps	Mega symbols per second
MU	Multiuser
NR	Noise Reduction
OD	Optimum Detection
OFDM	Orthogonal Frequency Division Multiplexing
OM	Orthogonal Multilevel
OQPSK	Offset Quadrature Phase Shift Keying
PAPR	Peak-to-Average Power Ratio
PDF	Probability Density Function
PI	Permutation Index
PPP	Public Private Partnership
QCSK	Quadrature Chaos Shift Keying
QPSK	Quadrature Phase Shift Keying
RCG	Repeated Chaotic Generators
RF	Radio Frequency
SER	Symbol Error Rate
SIM	Subcarrier Index Modulation

SIMO	Single-Input Multiple-Output
SISO	Single-Input Single-Output
SLED	Square-Law Envelope Detector
SM	Spatial Modulation
SME	Small and Medium Enterprise
SS	Spread Spectrum
SSK	Space-Shift Keying
STBC	Space-Time Block Codes
TR	Transmitted Reference
UWB	Ultra Wide Band
WBAN	Wireless Body Area Networks
WSN	Wireless Sensor Networks
ZF	Zero Forcing
ZMCG	Zero-Mean Complex Gaussian

INTRODUCTION

The fifth generation (5G) Infrastructure Public Private Partnership known as the 5G-PPP is a joint initiative between the European Commission and European information and communications technology (ICT) manufacturers, telecommunications operators, service providers, small or medium-sized enterprises (SMEs) and researcher Institutions. The 5G-PPP is now in its second phase where 21 new projects were recently launched in Brussels in 2017. The 5G PPP will deliver solutions, architectures, technologies and standards for the ubiquitous next generation communication infrastructures of the coming decade across the globe. The challenge for the 5G Public Private Partnership (5G PPP) is to secure leadership in the particular areas where there is potential for creating new markets such as smart cities, e-health, intelligent transport, education or entertainment and media. The 5G PPP initiative will reinforce the success of the telecommunications industry in global markets and open new innovation opportunities. According to European Commission & European ICT Industry (2014), it will open a platform that helps reaching the common goal to maintain and strengthen the global technological lead.

The key challenges for the 5G Infrastructure PPP may be summarized as

- Providing 1000 times higher wireless area capacity and more varied service capabilities compared to 2010;
- Saving up to 90% of energy per service provided. The main focus will be in mobile communication networks where the dominating energy consumption comes from the radio access network;
- Reducing the average service creation time cycle from 90 hours to 90 minutes.
- Creating a secure, reliable and dependable Internet with a *zero perceived* downtime for services provision;

- Facilitating very dense deployments of wireless communication links to connect over 7 trillion wireless devices serving over 7 billion people;
- Ensuring for everyone and everywhere the access to a wider panel of services and applications at lower cost.

0.1 Modulation for 5G Wireless Communications

Concerning the physical layer and the modulation techniques involved therein, Orthogonal Frequency Division Multiplexing (OFDM) is known to be the main platform for 5G wireless communications modulation. But as OFDM has a set of drawbacks like the need to a cyclic prefix (CP), side-lobe frequencies, peak to average power ratio (PAPR) and high sensitivity to carrier frequency offsets, a new technique called Filter Bank Multi-Carrier (FBMC) has been developed to compensate the deficiencies of OFDM and to offer ways of overcoming the known limitations of OFDM of reduced spectral efficiency and strict synchronization requirements. These advantages have led it to being considered as one of the modulation techniques for 5G communication systems Schellmann *et al.* (2014); Wunder *et al.* (2014). Note that FBMC is a development of OFDM, which uses banks of filters that are implemented, typically using digital signal processing techniques. Furthermore, when carriers are modulated in an OFDM system, side-lobes spread out either side. With a filter bank system, the filters are used to remove these side-lobes and much cleaner carriers are obtained. FBMC is, however, more complex than OFDM and less flexible for multiple-input multiple-output (MIMO) applications. In addition, OFDM has been around for more than 3 decades and is already incorporated into many platforms in various applications, therefore, any shift to a newer technology like FBMC will need time.

0.2 Index Modulation

Since 5G wireless networks have drawn great attention over the past few years Andrews *et al.* (2014), Wang *et al.* (2014) as the wireless infrastructure for the future, research is ongoing to further enhance this yet to-be implemented technology in terms of bandwidth, data rate and latency. Since almost everything will be connected to the internet in what is known as the Internet of Things (IoT) Weber & Weber (2010), it is necessary to develop novel spectrum and energy efficient physical layer techniques for 5G wireless communication networks. Some techniques such as massive MIMO systems, millimetre wave (mmWave) communications and flexible waveform designs have already been developed; however, research community is still working to propose new and more influential physical layer solutions toward 5G wireless networks.

The Index Modulation (IM) technique, which considers innovative ways to convey extra information bits compared to traditional communication systems, appears as a competitive candidate for next generation wireless networks due to the attractive features it offers in terms of spectral and energy efficiencies as well as hardware simplicity. The interest in IM techniques has grown in the past few years as it augments energy and spectrum efficiencies while remaining simple and being possible to merge with theoretically any digital modulation technique. IM accommodates substitute manners to transfer extra information compared to classical digital modulation schemes that depend on amplitude, phase or frequency of a sinusoidal carrier signal for communication.

In fact, IM schemes map extra information bits by altering the on/off status of an entity in the communication system into which it is merged, such as transmit antennas, subcarriers, radio frequency (RF) mirrors, transmit light emitting diodes (LEDs), relays, modulation types, time slots, precoder matrices, dispersion matrices, spreading codes, signal powers, etc. Brief, IM establishes totally novel dimensions for data transmission.

In IM, a considerable part of the outgoing bits are inherently transmitted, so their transmission energy is saved and transferred to the actually –physically– transmitted bits, which results in an improved error performance compared to classical schemes that utilise the same total transmission energy. That is to say, IM schemes convey extra information in an energy-efficient fashion.

As IM suggests new dimensions for conveying digital information, the spectral efficiency of the considered communication system can be effectively enhanced without increasing hardware complexity. In the following sections, we will have a glance at spatial modulation, code index modulation, frequency index modulation and initial-condition chaos shift keying modulation as examples of concern of IM.

0.3 Spatial Modulation

SM is a technique in which indices of the transmit antennas of a MIMO architecture are used for conveying additional information, and is indeed one of the earliest applications of IM, where it represents a novel method to transmit information by means of the indices of the transmit antennas of a MIMO architecture in addition to the conventional $M-$ary signal constellations. In fact, SM appeared in some works like Chau *et al.* (2001) and Haas *et al.* (2002) for the first time but under different names and terminologies, however, the term *spatial modulation* is utilised for the first time in the studies of Ganesan *et al.* (2006) and Mesleh *et al.* (2006a).

To be specific, two information-carrying units exist in SM, the indices of the available transmit antennas and the $M-$ary constellation symbols. For each transmission interval, a total of $\log_2(N_t)+\log_2(M)$ outgoing bits enter the transmitter of an SM system, where N_t is the number of antennas in the transmit antenna array and M is the modulation order. To provide some detail, the first $\log_2(M)$ bits of the outgoing bit sequence are used to modulate the phase and/or amplitude of a carrier signal, while the remaining $\log_2(N_t)$ bits of the outgoing bit sequence

are considered for the selection of the index of the active transmit antenna that will be turned on to perform the transmission of the corresponding modulated signal. A 3-dimensional constellation diagram of SM with $N_t = 4$ antennae and Quadrature Phase Shift Keying (QPSK) constellation $M = 4$ is shown in Figure 0.1.

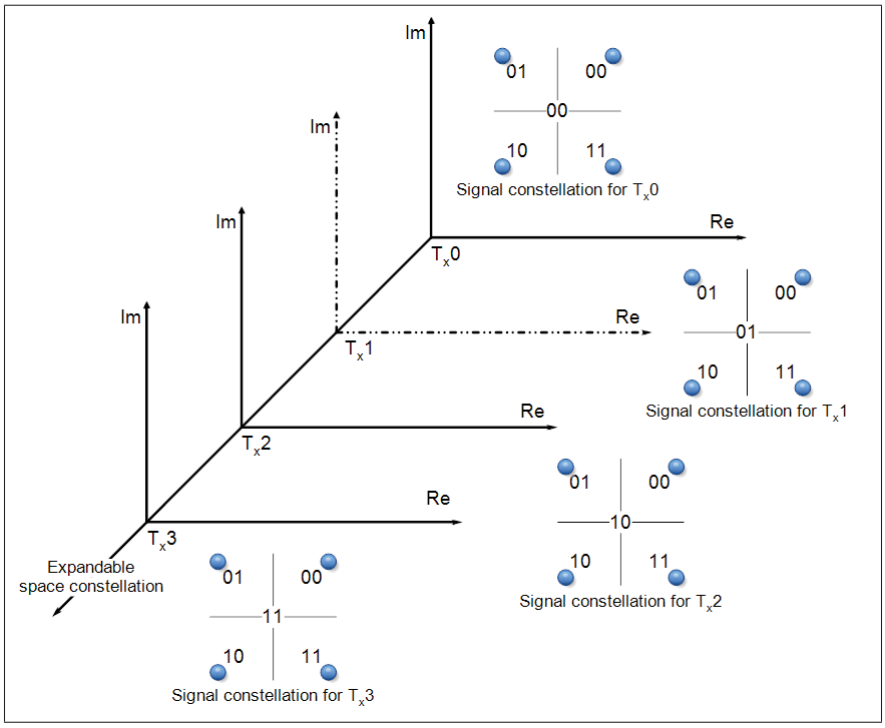

Figure 0.1 3-D signal constellation for SM systems with $M = 4$ and $N_t = 4$

Note that a simpler implementation of the SM that relies only on antenna indices and does not incorporate any signal modulation that is known as space-shift keying (SSK) is investigated and developed by Jeganathan *et al.* (2008b), Jeganathan *et al.* (2009). Compared to SM, SSK requires neither in-phase and quadrature (IQ) modulation nor pulse shaping, and thus, has a simpler form and less complexity.

0.3.1 SM Receiver

The receiver of the SM scheme has to deal with the following two major tasks: detection of the active transmit antenna for the demodulation of IM bits and detection of the data symbol transmitted over the activated transmit antenna for the demodulation of the bits mapped to the $M-$ary signal constellation. As a matter of fact, the optimum ML detector of SM has to jointly search over all transmit antennas and constellation symbols to decode both of the bits. Although the suboptimal detector can obtain a significant complexity reduction for increasing number of transmit antennas and higher order constellations, its error performance is considerably worse than that of the ML detector. Therefore, the implementation of the suboptimal detector can be problematic for critical applications that require a low error rate. Additionally, the sparse structure of SM transmission vectors paves the way for the implementation of near/sub-optimal low-complexity detection methods for SM systems such as matched filter-based detection Tang *et al.* (2013) and compressed sensing (CS)-based detection Yu *et al.* (2012).

0.3.2 Features and Drawbacks of SM

In light of the above discussion on the concept of SM, MIMO systems employing SM provide attractive advantages over their traditional counterparts Di Renzo *et al.* (2016). The main advantages of SM over classical MIMO systems could be summarized as Basar *et al.* (2017):

- High spectral efficiency: The spectral efficiency of SM is superior to that of traditional single-input single-output (SISO) systems as well as orthogonal space-time block codes (STBCs) due to indexing the transmit antenna number as a supplementary approach of ferrying extra information;

- High energy efficiency: The SM transmitter power consumption is unconnected to the number of transmit antennas, while the information can still be transferred via these antennas. In fact, SM may be regarded as a green and energy-efficient MIMO technology as it may deploy a transmission system without requiring additional transmission energy but by using a higher number of transmit antennas;
- Simple transceiver design: One RF chain is sufficient for the SM scheme compared to MIMO where many are required, as SM activates a single antenna during a given transmission;
- Elimination of Inter-antenna synchronization (IAS) and inter-channel interference.

While the SM scheme has the aforementioned appealing advantages, it also has some disadvantages, which are summarized as follows:

- It is mainly solely suitable for base stations of wireless networks, where space is abundant to host multiple antennas. This is because smaller devices such as cell phones do not have the necessary physical space to provide, especially considering that a spacing of $\lambda/2$ between antennas must be respected, where λ is the transmission wavelength;
- SM is also not applicable to sensor networks and IoT devices as most these devices are tiny and may not have the physical space to handle multiple antennas;
- The spectral efficiency of SM increases logarithmically with N_t;
- The channel coefficients of different transmit antennas have to be sufficiently different for an SM scheme to operate effectively. In other words, SM requires rich scattering environments to ensure better error performance. This requirement is not guaranteed and renders SM impractical;

- The decoding complexity of the SM receiver, in terms of the total number of real multiplications, grows linearly with the product of the constellation size and the number of transmit antennas;

- Another impediment of SM techniques is switching time existing in current RF switch modules. Turning antennas *on* and *off* is costly in terms of power required for 'on-off' and the time duration needed for such repetitive 'on-off' operations to take place, as shown in Fig. 0.2. In fact, switching time intervals introduce systematic transmission gaps in SM systems which overshadow its overall communication performance. In this regard, parasitic antennas which rely on Micro Electro Mechanical Systems (MEMS) technology for RF applications that are being used in handheld mobile devices nowadays have switching times in the range of $2-50\,\mu$s which renders it inefficient for today's high-speed applications, if the antenna is to be switched on and off thousands or millions of times every single second. Indeed, since SM may require a transition (switching) to happen for the transmission of each individual symbol to materialize, it is clear that switching times in antenna controllers must be significantly smaller than the symbol period. This requirement makes the application of MEMS-based technology of today in SM very hard.

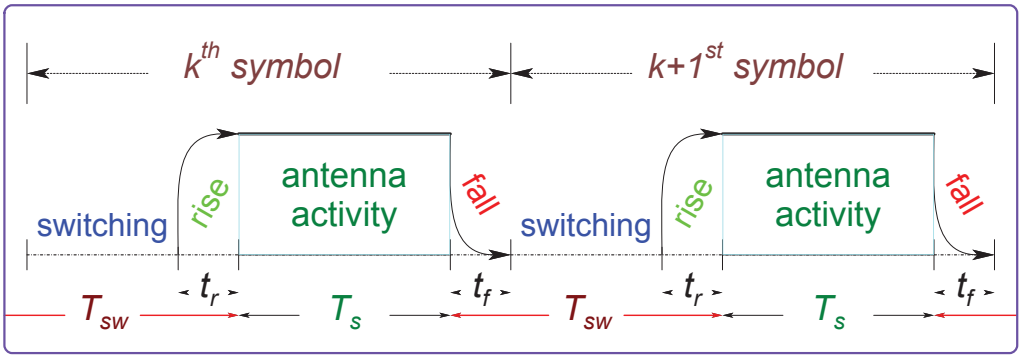

Figure 0.2 The concept of switching time and its influence on the system performance

Considering the advantages and disadvantages of SM systems mentioned above, we may conclude that SM scheme provides an interesting trade-off among encoding/decoding complexity, spectral efficiency, and error performance, however, further technological advancement especially in RF switching techniques is needed before its full implementation.

0.4 Code Index Modulation

A new technique that uses the index modulation domain is developed in Kaddoum *et al.* (2015b) where the spreading code domain is used as an indexing parameter in order to increase the data rate without adding extra computations complexity to the system. This scheme, which is called code index modulation-spread spectrum (CIM-SS), may also be integrated with MIMO or SM systems to achieve higher throughput. CIM-SS uses spreading codes to map additional outgoing data in conjunction with constellation symbols. A system model incorporating the CIM-SS transmitter and receiver structures extracted from Kaddoum *et al.* (2015b) is shown in Fig. 0.3.

The basic form of CIM-SS considers the outgoing data in pairs, where for each pair of bits, one bit chooses a spreading code from a pre-assigned set of codes, and the other bit is spread by the selected code. At the receiver, the spreading code is first detected which allows the recovery of the mapped bit then the transmitted bit is demodulated via despreading. With this elegant scheme, only half of the bits are physically transmitted over the channel and the other half are mapped into spreading codes. Consequently, CIM-SS increases throughput and decreases energy consumption while retaining the system easy to implement. Furthermore, the gains of the spread spectrum modulation are maintained in the proposed CIM-SS scheme.

In fact, CIM-SS is among the earliest *soft*-indexing techniques that appeared as a rival for the *hardware*-based SM technique. A generalized form of this technique which uses $M-$ary constellation instead of a binary one is developed in Kaddoum *et al.* (2016b).

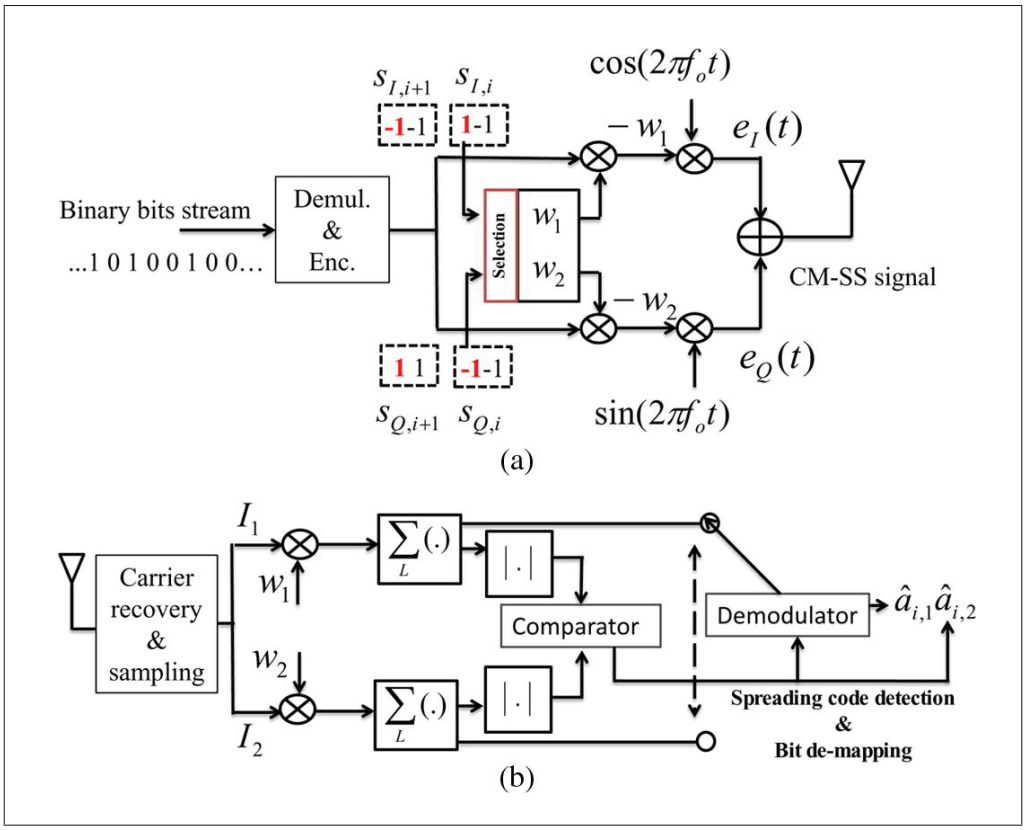

Figure 0.3 CIM-SS system model: (a) Transmitter (b) In phase receiver structure
Taken from Kaddoum *et al.* (2015b)

0.5 Frequency Index Modulation

Within the context of soft-index modulation, subcarrier index modulation (SIM) scheme has been proposed in Abu-Alhiga & Haas (2009) where it has been merged with orthogonal frequency division multiplexing (OFDM) to constitute SIM-OFDM. Moreover, enhanced subcarrier index modulation (ESIM) has been proposed to avoid the propagation of error by replacing the concept of majority counting by a simpler method in which a pair of *off-on* or *on-off* subcarriers is used to represent a single bit Tsonev *et al.* (2011), however, the fact that two subcarriers are used to transmit a single bit doubles the required bandwidth necessary for transmission in this method.

Eventually, a transmission scheme called OFDM with index modulation (OFDM-IM) is proposed Başar *et al.* (2013). In this scheme, information is conveyed not only by M-ary signal constellations as in classical OFDM, but also by the indices of the subcarriers, which are activated according to the incoming information bits. But from the practical point of view, the implementation of this scheme is difficult as it relies on the maximum likelihood (ML) detection that requires heavy computing charges as it needs to search over all the possibilities (subcarrier combinations) within a bandwidth. This is costly as it makes a joint search over all possibilities Başar (2015) and is impractical for large combination values due to its exponentially growing decoding complexity Başar *et al.* (2013), which makes it unsuitable for WSN applications. Furthermore, the Log-Likelihood Ratio (LLR) detection strategy is another detection method proposed for this scheme for high number of subcarriers, but this detector may produce an undefined set of active indices not at all included in the original mapping table Başar *et al.* (2013).

In the work of Soujeri *et al.* (2017), a modified frequency index modulation (FIM) scheme that is simpler than the approach of Başar *et al.* (2013) is introduced. This system has a lower complexity compared to OFDM-IM, lower power consumption profile and does not sacrifice data rate as it makes use of the frequency hops in a smart and wise way. As the proposed system does not use all of the available subcarriers, it will also enjoy inter-carrier interference -free transmission while it allows the transmission of additional bits in the index domain. Therefore, this work is an excellent choice for WSNs and IoT applications.

In the FIM scheme, the OFDM bandwidth is divided into equal N_B sub-bands of N subcarriers each. A message is divided into mapped and modulated blocks where the mapped block activates a single corresponding subcarrier in its predefined sub-band in order to carry the data of the modulated block. At the receiver side, FFT is first performed on the received signal followed by sub-sectioning the bandwidth into N_B sub-bands where square-law envelope detector

(SLED) is used in each sub-band to identify the active subcarrier. Then, the mapper chooses the corresponding indexed message and demodulates the received signal over the channel to get the remainder. The FIM system keeps the architecture simple and constitutes an excellent substitution for the conventional frequency-hopping (FH) technique in which hops carry no additional information. Despite the simplicity, FIM enjoys all the specifications associated with frequency hopping systems from the signal, interference, channel and anti-jamming points of view. Furthermore, the system has a low PAPR profile and may be used in multi-user or multi-node scenarios thanks to OFDMA multiple access technique. These properties make FIM scheme suitable for WSNs and IoT applications as size, simplicity and efficiency are of great importance in these schemes Barnaghi *et al.* (2012).

While the structure of FIM introduces an important enhancement to personal area networks like Bluetooth and ZigBee, it is quite competitive in high speed 5G networks like UWB and Wi-Fi architectures too.

Q. What is the cost of transmission in terms of Hz/bits in FIM systems?

For the transmission of b_{map} mapped and b_{map} modulated bits, a total of $b_{\text{tot}} = b_{\text{map}} + b_{\text{mod}}$ bits is transmitted in a FIM system such that, for N_B sub-bands, the symbol time T_{FIM} becomes $T_{\text{FIM}} = N_B b_{\text{tot}}$.

As the frequency separation between subcarriers must be at least $1/T_{\text{FIM}}$ to respect orthogonality, the total bandwidth requirement per bit will be

$$N_{\text{FIM}}/T_{\text{FIM}} = N_B N/N_B(b_{\text{map}} + b_{\text{mod}}) = N/b_{\text{tot}} \quad \text{Hz / bits.}$$

This may be verified for any choice of N, b_{map} and b_{mod}.

Note that in Chapter 2, the variables are adjusted such that $p_1 = b_{\text{map}}$, $p_2 = b_{\text{mod}}$ and $b_T = b_{\text{tot}}$.

0.6 Chaotic Index Modulation

0.6.1 A Comprehensive Overview of Chaotic Modulations

Due to their highly non-linear dynamics, chaotic maps may produce infinite number of signals using different initial conditions. In fact, the sensitivity of chaotic maps upon initial conditions is very high and the produced chaotic signals show very low cross-correlation values that qualify such sequences to be used in spread spectrum applications. In this vein, chaotic spreading sequences can be considered as suitable candidates for spread spectrum applications Kaddoum (2016b).

In fact, chaos-based modulation provides the advantages of conventional spread-spectrum systems like jamming resistance, low probability of interception (LPI), fading mitigation and secure communications. Moreover, the non-periodic nature of chaotic codes adds further security and is a built-in feature of these codes Lynnyk & Čelikovskỳ (2010).

Furthermore, many studies that target the reduction of multi-user interference and PAPR show that chaotic sequences outperform sequences that have a periodic nature like Gold sequences Vitali *et al.* (2006).

To measure the performance of chaotic-based systems, a first study ever of the feasibility of using chaos shift keying (CSK) in a Multiple-Input Multiple-Output (MIMO) channels is covered in Kaddoum *et al.* (2011), the integration of space-time block code (STBC) tehcniques into a CSK system is approached in Kaddoum & Gagnon (2013b) and a computation of the BER for asynchronous chaos-based DS-CDMA is provided in Kaddoum *et al.* (2009d). Moreover, an investigation of the analysis of a cooperative decode-and-forward (DF) relay networks with chaos shift keying (CSK) modulation that constituted a first-ever application of CSK in the cooperative communications field is developed in Kaddoum & Gagnon (2013a).

An accurate approach to compute the bit error rate expression for the multiuser chaosbased DS-CDMA case is presented in Kaddoum *et al.* (2009b) and a comparison of different chaotic maps and their influence on the performance analysis of a direct-sequence code division multiple access (DS-CDMA) system when chaotic sequences are used instead of conventional pseudo-noise (PN) spreading codes is studied in Kaddoum *et al.* (2007).

Emphasizing that the application of chaos modulation in digital communications does not violate any basic principle, the potential use of chaotic signals in digital modulation is studied in Kaddoum *et al.* (2013c) and is found promising from an information theory point of view.

Principally, two categories of chaos-based communication systems have been set forth for consideration:

- Coherently detected chaotic codes. In this layout, the receiver generates a synchronized copy of the chaotic signal and uses the generated replica in accordance with a detection technique to recover the transmitted data Kolumbán *et al.* (1997b).

The coherent reception is similar to replacing the conventional binary spreading sequences such as Gold, Walsh or pseudo-noise sequences by chaotic sequences, where the implementation of chaotic codes adds to security because of its non-periodic nature. This form of reception is used in chaos shift keying (CSK), chaos-based direct sequence code division multiple access (DS-CDMA), a configuration in which the chaotic signal is used to spread the data information signal while chaotic synchronization is required at the receiver side in order to regenerate an exact replica of the chaotic sequence to demodulate the transmitted bits Kaddoum *et al.* (2009c).

The chaotic symbolic dynamic (CSD) modulation has also been introduced as an important class of coherent chaotic modulation in Kurian *et al.* (2005) and a spread spectrum communication system using chaotic symbolic dynamics modulation is studied in Kaddoum *et al.*

(2013b). In this latter work, the authors combine spread spectrum and chaotic modulation for the sake of increased security in a multiuser environment. The feasibility of having chaos-based communication in a 2 by 2 MIMO system using Alamouti space-time codes is presented in Kaddoum *et al.* (2012b), and an enhanced transceiver design has been proposed in Kaddoum *et al.* (2012a) to overcome the performance degradation that arises because of synchronization in noisy environments.

- Non-coherently detected chaotic codes. In this strategy, the receiver recovers the transmitted data by detecting features of the received signal with no knowledge of neither the chaotic codes nor the channel state information Kennedy *et al.* (2000).

The fact that non-coherent reception requires neither synchronization of chaotic codes nor the knowledge of CSI makes this reception approach a resilient and robust one. Examples of techniques that depend on non-coherent reception are differential chaos shift keying (DCSK) systems and chaos-based on off Keying (COOK) systems Kaddoum (2016b).

Additionally, an improved continuous-mobility differential chaos-shift-keying system (CM-DCSK) that provides improved performance in fast fading channels without accurate channel estimation is presented in Escribano *et al.* (2016) and a secure Multi-Carrier Differential Chaos Shift Keying (MC-DCSK) system in which a hybrid of MC modulation and DCSK is used is proposed in Kaddoum & Gagnon (2012). Besides, the application of chaos modulation has grown to include fields like power line applications Kaddoum & Tadayon (2017) and relay-based communication systems Kaddoum *et al.* (2014).

The concept has also been extended to energy harvesting, where a simultaneous wireless information and power transfer scheme for short reference DCSK communication systems to overcome limited energy needs is provided in Kaddoum *et al.* (2017).

0.7 The Application of Index Modulation to Chaotic Modulation

Index modulation in chaotic systems is to use a certain property of chaotic sequences to ferry extra information per transmission, seeking further security, energy- and spectral- efficiency. Since the combination of IM and chaotic modulation techniques remains open, new forms and designs may be achieved. Here, we have a look at the studies carried out in this field.

0.7.1 Non-coherent Chaotic Index Modulation

Many works have considered IM for non-coherent chaotic modulation. The works called Carrier Index Differential Chaos Shift Keying Modulation Cheng *et al.* (2017) and Permutation Index Differential Chaos Shift Keying (PI-DCSK) modulation that targets enhanced data security and improved energy and spectral efficiencies Herceg *et al.* (2017) constitute prominent examples. In the PI-DCSK scheme, each data frame is divided into two time slots in which the reference chaotic signal is sent in the first time slot and a the product of the permuted replica of the reference signal into the modulating bit is sent in the second time slot. In particular, the bit stream is divided at the transmitter into blocks of $n+1$ bits, where n mapped bits are used to select one of the predefined reference sequence permutations, while a single modulated bit is spread by the permuted reference signal just mentioned. At the receiver side, the reference signal is recovered first, then all permuted versions of it are correlated with the data bearing signal. The index of the correlator output with the maximum magnitude will estimate the mapped bits, while the output of the corresponding correlator is compared to a zero threshold to recover the modulated bit. This technique may also be extended to the multiple access (MA) case.

With respect to hybrid modulation, a differentially spatial modulated chaos shift keying modulation communication system where a part of outgoing symbols at the transmitter map an antenna index for transmission is proposed in Hu *et al.* (2017).

0.7.2 Coherent Chaotic Index Modulation

The application of index modulation to coherent chaotic schemes can enhance the data rate and enjoys the properties offered by these coherent schemes such as excellent performance, and high security. In fact, the coherent chaotic index modulation has followed the application of various index modulation techniques like SM, CIM, FIM and PI-DCSK. In particular, we have applied for the first time the index modulation to a coherent secure chaos-based scheme named chaos shift keying (CSK) in Soujeri *et al.* (2018). This unique scheme termed initial condition-index CSK (ICI-CSK) aspires the enhancement of spectral and energy efficiencies. In this vein, the proposed ICI-CSK scheme exploits the chaotic maps sensitivity on initial conditions to generate a large number of uncorrelated chaotic signals from the same chaotic map. In particular, at the transmitter, the data stream is formed in blocks of $p_{\text{tot}} = n + 1$ bits where the first n bits select an initial condition index from a set of N available initial conditions used to generate a chaotic sequence of a predetermined length, while the remaining single bit is spread by the selected chaotic sequence.

In this Thesis, we consider index modulation for both coherent and non-coherent chaotic reception schemes.

0.8 Author Contributions

Besides the papers that constitute the core of this Thesis, the author of this Thesis has been involved in and contributed to many other scientific papers not included in this Thesis. The contribution varied from a paper to another and took many forms, from partially performing simulation to verifying the integrity of the article, checking math, editing content, linguistic verification, cross-checking references and auditing survey.

The articles to which the Author has contributed so far, before the publication of this Thesis, are as listed here:

A. Conference Articles:

Georges Kaddoum, Navid Tadayon and Ebrahim Soujeri, 2016. « Performance of DCSK system with blanking circuit for power-line communications ». Proceedings of IEEE International Symposium on Circuits and Systems (ISCAS), Montreal, Canada, May 22-25, 2016.

Georges Kaddoum and Ebrahim Soujeri, "On the Comparison Between Code-Index Modulation and Spatial Modulation Techniques", ICTRC 2015, UAE, 17-19 May 2015, pages 1-4.

B. Journal Articles:

Minh Au, Georges Kaddoum, François Gagnon and Ebrahim Soujeri, "A Joint Code-Frequency Index Modulation for Low-complexity, High Spectral and Energy Efficiency Communications", IEEE Transactions on Communications, submitted: Dec 2017.

Marijan Herceg, Denis Vranješ, Georges Kaddoum and Ebrahim Soujeri, "Commutation Code Index DCSK Modulation Technique for High-Data-Rate Communication Systems", IEEE Transactions on Circuits and Systems II: Express Briefs, 2018. DOI: 10.1109/TCSII.2018.2817930

Marijan Herceg, Georges Kaddoum, Denis Vranješ and Ebrahim Soujeri,"Permutation Index DCSK Modulation Technique for Secure Multi-User High-Data-Rate Communication Sys-

tems", IEEE Transaction on Vehicular Technology, November 2017.

Georges Kaddoum and Ebrahim Soujeri, "NR-DCSK: A Noise Reduction Differential Chaos Shift Keying System", IEEE Transactions on Circuits and Systems II: Express Briefs, Year: 2016, Volume: PP, Issue: 99 Pages: 1 - 1, DOI: 10.1109/TCSII.2016.2532041.

Georges Kaddoum, Ebrahim Soujeri and Yogesh Nijsure, "Design of a Short Reference Noncoherent Chaos-Based Communication Systems", IEEE Transactions on Communications, Year: 2016, Volume: 64, Issue: 2 Pages: 680 - 689, DOI: 10.1109/TCOMM.2015.2514089.

Georges Kaddoum, Ebrahim Soujeri, Carlos Arcila and Khaled Eshteiwi, "I-DCSK: An Improved Non-Coherent Communication System Architecture", IEEE Trans. on CAS II, 2015.

0.9 Thesis Outline

This Thesis is organized as follows:

Chapter 1 discusses the impact of antenna switching time on the performance of SM techniques. This is to show the cost associated with the implementation of SM techniques and the unsuitability of this technique to IoT and WSN applications. In Chapter 2, we study the frequency index modulation technique as a soft indexing substitute for the SM technique. In Chapter 3, we investigate initial condition index chaos shift keying modulation for high data rate, secure and high energy efficiency communications. This represents an example of the application of coherent CSK technique to index modulation. We also consider permutation index DCSK modulation as an example of noncoherent DCSK application to index modulation,

that is placed in Appendix II. Finally, we have concluded this Thesis, included discussion and future work proposals in Conclusion and Recommendations.

CHAPTER 1

THE IMPACT OF ANTENNA SWITCHING TIME ON SPATIAL MODULATION

Ebrahim Soujeri[1], Georges Kaddoum[1]

[1] Department of Electrical Engineering, École de Technologie Supérieure,
1100 Notre-Dame West, Montreal, Quebec, Canada H3C 1K3

Paper published in *IEEE Wireless Communications Letters*, June 2016.

Abstract

Spatial Modulation (SM) is an emerging technology that reduces hardware complexity, power consumption, inter-channel interference and antenna synchronization problems of multiple-input multiple-output (MIMO) communications. However, SM depends on continuous antenna transitions that rely on RF antenna switches which consume considerable time. Because of this, the data rates of SM schemes face a cap and are bound to certain limitations and the effective SM transmission is much less than the nominal value. In this letter, we study the impact of switching time on SM and we develop expressions for the effective transmission rate, effective capacity and spectral efficiency. An upper bound on the switching time is derived such that SM sustains capacity superiority in comparison with SIMO systems.

1.1 Introduction

Spatial modulation (SM) is an antenna-transition-based scheme that has been developed in the last decade Mesleh *et al.* (2008); Jeganathan *et al.* (2008b) with unique features. Data rate increment achieved via the utilization of the index of actively transmitting antenna is the core of this modulation scheme. Other benefits of using such modulation schemes comprise improved capacity, spectral and energy efficiency, the reduction to a single RF chain and the removal of inter-channel interference and inter-antenna synchronization requirements. Despite the existence of some drawbacks in this system like the absolute reliance of its performance on channel state information (CSI), i.e. being sensitive to channel correlation and erroneous

CSI Soujeri & Kaddoum (2015), it has been the focus of many research studies in the last decade. While bit error rate (BER) performance evaluation has received most attention, very little has been discussed about antenna transitions that constitute a critical property of SM systems. In fact, a study of MIMO antennas for mobile handsets has been carried out in Shoaib *et al.* (2015) where the isolation properties of decoupling mechanism of certain antennas are discussed. In this regard, parasitic antennas which rely on Micro Electro Mechanical Systems (MEMS) technology for RF applications are already being used in handheld mobile devices. Further, the switching time in MEMS technology is known to be in the range of $2-50\mu$s which renders it inefficient for today's high-speed applications. Indeed, since SM may require a transition (switching) to happen for the transmission of each individual symbol to materialize, it is clear that switching times in antenna controllers must be significantly smaller than the symbol period. This requirement puts the option of MEMS-based switching technology off the table. According to Kalis *et al.* (2014), parasitic antenna arrays for MIMO applications using semiconductor diodes faster than 0.1μs (100 ns) are available. While in Ishibashi & Sugiura (2014), the effects of antenna switching on band-limited spatial modulation is investigated, where the employment of an SM-specific practical time-limited shaping filter is taken into account and the use of multiple RF chains is considered to transmit the side-lobes of band-limited pulses, in many recent works, i.e. Serafimovski *et al.* (2013) and Di Renzo *et al.* (2014), this issue has never been tackled or debated. This work is the first in this regard to shed the light on the feasibility of implementation of SM technology under the speed constraints of currently existing antenna switching technologies.

Contributions

Encouraged by the fact that RF antenna switches constitute an important part of the RF front end Bowick (2011) utilized in SM systems and we admit that these RF switches are neither cost-free nor steeply climbing (in zero-time) and require certain advanced technologies to perform, i.e. acknowledging that switching time intervals introduce systematic transmission gaps in SM systems which overshadow its overall communication performance. In this letter, we

calculate the effective data rate, the effective capacity and the spectral efficiency of SM systems for the first time under this practical constraint. In fact, we explore the speed limitations of industrial RF switches to analyse the SM system and to develop expressions for the effective data rate, effective capacity and spectral efficiency. We also identify the upper bound on the switching time interval such that the capacity superiority of SM with respect to single antenna transmission systems is sustained.

1.2 System Model

In SM, bits to be transmitted are grouped into $m+n_t$ blocks, where the information is transmitted via $N_t = 2^{n_t}$ number of antennas, where each antenna is loaded with a symbol from the constellation pool that has a size of 2^m Mesleh *et al.* (2008); Jeganathan *et al.* (2008b). We add that the SM scheme would be equipped with an RF switch at the transmitter in the fashion shown in Fig. 1.1. Further details on RF switching can be found in CEL (2015) and in

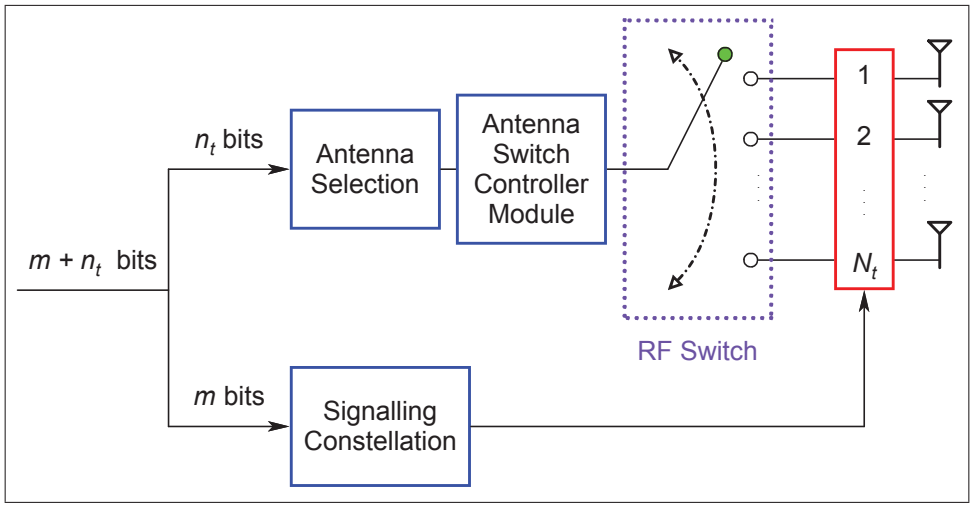

Figure 1.1 Block diagram of the SM transmitter

nxp (2014), and are omitted from this letter for lack of space. Literally, the fastest RF switch fabricated today has a switching time of 20 ns.

1.3 Analytical View

In an RF front end, we view the switching time as the time needed for the RF switch to forward an incoming signal to an antenna on one of its branches. In an SM system with N_t antennas at the transmitter, the process of choosing an antenna at every transmission period is a mutually exclusive event that follows a discrete uniform distribution. Since the antenna index is chosen from a constellation, a given antenna, i.e. the k^{th} antenna is chosen with a probability of

$$P_s = \Pr(a = a_k) = 1/N_t, \tag{1.1}$$

where P_s denotes the probability that the transmission stays on the k^{th} antenna to transmit the next symbol, i.e. no switching happens. Likewise, the probability of switching to another antenna P_{sw} to transmit the next symbol would become

$$P_{sw} = 1 - P_s = 1 - 1/N_t. \tag{1.2}$$

In fact, (1.2) shows the probability of hopping or jumping to another antenna in a set of N_t antennas. Considering these two probabilities and the fact that if a switching occurs then the symbol duration will be the switching time plus the SM symbol time, i.e. $T_{sw} + T_s$, we may now discuss the effective SM symbol duration T_{av} which we define as

$$T_{av} \equiv P_s \cdot \underbrace{T_s}_{\text{(duration if not switching)}} + P_{sw} \cdot \underbrace{(T_s + T_{sw})}_{\text{(duration if switching)}} \tag{1.3}$$

which, after substituting (1.1) and (1.2) into (1.3), may expand as

$$T_{av} = \frac{(T_s + T_{sw})N_t - T_{sw}}{N_t}. \tag{1.4}$$

As observed in (1.4), the effective SM symbol duration depends on the number of antennas involved in transmission and on the *switching* time in relationship with the RF switch. On the one hand, it is clearly noticed that T_{av} reduces to $T_{av} = T_s$ in the hypothetical case of $T_{sw} = 0$.

This hypothesis is, however, unachievable in practical systems. On the other hand, a practical implementation of some SM receivers may require the insertion of a vacant pause of duration T_{sw} whether or not switching takes place, to maintain synchronization and to avoid receiver oversampling of the received signals which may complicate the reception process. Hence, this hardware configuration can by analysed with the given analytical models by letting $P_s = 0$ and $P_{sw} = 1$ in (1.3), or equivalently, by having N_t very large in (1.4). Moreover, the performance of this SM system configuration is discussed in the discussion and simulation results section (section IV). Considering (1.4), the effective data rate R_{ef} of SM will be expressed in symbols per second (sps) as

$$R_{\text{ef}} = 1/T_{av} = \frac{N_t}{(T_s + T_{sw})N_t - T_{sw}} \quad \text{sps.} \tag{1.5}$$

1.3.1 Effective SM Capacity

We use the conventional information theory approach Prisecaru (2010) to calculate the capacity of SM systems as

$$C_{\text{SM}} = \Big(m + n_t\Big)\Big(1 + p_e \log_2(p_e) + p_c \log_2(p_c)\Big) \quad \text{bpcu} \tag{1.6}$$

where p_e represents the probability of error of SM detection in fading channels, $p_c = 1 - p_e$ is the probability of correct detection and $m + n_t$ represents the total number of bits conveyed by the SM system, where m bits choose a constellation symbol and n_t bits choose an antenna for transmission. Furthermore, the capacity of SM is not calculated the way it is done for MIMO communications, this is because the calculation of MIMO capacity C_{MIMO} does not apply Prisecaru (2010). In fact, the antenna number in SM represents added information and the antenna pattern is considered as spatial constellation, not as an information source as in MIMO. Moreover, other forms of determining the SM capacity based on mutual information may also be found in An *et al.* (2015). Note that p_e is calculated in a fading channel environment since SM is not defined for AWGN channels in which it is impossible to detect the antenna indices

which require the uniqueness of channel coefficients. Ideally, the achievable SM data rate R_s would be

$$R_s \leq C_{\text{SM}}, \tag{1.7}$$

where $R_s = 1/T_s$ and in practical situations where $T_{sw} \neq 0$, the effective SM data rate would be bounded as

$$R_{\text{ef}} \leq C_{\text{ef}}, \tag{1.8}$$

where C_{ef} is the effective capacity. Dividing (1.8) by (1.7) and considering the equality to compute an upper bound, we may now without loss of generality express C_{ef} in terms of C_{SM} in combination with (1.5) and (1.6) as

$$\begin{aligned} C_{\text{ef}} &= R_{\text{ef}}/R_s \cdot C_{\text{SM}} \\ &= \frac{N_t T_s}{(T_s + T_{sw})N_t - T_{sw}} \cdot C_{\text{SM}} \\ &= \frac{1}{1 + (1 - 1/N_t)\beta} \cdot C_{\text{SM}} \end{aligned} \tag{1.9}$$

where $\beta = T_{sw}/T_s$ in (1.9) plays a fundamental role in determining the effective capacity for a given SM configuration with N_t transmitting antennas. It is also crucial to note that

$$\lim_{\beta \to 0} C_{\text{ef}} = C_{\text{SM}}. \tag{1.10}$$

1.3.2 Restrictions on β

Using (1.9) along with Soujeri & Kaddoum (2015); Tse & Viswanath (2005) we may state the following order: $C_{\text{SIMO}} \leq C_{\text{ef}} \leq C_{\text{SM}} \leq C_{\text{MIMO}}$, where C_{SIMO} is the capacity of SIMO systems. Note that if β grows then C_{ef} will drop even below C_{SIMO} and as a result, the capacity gain achieved by SM will be lost which renders this modulation scheme useless and obsolete. Therefore, it is crucial to find a threshold value β_{th} that will keep C_{ef} above C_{SIMO} such that investing in SM systems would be feasible from the capacity point of view. In order to find the threshold value β_{th} that achieves this, we proceed following the requirement that $C_{\text{SIMO}} \leq C_{\text{ef}}$

where for N_t degrees of freedom, C_{SIMO} is calculated as described by (8.33) in Tse & Viswanath (2005) and C_{ef} is calculated according to (1.6) and (1.9). Noting the above, we pursue as

$$\frac{1}{1+(1-1/N_t)\beta} \cdot C_{\text{SM}} \geq C_{\text{SIMO}} \tag{1.11}$$

which results in the following β values

$$\beta \leq \beta_{\text{th}} = \frac{N_t}{N_t - 1}\Big(\frac{C_{\text{SM}} - C_{\text{SIMO}}}{C_{\text{SIMO}}}\Big) \tag{1.12}$$

and this forces T_{sw} to remain capped in the range

$$T_{sw} \leq \frac{T_s N_t}{N_t - 1}\Big(\frac{C_{\text{SM}} - C_{\text{SIMO}}}{C_{\text{SIMO}}}\Big). \tag{1.13}$$

Note that (1.13) above is extremely important and shows a critical relationship between the switching time T_{sw} and the symbol period T_s if SM capacity achievement is to be retained. As a matter of fact, (1.13) introduces an upper bound on the switching time T_{sw} in terms of the SM symbol duration T_s such that the capacity achievement of SM, as a system that uses multiple antennas to enhance capacity, in comparison to single-antenna systems is to preserve its superiority. Moreover, the upper bound on the switching time for a given scenario involves the calculation of C_{SM} and C_{SIMO} as described earlier under similar channel conditions.

1.3.3 Spectral Efficiency

For an SM symbol with duration T_s, the raised cosine filter occupies a bandwidth B_{SM} for each pulse Ishibashi & Sugiura (2014) that is given by

$$B_{\text{SM}} = (1+\alpha)/T_s, \tag{1.14}$$

where $0 \leq \alpha \leq 1$. Keeping this in mind, we observe that switching introduces continuous vacant (empty) pauses in the time domain that interrupt and slow down the effective data rate. Note that while the SM system occupies a bandwidth B_{SM} as indicated in (1.14) its effective

data rate reduces as given in (1.5). Inspired by Chung *et al.* (2007), we calculate the spectral efficiency η of our system as the effective data rate divided by the bandwidth as

$$\begin{aligned}\eta(\beta) \equiv \frac{R_{\text{ef}}}{B_{\text{SM}}} &= \frac{N_t}{(T_s+T_{sw})N_t - T_{sw}}\Big(\frac{T_s}{1+\alpha}\Big) \\ &= \frac{N_t}{N_t+\beta(N_t-1)}\Big(\frac{1}{1+\alpha}\Big).\end{aligned} \tag{1.15}$$

The spectral efficiency described in (1.15) is expected to degrade and vanish for large values of β since

$$\lim_{\beta\to\infty} \eta = 0, \tag{1.16}$$

and to become inversely proportional to β for large N_t as

$$\eta_{\min} = \lim_{N_t\to\infty} \eta = \frac{1}{(1+\beta)(1+\alpha)}. \tag{1.17}$$

Furthermore, the maximum achievable spectral efficiency is independent of N_t and only occurs in the ideal case, i.e.

$$\eta_{\max} = \eta|_{\beta=0} = \frac{1}{(1+\alpha)}, \tag{1.18}$$

however, the spectral efficiency can never reach unity in practical systems because neither the switching time T_{sw} nor the roll-off factor α are zero.

1.4 Discussions and Numerical Results

Switching time has an undeniable direct influence on the achievable data rate, spectral efficiency and capacity. The results obtained in this work confirm that industrial RF switches which are known to have a quantified and limited transition speed, impose an upper bound on the achievable data rate. In other words, moving to higher data rates will only be possible with advancements in RF switching technology, specifically from the *switching speed* point of view. Our results concerning the effects of switching time on these parameters will be presented in

the remaining part of this letter. Fig. 1.2 shows the effective SM transmission rate in mega symbols per second (Msps) in realistic scenarios at various RF switching speeds for $N_t = 4$ and 16 antennas. Judged by the wide gap in the effective SM data rates for $T_{sw} = 0$ and

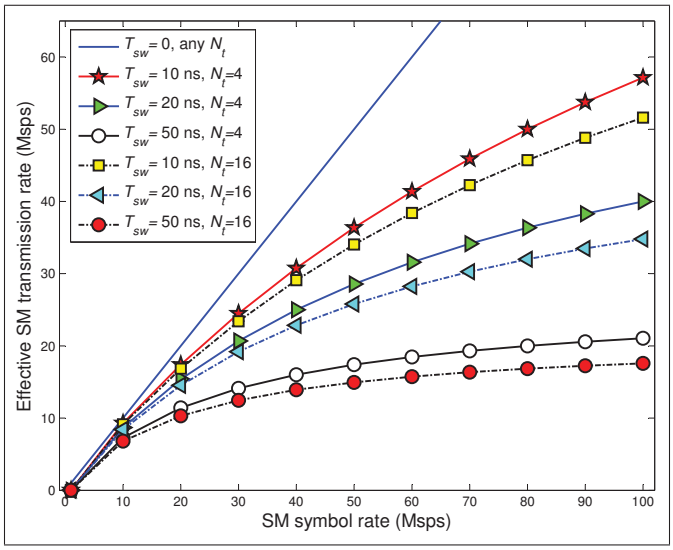

Figure 1.2 The effective SM data rate versus SM symbol rate

$T_{sw} = 20$ ns (the fastest RF switch available today), the important message that is conveyed by Fig. 1.2 is that ignoring T_{sw} leads to unrealistic transmission rate expectations. It is also observed that as N_t increases the effective data rate decreases, since the probability of hopping to a different transmitting antenna at every transmission instant rises. In Fig. 1.3, the capacities of MIMO, SIMO and SM are shown where the capacities of MIMO and SIMO are reproduced using the formulations given in Tse & Viswanath (2005) at SNR$= 0$ dB in a fading channel. The capacity of SM is calculated according to (1.6) where p_e is based on the optimum maximum likelihood (ML) detection outcome at the same SNR with a modulation order of $M = 8$, i.e. $m = 3$. Note that since N_t has to be a power of 2 in SM systems, we have compared the capacity of SM with the rival systems at these values of N_t only. Moreover, the relationship $N_t = N_r$ is preserved in order to have a fair comparison between SM and MIMO systems given in Tse & Viswanath (2005). Table 1.1 shows capacity and switching parameters versus antenna configurations. As seen in Fig. 1.3, longer SM switching times cause C_{ef} to reduce to the capacity of single antenna transmission schemes C_{SIMO}. As a result, the capacity gain achieved

Table 1.1 Capacity and switching parameters vs. antenna setup

$N_r = N_t$	**2**	**4**	**8**	**16**
n_t	1	2	3	4
p_e	0.136	0.080	0.031	0.006
SM & MIMO ($N_t \times N_r$)	2×2	4×4	8×8	16×16
SIMO ($1 \times N_r$)	1×2	1×4	1×8	1×16
β_{th} based on (1.12)	0.3634	0.4693	0.6281	0.6783

by spatial modulation is lost and, effectively, using SM to enhance capacity becomes useless and obsolete when β exceeds the threshold β_{th}. Fig. 1.3 clearly shows that SM achieves a higher capacity in comparison to SIMO as long as β does not exceed β_{th}, which confirms our analytical results with respect to the threshold value β_{th}. In summary, growing β values push the C_{ef} curves down towards C_{SIMO}, which is in line with our analysis. Finally, the spectral

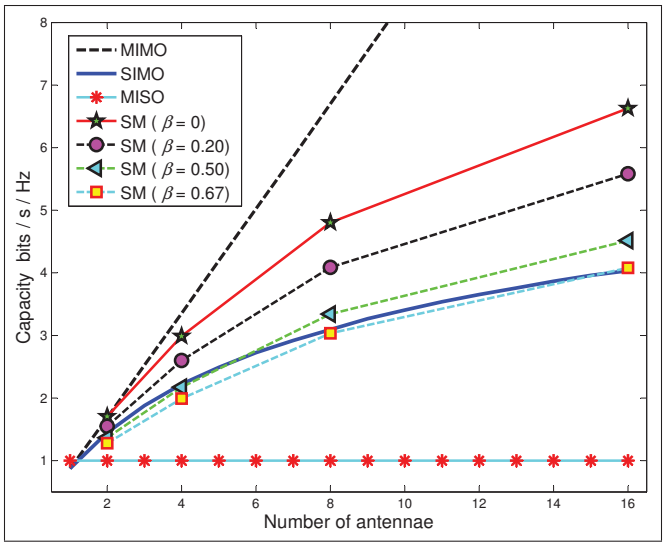

Figure 1.3 Capacities of MIMO, SM and SIMO systems

efficiency η vs. β calculated according to (1.15) is shown in Fig. 1.4 for various values of N_t and for a roll-off factor $\alpha = 0.22$ which is recently adopted in long-term evolution (LTE) filters Dahlman *et al.* (2013). The asymptotic lower bound in Fig. 1.4 concerns the insertion of an empty slot of duration T_{sw} at every transmission to relax receiver synchronization, whether antennas switch or not, which also corresponds to very large N_t, as remarked in (1.4).

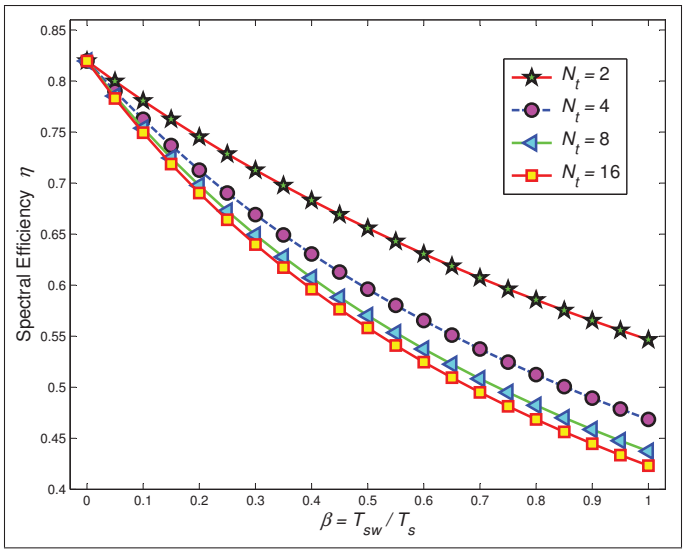

Figure 1.4 SM Spectral efficiency η versus β for various values of N_t

1.5 Conclusions

In this work, we consider the effect of switching time which is an inherent property of RF industrial switches on SM systems. Switching time being in the order of nanoseconds naturally influences the transmission rate of SM systems because of introducing systematic transmission pauses. Given the speed limitation of practical RF switches in performing transitions, antenna transition-based technologies like SM schemes are capped in terms of data rate performance. In fact, the effective data rate of SM will remain hostage to developments in industrial RF switches. This brings restrictions to the implementation and operation issues when extremely high data rates become a necessity. Since the technology marches towards emerging systems where bandwidth efficiency and data rate are both essential requirements, it is necessary to develop new SM techniques based on minimum transition of antennas, or on the transition of a group of antennas at a time rather than schemes that require a transition at every transmission instant. It is shown by the assemblage of our results that the switching time T_{sw} which is a requirement for transitions between antennas to happen, dictates restrictions on data rate, capacity and spectral efficiency of SM systems.

CHAPTER 2

FREQUENCY INDEX MODULATION FOR LOW COMPLEXITY LOW ENERGY COMMUNICATION NETWORKS

Ebrahim Soujeri[1], Georges Kaddoum[1], Minh Au[1] and Marijan Herceg[2]

[1] Department of Electrical Engineering, École de Technologie Supérieure,
1100 Notre-Dame West, Montreal, Quebec, Canada H3C 1K3
[2] Department of Communications, Faculty of Electrical Engineering, Computer Science and Information Technology Osijek, Croatia

Paper published in *IEEE Access*, June 2017.

Abstract

In this paper, we propose a low complexity multi-user communication system based on frequency index modulation that suits Internet of Things (IoT) applications. This system aims to reduce the transmitted energy and the peak-to-average-power ratio (PAPR) of orthogonal frequency-division multiplexing (OFDM) systems and to perform without sacrificing data rate in comparison to conventional OFDM. In this design, OFDM-like signals are used to make the implementation of the system easy by virtue of fast Fourier transform (FFT). In the proposed scheme, the OFDM bandwidth of N_{FIM} total sub carriers is divided into N_B equal number of sub-bands, with N subcarriers in every sub-band. At the transmitter side of each sensor, the bit stream is divided into two blocks: mapped and modulated. The bits within the mapped block are used to activate the corresponding subcarrier in its predefined sub-band in order to carry the data of the modulated block, while the other $N-1$ subcarriers are nulled out. At the receiver, the FFT is performed first, then the square-law envelope detector is applied to estimate the active frequency index to recover the mapped bits, followed by a conventional demodulation to demodulate the transmitted bits. Once the system is presented and analysed, energy efficiency, PAPR and complexity are studied to show the features of the proposed scheme. Moreover, we derive closed-form expressions of the bit error rate (BER) performance over Rayleigh fading channels and we validate the outcome by simulation results. With the characteristics exhibited in this work, the proposed system would constitute an excellent candidate for wireless sen-

sor applications, where it represents a simpler substitution for frequency-hopping (FH) based architectures, in which the hops carry extra bits.

2.1 Introduction

Recently, there has been an escalating demand for higher data rate communication systems that is associated with an increasing need in the number of devices, gadgets and wireless services. On the one hand, the 5G infrastructure public private partnership has set the goal of reaching 1000 times more speed compared to what we had in 2010, while the power to-be-consumed to run such networks are desired to be around 10% of the consumption at that time Pirinen (2014). On the other hand, the concept of internet of things (IoT) has advanced in parallel to the developments in 5G networks by virtue of wireless sensor networks (WSN) that have emerged as the most promising technologies for the future that touch various aspects of our life like fitness, automation, security, localization, consumer electronics, smart grid devices and many more Rawat *et al.* (2014). In fact, WSNs have been among one of the most researched areas in the last decade. The emergence of this technology has only been possible via advances in and availability of small, inexpensive and smart sensors that are cost effective and easily deployable Rawat *et al.* (2014). Various modulation types have so far been used in wireless sensor nodes, among these schemes are $M-$ary quadrature amplitude modulation (MQAM), offset quadrature phase-shift keying (OQPSK) and multiple frequency-shift keying (MFSK), which is also known as the *green modulation* scheme providing the advantage of low complexity and low cost of implementation in comparison to other schemes Abouei *et al.* (2010).

It is to be mentioned that in order to increase data rate, alternative index modulation schemes such as spatial modulation, code index modulation, subcarrier-index modulation, etc, have been proposed to achieve both high data rate and energy efficiency in emerging networks. To achieve this goal, indexing certain parameters of the communication system into the transmission mechanism in order to enable the conveyance of extra bits per symbol, at neither exaggerated bandwidth cost nor increased transmission power cost has been seriously considered in the last decade.

In this context, spatial modulation (SM) which uses index modulation by multiple antennae in order to increase the data rate and partially enhance the transmission capacity, has been considered in Mesleh *et al.* (2006a, 2008); Jeganathan *et al.* (2008b); Di Renzo *et al.* (2014). In this approach, antenna number or antenna index is used as an extra parameter to convey information and enhance transmission data rate. At each transmission instant, only one transmit antenna in the set is active while all other antennae are inactive. Nonetheless, this scheme has not been cost free either, since it totally depends on the channel characteristics, requires a continuous *update* of the CSI which imposes noticeable transmission overheads Di Renzo *et al.* (2011) and is very fragile with respect to both noisy CSI estimation as well as correlated channels Chang *et al.* (2013); Soujeri & Kaddoum (2015). Besides, switching time is a major impediment that caps the ambitions related to the implementation of this system in real-life scenarios. The recent study of Soujeri & Kaddoum (2016) has shown that switching time, i.e. the duration of time needed by RF switches to carry out transitions between antennae, limits the ambitions of SM and introduces noticeable gaps between projected and actual data rates.

Furthermore, code index modulation-spread spectrum (CIM-SS) has also been proposed as an alternative index-based modulation to achieve higher throughput Kaddoum *et al.* (2015b). This system uses spreading codes to map the data in conjunction with the constellation symbols. In this configuration, bits are grouped into two categories, mapped bits and modulated bits. Mapped bits choose a spreading code from a set of predetermined codes in order to spread the modulated bit. At the receiver, the spreading code is first detected using the maximum autocorrelation value and then the transmitted bit is demodulated.

Additionally, subcarrier index modulation (SIM) scheme has been proposed in Abu-Alhiga & Haas (2009) where it is merged with orthogonal frequency division multiplexing (OFDM) to constitute SIM-OFDM. Moreover, enhanced subcarrier index modulation (ESIM) has been proposed to avoid the propagation of error by replacing the concept of majority counting by a simpler method in which a pair of *off-on* or *on-off* subcarriers is used to represent a single bit Tsonev *et al.* (2011), however, the fact that two subcarriers are used to transmit a single bit doubles the required bandwidth necessary for transmission in this method.

Eventually, a transmission scheme called OFDM with index modulation (OFDM-IM) is proposed Başar *et al.* (2013). In this scheme, information is conveyed not only by M-ary signal constellations as in classical OFDM, but also by the indices of the subcarriers, which are activated according to the incoming information bits. But the implementation of this last scheme is hard as it relies on maximum likelihood (ML) detection that requires a lot of computing charges as it needs to search over all the possibilities (subcarrier combinations) within a bandwidth. This is costly as it makes a joint search over all possibilities Başar (2015) and is impractical for large combination values due to its exponentially growing decoding complexity Başar *et al.* (2013), which makes it unsuitable for WSN applications. Furthermore, the Log-Likelihood Ratio (LLR) detection strategy is another detection method proposed for this scheme for high number of subcarriers, but this detector may produce an undefined set of active indices not at all included in the original mapping table Başar *et al.* (2013).

In this work, we introduce a modified frequency index modulation (FIM) scheme that is simpler than the approach of Başar *et al.* (2013). This system has a lower complexity compared to OFDM-IM, low power consumption profile and does not sacrifice data rate as it makes use of the frequency hops in a smart and wise way. As the proposed system does not use all of the available subcarriers, it will also enjoy inter-carrier interference -free transmission while it allows the transmission of additional bits in the index domain. Therefore, the proposed system is an excellent choice for WSNs.

In the proposed FIM scheme, the OFDM bandwidth is divided into equal N_B sub-bands of N subcarriers each. A message is divided into mapped and modulated blocks where the mapped block activates a single corresponding subcarrier in its predefined sub-band in order to carry the data of the modulated block. At the receiver side, FFT is first performed on the received signal followed by sub-sectioning the bandwidth into N_B sub-bands where square-law envelope detector (SLED) is used in each sub-band to identify the active subcarrier. Then, the mapper chooses the corresponding indexed message and demodulates the received signal over the channel to get the remainder. While the proposed system keeps the architecture simple and constitutes an excellent substitution for the conventional frequency-hopping (FH) technique in which hops

carry no additional information. Moreover, despite the simplicity, the proposed system enjoys all the specifications associated with frequency hopping systems from the signal, interference, channel and anti-jamming points of view. Furthermore, the system has a low PAPR profile and may be used in multi-user or multi-node scenarios thanks to OFDMA multiple access technique. These properties make FIM scheme suitable for IoT applications where size, simplicity and efficiency say the final word Barnaghi *et al.* (2012).

In summary, the low complex FIM system with its simple mapping method is briefly described. The analytical bit error rate (BER) expressions over Rayleigh fading channel are derived and are cross-checked with simulation results to show the accuracy extent of our analytical expressions. Further, the energy efficiency and PAPR of the proposed system are analysed. Finally, the BER performance of this scheme is compared with similar modulation techniques to show the FIM system superiority compared to is counterparts.

The rest of the paper can be summarized as follows. In Section 2.2, the proposed system model is presented. Performance analysis of the FIM is demonstrated in Section 2.3. Energy efficiency and complexity are discussed in 2.4. In Section 2.5, we present numerical and simulation results and Section 2.6 provides concluding remarks.

2.2 System Model

In this section, the FIM transmitter and the receiver architectures will be described in detail.

2.2.1 The Transmitter

A block diagram of the proposed FIM system is presented in Fig. 2.1. The FIM scheme divides the OFDM bandwidth of N_{FIM} total sub carriers into N_B equal sub-bands of N subcarriers each. Since each FIM sub-block has the same processing procedure, we consider the i^{th} sub-band for simplicity hereafter. In the FIM transmitter, the bit stream in every sub-band is divided into blocks of $p_n = p_1 + p_2$ bits, where p_1 denotes the number of mapped bits while p_2 represents the number of modulated bits. As such, the outgoing bit stream can be written as $\mathbf{b}_i = [\mathbf{b}_i^{p_1}, \mathbf{b}_i^{p_2}]$,

where $\mathbf{b}_i \in \{0,1\}^{(p_1+p_2)}$, $\mathbf{b}_i^{p_1} = [b_i^1, \cdots, b_i^{p_1}]$ and $\mathbf{b}_i^{p_2} = [b_i^{p_1+1}, \cdots, b_i^{p_2}]$ are the two sub-blocks that represent p_1 mapped and p_2 modulated bits, respectively. Subsequently, the vector $\mathbf{b}_i^{p_1} \in \{0,1\}^{p_1}$, of $p_1 = \log_2(N)$ bits, chooses one active subcarrier index $I \in \{0, \cdots, N-1\}$ out of N available indices in the sub-band. The transformation of mapped bits into an active subcarrier *index* is performed by the index selector module. Fig. 2.2 illustrates the case where $\mathbf{b}_i^{p_1} = [0 \;\; 1]$ which leads to the activation of the second subcarrier, i.e. $I_i = 2$ out of 4 available subcarriers in the sub-band.

On the other hand, the vector $\mathbf{b}_i^{p_2} \in \{0,1\}^{p_2}$, of $p_2 = \log_2(M)$ bits, is mapped onto the considered M-ary signal constellation to produce the transmitted symbol s_i. The symbol s_i is transmitted over the selected subcarrier indexed by I_i, while the other $N-1$ subcarriers are inactive and set to zero. The transmitted symbol s_i has an energy $E_s = \mathrm{E}[s_i s_i^*] = p_2 E_b$ where E_b is the bit energy.

2.2.2 Total Mapped Bits p_T

Once the frequency modulation system with a total number of available frequencies $N_{\mathrm{FIM}} = N_B \times N$ that is split into N_B number of sub-bands such that $N_{\mathrm{FIM}} = N_B \times N$ is set up, the records shown in Table 2.1 may be discussed. In fact, Table 2.1 describes the total number of transmittable mapped bits $p_T = N_B \times p_1 = N_B \times \log_2(N)$ in the FIM system with respect to the number of sub-bands N_B for different N_{FIM}. Observe that the FIM system has a capacity to transmit a total of $N_B \times p_n$ bits in every transmission instant. Since both the peak power in the system as well as the BER performance depend on the number of active frequencies in a sub-band, Table 2.1 will be revisited again later, when we discuss PAPR analysis and simulation results in the sections that follow.

Also, since part of transmitted bits are conveyed by the frequency index, and to have a fair comparison with other conventional systems, we define an equivalent system bit energy E_{b_S} which represents the effective energy consumed per transmitted bit. This equivalent system bit

Table 2.1 FIM transmits a total of p_T mapped bits using N_B number of sub-bands with N frequencies each

N_{FIM}	4	8	16	32	64	128	256
N_B	2	2	2	2	2	2	2
N	2	4	8	16	32	64	128
p_T	2	4	6	8	10	12	14
N_B		4	4	4	4	4	4
N		2	4	8	16	32	64
p_T		4	**8**	12	16	20	24
N_B			8	8	8	8	8
N			2	4	8	16	32
p_T			**8**	**16**	24	32	40
N_B				16	16	16	16
N				2	4	8	16
p_T				**16**	**32**	48	64
N_B					32	32	32
N					2	4	8
p_T					**32**	**64**	96
N_B						64	64
N						2	4
p_T						**64**	**128**
N_B							128
N							2
p_T							**128**

energy is related to the physically modulated bit energy by the relationship

$$E_{b_S} = \frac{p_1 + p_2}{p_2} E_b = \frac{p_n}{p_2} E_b. \tag{2.1}$$

While the energy described in (2.1) allows the comparison of our system to other systems from the performance point of view, it also is an indication of the energy efficiency achieved by the proposed system. Furthermore, to construct the FIM sub-block of N elements in the frequency domain, we consider the selected active subcarrier index I_i and the modulated M-PSK symbol s_i, in order to form the vector

$$\mathbf{X}_i = [X_i(0), \cdots, X_i(N-1)], \tag{2.2}$$

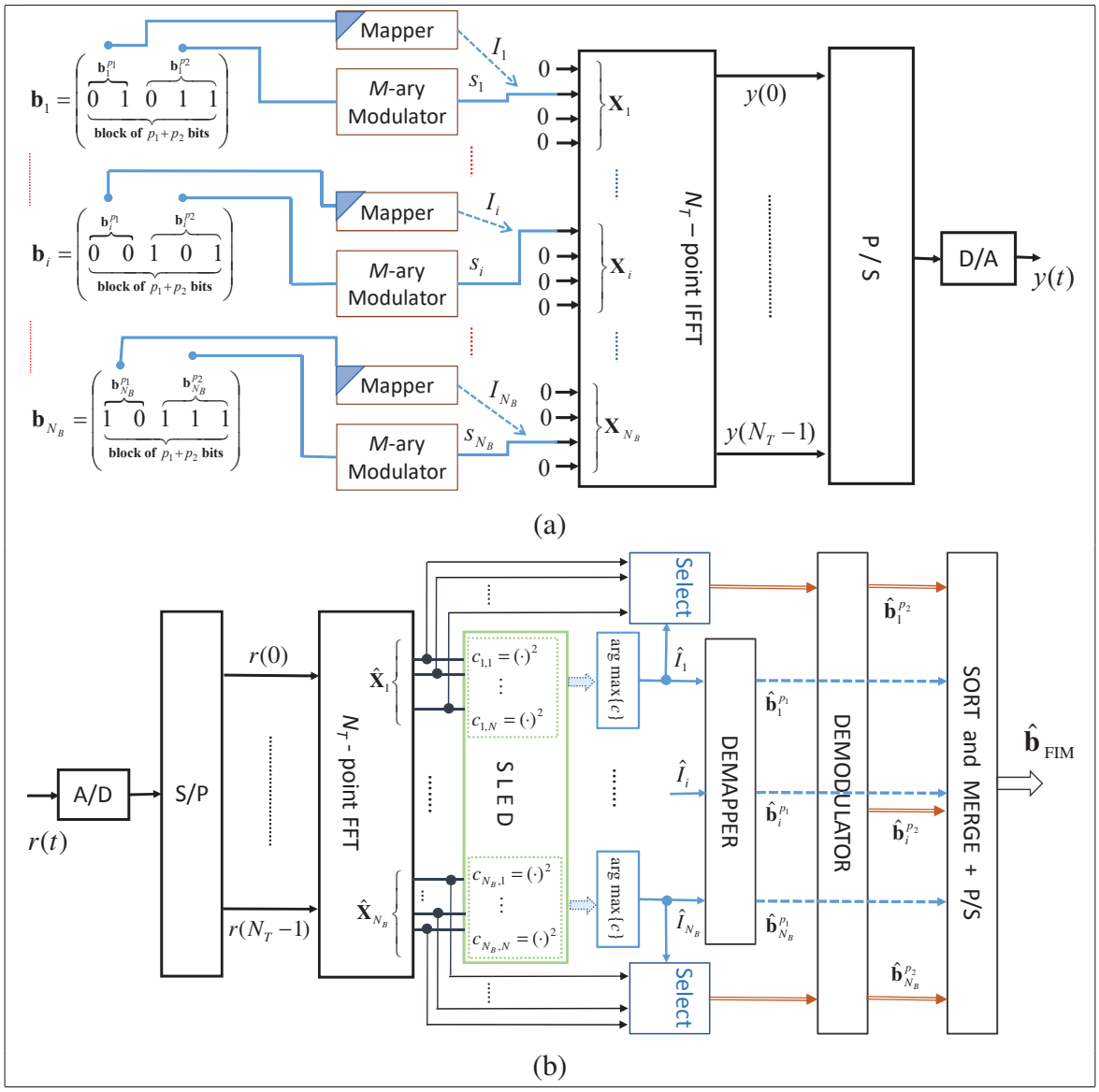

Figure 2.1 Block diagram of the general structure of FIM communication system: a) the transmitter, and b) the receiver

where

$$X_i(k) = \begin{cases} 0, & k \neq I, \\ s_i, & k = I, \quad \text{for} \quad k = 0, \cdots, N-1. \end{cases} \tag{2.3}$$

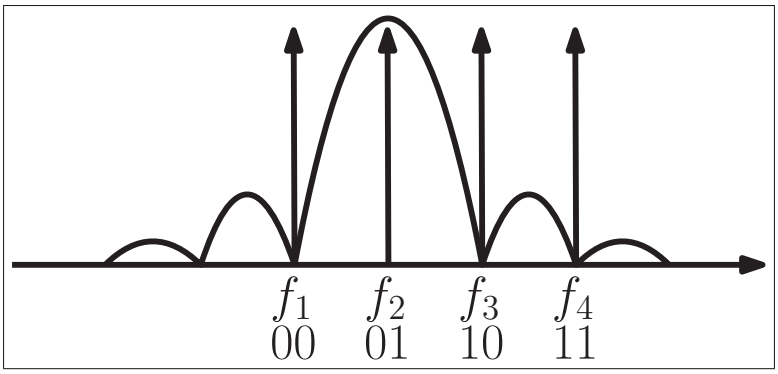

Figure 2.2 A given FIM system with 4 subcarriers. In the illustration, the transmitter has indexed the message 01 and transmits the rest of the message via the subcarrier f_2 only

For simplicity, the insertion and removal of cyclic guard prefix is not expressed in our mathematical equations.

The frequency index modulators in each sub-band of the transmitter obtain the FIM subblocks first and then concatenate these subblocks to form the main FIM blocks. So, the complete FIM transmitted block that incorporates all sub-bands (from 1 until N_B) would be stated as

$$y(t) = \frac{1}{\sqrt{T_N}} \sum_{i=1}^{N_B} \sum_{k=0}^{N-1} X_i(k) e^{j2\pi f_{i,k} t}, \quad 0 \le t \le T_N, \tag{2.4}$$

where $f_{i,k}$ is the k^{th} subcarrier frequency in the i^{th} sub-band with a predefined bandwidth of $f_{i,k} = N(i-1)/T_N + k/T_N$ with T_N being the time duration of a FIM symbol.

2.2.3 The Receiver

In this paper, we consider transmissions over a Rayleigh fading channel corrupted by an additive Gaussian noise channel. The received signal in the i^{th} sub-block can be expressed as a vector of N samples $\hat{\mathbf{X}}_i = \left[\hat{X}_i(0), \cdots, \hat{X}_i(N)\right]$ such that

$$\hat{X}_i(k) = \begin{cases} Z_i', & k \neq I, \\ H_i s_i + Z_i, & k = I, \quad \text{for} \quad k = 0, \cdots, N-1. \end{cases} \tag{2.5}$$

where $H_i \sim \mathbb{C}\mathcal{N}(0,1)$ is the FFT output produced by the Rayleigh fading channel effect, Z_i' and Z_i are independent complex AWGN, with zero mean and variance N_0. In order to reduce the complexity of the receiver, a SLED is used to estimate the active subcarrier index in the i^{th} sub-block. Thus, the output variables in the vector $\hat{\mathbf{X}}_i$ are fed to SLED forming N decision variables such that for $k = 0, \cdots, N-1$, we have

$$c_{i,k} = |\hat{X}_i(k)|^2 = \begin{cases} |Z_i'|^2, & \mathscr{H}_0 \\ |H_i s_i + Z_i|^2, & \mathscr{H}_1 \end{cases} \tag{2.6}$$

where $\mathscr{H}_0$ and $\mathscr{H}_1$ are two hypotheses with which $\mathscr{H}_0$ is verified if there is no signal, and $\mathscr{H}_1$ is the alternative that indicates the presence of s_i. The SLED chooses the maximum value in order to estimate the active subcarrier *index*, such that the estimate of the active subcarrier index would be expressed as

$$\hat{I}_i = \arg\max_k \{c_{i,k}\}, k \in \{0, \cdots, N-1\}. \tag{2.7}$$

Therefore, the decision variable might land in $\mathscr{H}_1$ if $\hat{I}_i = I_i$. By estimating the active subcarrier index $\hat{I}_i$, the receiver can extract p_1 mapped bits. The receiver then demodulates the corresponding branch output using a conventional M-PSK demodulator to extract the remaining p_2 modulated bits.

2.3 FIM Performance Analysis

In this section, we determine the performance of the proposed FIM system, in order to examine the advantages of mapping information bits into subcarrier indices.

2.3.1 BER Analysis of FIM

In the FIM scheme, the transmitted data in every sub-band is divided into two blocks; the *mapped bits* block and the *modulated bits* block. The mapped bits block determines which subcarrier will be active and, hence, will be modulated by the modulating bits, contained in

the *modulated bits* block. Therefore, the FIM system BER probability consists of the BER probability of mapped bits P_{map} and the BER probability of modulated bits P_{mod}. Subsequently, the FIM BER could be described as

$$P_{\text{FIM}} = \frac{p_1}{p_1 + p_2} P_{\text{map}} + \frac{p_2}{p_1 + p_2} P_{\text{mod}}. \tag{2.8}$$

In (2.8) above, the probability of error is prorated to the number of bits in every category and the errors committed in that category. In order to derive the BER probability of mapped bits P_{map}, the erroneous probability of active subcarrier index detection P_{ed} should be derived. Erroneous active subcarrier index detection causes a wrong mapped bits combination estimation. Each wrong combination can have a different number of incorrect bits compared to the correct combination. Therefore, the probability of erroneous active subcarrier index detection is converted into the corresponding BER probability of mapped bits by using

$$P_{\text{map}} = \frac{2^{(p_1 - 1)}}{2^{p_1} - 1} P_{\text{ed}}. \tag{2.9}$$

In order to calculate the BER of the modulated bits P_{mod}, we consider that this probability depends on the correct estimation of the active subcarrier index and the BER probability of M-ary PSK modulation. Therefore, an error may occur in two different ways. The first case is when the active subcarrier index is correctly estimated but an error occurs in the $M-$PSK demodulation process. The second case is when an error occurs in the estimation of the active subcarrier index, and the modulated bits are estimated using the wrong subcarrier. In this case, the $M-$PSK modulated symbol will have to be guessed. In fact, the probability of correct detection will be simply equal to $\frac{1}{M}$. Consequently, the BER probability of the modulated bits would be expressed as

$$P_{\text{mod}} = \frac{1}{p_2} \left[P_{S,\text{MPSK}} (1 - P_{\text{ed}}) + \frac{M-1}{M} P_{\text{ed}} \right], \tag{2.10}$$

where $P_{S,\mathrm{MPSK}}$ is the conventional SER probability of $M-$PSK modulation. As both (2.9) and (2.10) in the above depend on P_{ed}, we have a detailed look at this in the next subsection.

2.3.2 Erroneous Active Subcarrier Index Detection P_{ed}

Since a SLED is used for active subcarrier index estimation, we shall determine the probability of erroneous active subcarrier index detection P_{ed}. To do so, we assume equiprobable transmitting active subcarriers. Moreover, for the sake of clarity, we focus on a single sub-band, i.e the i^{th} sub-band, in which $c_{i,k}$ in (2.6) becomes c_k for $k = 0, \cdots, N-1$. Therefore, P_{ed} the probability of error conditioned on the transmitting subcarrier index being $I \in \{0 \cdots N-1\}$ would be given as

$$\begin{aligned} P_{\mathrm{ed}} &= P\left(c_I < \max\left(c_k\right) | I\right), \\ &\text{for} \quad 1 \leq \underset{k \neq I}{k} \leq N. \end{aligned} \tag{2.11}$$

As deduced from (2.11), an error in the estimation of the active subcarrier index will occur if the decision variable $\max(c_k)$ is larger than c_I. It can be observed from (2.6) that the variable c_k may assume two values as

$$c_k = \begin{cases} |Hs + Z_I|^2, & k = I, \\ |Z_k|^2 \qquad , & k \neq I. \end{cases} \tag{2.12}$$

Since the complex-valued random variables $\{Hs\}$, $\{Z_I\}$ and $\{Z_k\}$ are mutually independent zero mean Gaussian random variables, the decision variables c_I and c_k are distributed according to a chi-square distribution with two degrees of freedom. Subsequently, its probability density functions (PDF) can be written as

$$p(c_I) = \frac{1}{2\sigma_I^2} e^{-c_I/2\sigma_I^2}, \tag{2.13}$$

where the variance σ_I^2 is given by

$$\begin{aligned}\sigma_I^2 &= \mathbb{E}\left(|Hs+Z_I|^2\right)\\ &= \mathbb{E}\left((Hs+Z_I)(Hs+Z_I)^*\right)\\ &= \mathbb{E}(|H^2|)E_s+N_0 = N_0(1+\bar{\gamma}_s),\end{aligned} \tag{2.14}$$

where $\bar{\gamma}_s = \mathbb{E}(|H|^2)E_s/N_0$ is the average signal-to-noise ratio (SNR). Since the usual metrics for BER performance analysis in digital communications is the E_b/N_0, the expression (2.14) can be rewritten as

$$\sigma_I^2 = N_0(1+p_2\bar{\gamma}_b), \tag{2.15}$$

where $\bar{\gamma}_b = \mathbb{E}(|H|^2)E_b/N_0$. Similarly, for $k \neq I$, the variance σ_k^2 is calculated based on the PDF

$$p(c_k) = \frac{1}{2\sigma_k^2}e^{-c_k/2\sigma_k^2} \tag{2.16}$$

that results in

$$\sigma_k^2 = \mathbb{E}\left(|Z_k|^2\right) = N_0, \quad \text{for} \quad 1 \leq \underset{k\neq I}{k} \leq N. \tag{2.17}$$

The probability of erroneous active subcarrier index estimation is equal to 1 minus the probability that $c_I > c_k$, for $1 \leq \underset{k\neq I}{k} \leq N$. Since the signals are orthogonal and the AWGN are statistically independent, the random variables in (2.12) are mutually statistically independent. Hence, for a given I the joint probability $P(\{c_I > c_k\}|I)$, for $1 \leq \underset{k\neq I}{k} \leq N$ is equal to $P(c_I > c_k|I)$, for $k \neq I$, raised to the $N-1$ st power. Furthermore, we may now evaluate the probability $P(c_I > c_k|I)$ by applying

$$P(c_I > c_k|I) = \int_0^{c_I} p(c_k)dc_k. \tag{2.18}$$

The evaluation of the above integral results in Proakis (2001)

$$P(c_I > c_k|I) = 1 - e^{-\frac{c_I}{2\sigma_k^2}}. \tag{2.19}$$

Raising the result of (2.19) to the power $N-1$ and averaging over all possible values of c_I will yield the probability of correct decision P_{cd}.

$$P_{\text{cd}} = \int_0^\infty p(c_I)\left[1 - e^{-\frac{c_I}{2\sigma_k^2}}\right]^{N-1} dc_I. \tag{2.20}$$

Since $p(c_I)$ as been defined in (2.13), we get

$$\begin{aligned} P_{\text{cd}} &= \int_0^\infty \frac{1}{2\sigma_I^2} e^{-\frac{c_I}{2\sigma_I^2}}\left[1 - e^{-\frac{c_I}{2\sigma_k^2}}\right]^{N-1} dc_I \\ &= \int_0^\infty \frac{1}{1+p_2\bar{\gamma}_b} e^{-\frac{c_I}{1+p_2\bar{\gamma}_b}}\left[1 - e^{-c_I}\right]^{N-1} dc_I, \end{aligned} \tag{2.21}$$

Note that the term $\left[1 - e^{-c_I}\right]^{N-1}$ which appears in (2.21) may be expressed in a reduced form as

$$\left[1 - e^{-c_I}\right]^{N-1} = \sum_{k=0}^{N-1} (-1)^k \binom{N-1}{k} e^{-kc_I}. \tag{2.22}$$

Now, substituting (2.22) into (2.21), we get Proakis (2001)

$$\begin{aligned} P_{\text{cd}} = \frac{1}{1+p_2\bar{\gamma}_b} &\sum_{k=0}^{N-1} (-1)^k \binom{N-1}{k} \\ &\times \int_0^\infty e^{-\frac{c_I}{1+p_2\bar{\gamma}_b}} e^{-kc_I} dc_I. \end{aligned} \tag{2.23}$$

Unifying the exponential terms in the integral produces

$$\begin{aligned} P_{\text{cd}} = \frac{1}{1+p_2\bar{\gamma}_b} &\sum_{k=0}^{N-1} (-1)^k \binom{N-1}{k} \\ &\times \int_0^\infty e^{-\frac{(1+k+kp_2\bar{\gamma}_b)c_I}{1+p_2\bar{\gamma}_b}} dc_I. \end{aligned} \tag{2.24}$$

Replacing the integral term by its solution yields

$$P_{\text{cd}} = \frac{1}{1+p_2\bar{\gamma}_b}\sum_{k=0}^{N-1}(-1)^k\binom{N-1}{k}\left[\frac{1+p_2\bar{\gamma}_b}{(1+k+kp_2\bar{\gamma}_b)}\right], \tag{2.25}$$

which then simplifies to the final form of

$$P_{\text{cd}} = \sum_{k=0}^{N-1}\frac{(-1)^k}{1+k+kp_2\bar{\gamma}_b}\binom{N-1}{k}. \tag{2.26}$$

Subtracting the above result from unity gives the probability of subcarrier detection error, or the mapped symbol error i.e. $P_{\text{ed}} = 1 - P_{\text{cd}}$ as

$$P_{\text{ed}} = 1 - P_{\text{cd}} = \sum_{k=1}^{N-1}\frac{(-1)^{1+k}}{1+k+kp_2\bar{\gamma}_b}\binom{N-1}{k}. \tag{2.27}$$

2.3.3 BER of Mapped and Modulated Bits

Once the probability of subcarrier misdetection P_{ed} is evaluated as in (2.27), it is substituted in (2.9) and (2.10) to yield the BER of mapped and modulated bits, respectively. In the latter, the conventional M-PSK demodulation with the following closed-form SER expression over fading channels is considered Proakis (2001)

$$P_{S,\text{MPSK}} = \tfrac{M-1}{M} - \tfrac{V}{\pi\sqrt{1-W^2}}\cot^{-1}\left(\tfrac{-W}{\sqrt{1-W^2}}\right), \tag{2.28}$$

where $V = \mu\sin(\pi/M)$, $W = \mu\cos(\pi/M)$ and μ is given as

$$\mu = \sqrt{\frac{p_2\bar{\gamma}_b}{1+p_2\bar{\gamma}_b}}. \tag{2.29}$$

Substituting (2.27) and (2.28) into (2.9) and (2.10) respectively, and considering the expression for the probability of error for FIM systems introduced in (2.8), we end up with the final expanded form as shown on the top of the next page.

$$P_{\text{FIM}} = \frac{1}{p_n}\Bigg[\Big(\frac{M-1}{M} - \frac{\sqrt{\frac{p_2\bar{\gamma}_b}{1+p_2\bar{\gamma}_b}}\sin(\pi/M)}{\pi\sqrt{1-(\sqrt{\frac{p_2\bar{\gamma}_b}{1+p_2\bar{\gamma}_b}}\cos(\pi/M))^2}}\cot^{-1}\Big(\frac{-\sqrt{\frac{p_2\bar{\gamma}_b}{1+p_2\bar{\gamma}_b}}\cos(\pi/M)}{\sqrt{1-(\sqrt{\frac{p_2\bar{\gamma}_b}{1+p_2\bar{\gamma}_b}}\cos(\pi/M))^2}}\Big)\Big)$$
$$\times\sum_{k=0}^{N-1}\frac{(-1)^k}{1+k+kp_2\bar{\gamma}_b}\binom{N-1}{k} + \frac{M-1}{M}\sum_{k=1}^{N-1}\frac{(-1)^{1+k}}{1+k+kp_2\bar{\gamma}_b}\binom{N-1}{k}\Bigg]$$
$$+\frac{p_1}{p_n}\frac{2^{(p_1-1)}}{2^{p_1}-1}\sum_{k=1}^{N-1}\frac{(-1)^{1+k}}{1+k+kp_2\bar{\gamma}_b}\binom{N-1}{k}. \tag{2.30}$$

2.4 Energy Efficiency, PAPR and Complexity

In this section, we consider the energy efficiency, PAPR and complexity analyses for the proposed FIM system.

2.4.1 Energy Efficiency

Table 2.1 demonstrates various possible configurations for a given total number of subcarriers N_{FIM}. We observe that when N_{FIM} increases, we have more design options. In fact, we have $\log_2(N_{\text{FIM}}/2)$ possible configurations, where for each configuration, different number of bits are mapped. In the table, values of N_{FIM} from 4 to 256 are shown. As clearly observed in Table 2.1, the maximum number of mapped bits in a FIM system with a total of N_{FIM} frequencies is equal to $p_T = N_{\text{FIM}}/2$. This maximum mapping is achieved in two ways, choosing N either 2 or 4. That is to say, to divide N_{FIM} into sub-bands such that we have either 2 or 4 frequencies in each sub-band. Choosing $N = 2$ halves the transmitted power, but it does not render a BER performance improvement over the basic system. However, choosing $N = 4$ not only provides a lower PAPR and a better power efficiency compared to $N = 2$, as only 1 out of 4 frequencies becomes active, but achieves a BER enhancement and allows the system to carry an extra mapped bit compared to the $N = 2$ case.

In the proposed FIM only $N_B p_2$ bits from the total $N_B(p_1+p_2)$ are directly modulated using the M-ary modulation, whereas $N_B p_1$ bits are conveyed in the selection of subcarriers. Considering that each modulated bit requires an energy of E_b to be transmitted, then the mapping part to index subcarriers should reduce the total required transmission energy. Consequently, the percentage of the energy saving per subband in the proposed FIM is given by

$$\begin{aligned} E_{\text{saving}} &= \left(1-\frac{p_2}{p_1+p_2}\right)E_b\% \\ &= \left(1-\frac{1}{p_1/p_2+1}\right)E_b\% \end{aligned} \tag{2.31}$$

Since we have defined $p_1=\log_2(N)$ and $p_2=\log_2(M)$, the energy saving depends on the ratio of the number of subcarriers involved in indexing to the modulation order of the system. It should be noted that for a fixed modulation order, an augmentation in the number of subcarriers to be indexed yields more energy saving in the FIM system. Table 2.2 at the end of Section 2.5 provides a numerical example in relation to the energy saving discussed here.

2.4.2 PAPR Analysis

Taking into consideration the splitting of a full band that encompasses N_{FIM} frequencies into N_B sub-bands with N frequencies each, we will have a glance at the PAPR behaviour of the proposed system. The PAPR is a criterion to measure the success of a frequency modulation system and is defined in OFDM systems for a transmit signal $y(t)$ as Elavarasan & Nagarajan (2015)

$$\text{PAPR}_{\text{dB}} = 10\log_{10}\frac{\max|y(t)|^2}{E\{|y(t)|^2\}} \tag{2.32}$$

to represent an indication of the non-linearity in the transmitter amplifier. PAPR is ideally required to stay within the linear operational range of the RF amplifier at the transmitter. Assuming that the real and imaginary parts of $y(t)$ follow a Gaussian distribution, each with zero mean and variance $\frac{1}{2}$ in agreement with the central limit theorem, when N_{FIM} is sufficiently large, $|y(t)|$ becomes a Rayleigh distribution and the power distribution has central chi-square

distribution with two degrees of freedom Han & Lee (2005). The cumulative distribution function (CDF) of the amplitude of a signal sample is given by

$$F(\mathrm{PAPR}_0) = 1 - \mathrm{e}^{-\mathrm{PAPR}_0}. \tag{2.33}$$

If we assume that the average power of $y(t)$ is equal to one, then the sampling values of different sub-channels are mutually independent and identically distributed Rayleigh random variables normalized with its own average power. Hence, the probability distribution function for PAPR being less than a certain threshold value becomes

$$\begin{aligned} \Pr(\mathrm{PAPR} \leq \mathrm{PAPR}_0) &= F(\mathrm{PAPR}_0)^{N_B} \\ &= (1 - e^{-\mathrm{PAPR}_0})^{N_B}. \end{aligned} \tag{2.34}$$

However, when the performance for PAPR reduction techniques need to be evaluated, the complementary cumulative distribution function (CCDF) of the PAPR is more frequently used Litsyn (2007), *i.e.* the probability that PAPR exceeds a predefined threshold value PAPR_0, such that

$$\begin{aligned} \Pr(\mathrm{PAPR} > \mathrm{PAPR}_0) &= 1 - \Pr(\mathrm{PAPR} \leq \mathrm{PAPR}_0) \\ &= 1 - F(\mathrm{PAPR}_0)^{N_B} \\ &= 1 - (1 - e^{-\mathrm{PAPR}_0})^{N_B}. \end{aligned} \tag{2.35}$$

The partial selection of the subcarriers in FIM results in a reduction of the PAPR. Such a PAPR reduction considerably decreases the consumed power and is not associated with any form of penalty on the bit error rate (BER) performance.

2.4.3 System Complexity

The complexity of the FIM system can be evaluated by the number of operations required. Since the FIM uses IFFT and FFT operations with a length of N_{FIM}, the computational com-

plexity will be $\mathcal{O}_{\text{FFT/IFFT}} \sim \mathcal{O}(2N_{\text{FIM}}\log_2(N_{\text{FIM}}))$. Next, SLED multiplies the vector $\hat{\mathbf{X}}_i$ by its complex conjugate. Therefore, the computational complexity is simply $\mathcal{O}_{\text{SLED}} \sim \mathcal{O}(NN_B)$. Regarding the modulation and the demodulation, we assume that a modulator converts a stream of p_2 bits into an M-ary symbol by computing an inner product between the bit stream and the vector $\left[2^{p_2-1},\cdots,1\right]$. The demodulator will convert the symbol into a bit stream by computing p_2 Euclidean divisions. As a result, the computational complexity of a modulator and a demodulator will be $\mathcal{O}_{\text{Mod/Demod}} \sim \mathcal{O}(3p_2-1)$ per active subcarrier. In total, the complexity of the FIM system would be expressed as

$$\mathcal{O}_{\text{FIM}} = \mathcal{O}_{\text{FFT/IFFT}} + \mathcal{O}_{\text{SLED}} + N_B\mathcal{O}_{\text{Mod/Demod}}. \tag{2.36}$$

In the conventional OFDM scheme, since all subcarriers are activated during the transmission, the complexity will be

$$\mathcal{O}_{\text{OFDM}} = \mathcal{O}_{\text{FFT/IFFT}} + NN_B\mathcal{O}_{\text{Mod/Demod}}. \tag{2.37}$$

Aiming at comparing the FIM system to a system that shares the same modulation concept but with a different receiver design, we compare the complexity of FIM to that of OFDM-IM. In the latter, only k out of N subcarriers are activated. However, the complexity of the maximum likelihood detector is $\mathcal{O}_{\text{MLD}} \sim \mathcal{O}(2^{p_2}M^k)$ per subcarrier where $k = p_2/\log_2(M)$, Başar *et al.* (2013).

$$\mathcal{O}_{\text{OFDM-IM}} = \mathcal{O}_{\text{FFT/IFFT}} + kN_B\mathcal{O}_{\text{Mod/Demod}} + \mathcal{O}_{\text{MLD}}. \tag{2.38}$$

2.5 Simulation Results

In this section, we study the obtained analytical and simulation results for the proposed FIM system and show that analytical and simulation results are in good agreement. Then we compare the performance of FIM to other index-based schemes like SM and OFDM-IM system. Finally, we study the energy efficiency, PAPR and complexity analyses for the proposed system.

2.5.1 Performance of FIM

We shed light in this section on some of these parameters that influence the system the most, we investigate the performance of the proposed frequency-index modulation system in various scenarios and we compare the performance of our system to other modulation-index schemes to show the performance superiority.

As the system may ferry a certain number of symbols per sub-band in every transmission using various configurations, we start by plotting the overall BER performance of the FIM system described by (2.8) for the transmission of 7 bits per sub-band using different combinations of the modulation order M and the number of frequencies per sub-band N. The performance of such a case is shown in Fig. 2.3. The first observation is that all configurations of the FIM system show a superior BER performance to the conventional 128-ary PSK modulation in fading channels. As a matter of fact, the 128-ary PSK has been chosen to compare, as it represents the most basic well-known communication system that carries 7 bits. We also observe a great match and conformity between analytical and simulation results for the FIM system, which confirms the certitude of our approach. Furthermore, it also shows that under transmission rate restrictions, our system is design-flexible and is adaptable to acquire several forms in terms of M and N. This facilitates its practical application for WSNs. As both the modulation order M and the number of frequencies per sub-band N constitute the fundamental parts of the FIM design, we independently observe the BER performance of FIM with respect to each of these parameters individually in the next two plots. Fig. 2.4 shows the BER performance of the proposed FIM system versus the modulation order M, for $N = 4$ frequencies per sub-band. As seen in Fig. 2.4, increasing M tightens up the Euclidean distance between the transmitted symbols and degrades the BER performance, which is very well in line with communication theory. Fig. 2.5 exhibits the BER performance of the proposed FIM system with respect to the number of subcarriers per sub-band for a modulation order of $M = 8$. As witnessed in Fig. 2.5, the BER performance of the proposed system shows a marginal improvement with increased N. This is due to the fact that increasing N contributes to the total equivalent system bit energy described earlier in (2.1). As a matter of fact, the BER performance would deteriorate without

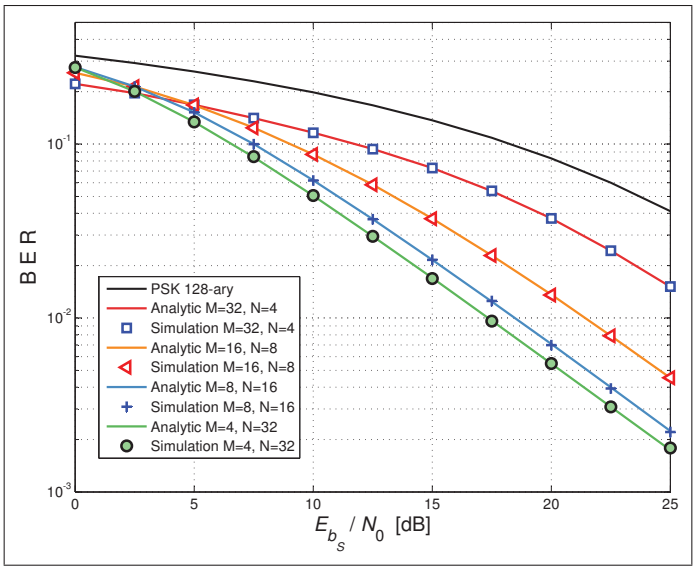

Figure 2.3 Performance of the proposed system with various values of M and N that facilitate the conveyance of 7 bits per transmission

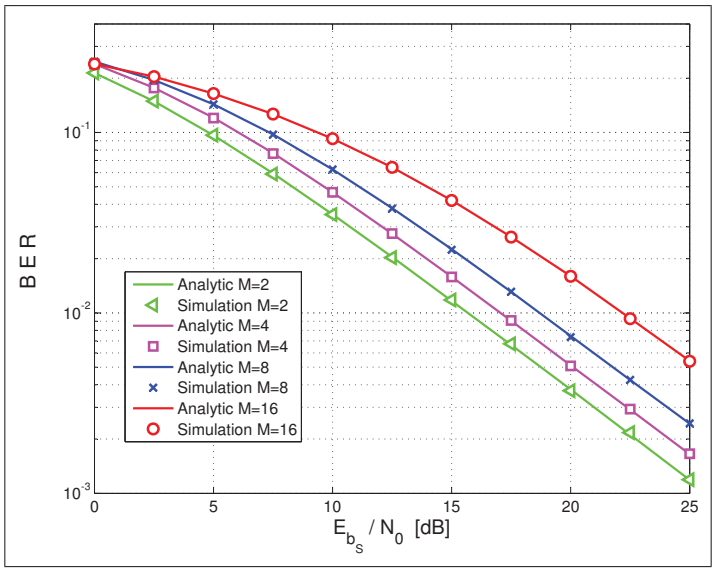

Figure 2.4 Performance of the proposed FIM system with various modulation order M for $N = 4$ subcarriers per sub-band

the contribution of the energy contained in the mapped bits, because increasing N challenges the receiver to choose a correct subcarrier from within a larger set and, therefore, deteriorates the BER performance. However the energy contribution made by the mapped bits balances the

performance. This figure affirms that the only price paid for conveying more mapped bits as N gets larger is bandwidth expansion, not BER performance alteration.

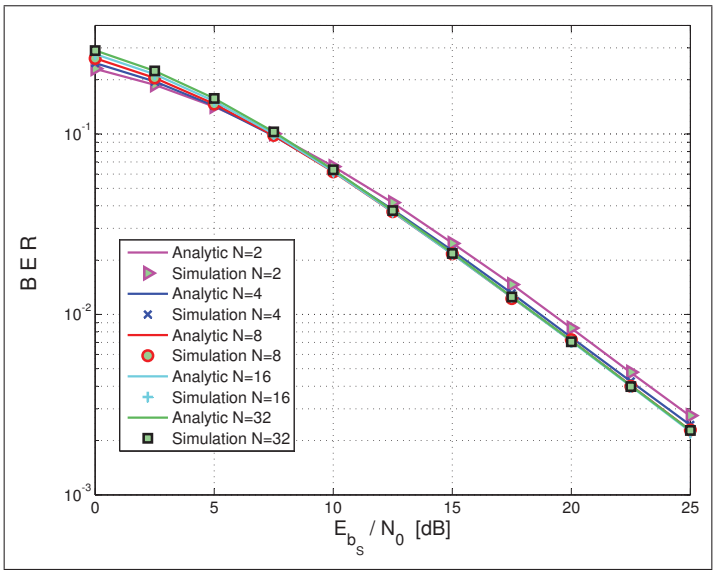

Figure 2.5 Performance of the proposed FIM system for various subcarriers per sub-band and a modulation order of $M = 8$

2.5.2 Performance Comparison with SM and OFDM-IM Systems

To exhibit the supremacy of the frequency index-modulation system despite its simplicity, we compare the performance of our proposed work to the performance of two other index-modulation based schemes, namely the spatial modulation (SM) and the orthogonal frequency division multiplexing with index modulation (OFDM-IM) techniques. These two works are very well explained in Mesleh *et al.* (2006a, 2008); Jeganathan *et al.* (2008b); Di Renzo *et al.* (2014) and Başar *et al.* (2013). For simplicity, we consider a comparison with SM and OFDM-IM for the case of dispatching 3 bits per transmission. In this case, the modulation order of SM is set to $M = 4$, while the number of transmitting antennae is fixed at $N_t = 2$ transmitting antennae versus a single receiving antenna, i.e. $N_r = 1$. We have chosen this case for SM as it shows a better performance compared to the other way round, e.g $N_t = 4$ and $M = 2$. Furthermore, the OFDM-IM system has 4 subcarriers in each sub-band, where 2 subcarriers are active. All the

three systems considered for comparison here are simulated under similar channel and fading conditions. In order to have a fair comparison in terms of energy with with respect to SM, the energy of SM has been reformulated in a fashion similar to (2.1) such that it incorporates the energy of the mapped bits too, i.e. $E_{b_{SM}} = \frac{log_2(N_t)+log_2(M)}{log_2(M)} \cdot E_{b_{SM0}}$ where $E_{b_{SM0}}$ is the default energy of the SM system. As depicted in Fig. 2.6, the FIM system achieves a noticeable

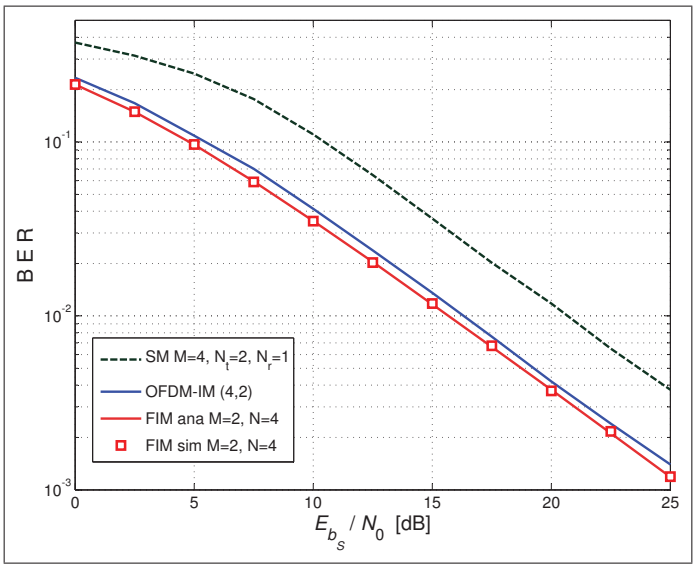

Figure 2.6 Performance of FIM in comparison to SM and OFDM-IM for the transmission of a total of 3 bits (mapped and modulated)

performance despite its simplicity and ease. The performance of the proposed FIM system is in tight competition with OFDM-IM. It is of course possible to enhance the performance of any of these index-modulation schemes by implementing more receiver antennae and increasing reception diversity, however this is absolutely impractical for wireless sensor cases, where size and simplicity are of extreme importance.

Indeed, the admirable advantage of the proposed system lies in its simplicity and suitability for application in WSNs. Unlike SM that requires expensive and bulky hardware with a performance totally antenna- and channel gain- dependent, and unlike OFDM-IM that is too complex for WSNs implementation. Furthermore, both SM and OFDM-IM are ML-detector dependent, the implementation of which becomes impractical for large combinations of M and N. In ad-

dition, neither SM nor OFDM-IM may function without the availability of perfect channel state information at the receiver. In the proposed FIM scheme, however, the performance is achieved without undergoing any expensive hardware expansion or complex algorithmic implementation. Added that the proposed scheme may very well convey p_1 bits per transmission and detect them using the SLED, without having any knowledge of the channel state information at all. This is absolutely not possible, neither with SM nor with OFDM-IM.

2.5.3 Energy Efficiency, PAPR and Complexity Analysis

In this subsection, we show the results concerning energy efficiency, PAPR and complexity analyses in 3 different consecutive and independent clauses for sake of clarity.

2.5.3.1 Energy Efficiency and PAPR Analysis

We compare the CCDF of the PAPR in terms of number of sub-bands N_B. This is because a single subcarrier is activated in every sub-band, and in effect, only N_B subcarriers are active per every FIM transmission. Fig. 2.7 shows the theoretical CCDFs of the proposed FIM system with different sub-bands for $N_{\text{FIM}} = 64$ based on evaluating (2.35). Notice that the case $N_B = 64$, $N = 1$ in Fig. 2.7 corresponds to the PAPR of a conventional OFDM system with 64 subcarriers, where no frequency-indexing takes place. As clearly illustrated in Fig. 2.7, increasing the number of subcarriers per sub-band N leads to lesser N_B which in turn causes the CCDF to diminish. It is observed here that the FIM system transmits fewer p_T bits and relaxes the PAPR for higher N and less N_B. Conversely, more p_T bits are transmitted for higher N_B and less N at the cost of higher PAPR values.

High PAPR can be avoided by reducing the number of subcarriers actually engaged in transmission, and in effect, the PAPR is reduced in a fashion similar to clustered OFDM Cimini Jr *et al.* (1996); Cimini Jr & Sollenberger (1997). Note that in the clustered OFDM technique mentioned in Cimini Jr *et al.* (1996); Cimini Jr & Sollenberger (1997) the subcarriers are clustered into several smaller blocks and transmitted over separate antennae. The PAPR is reduced

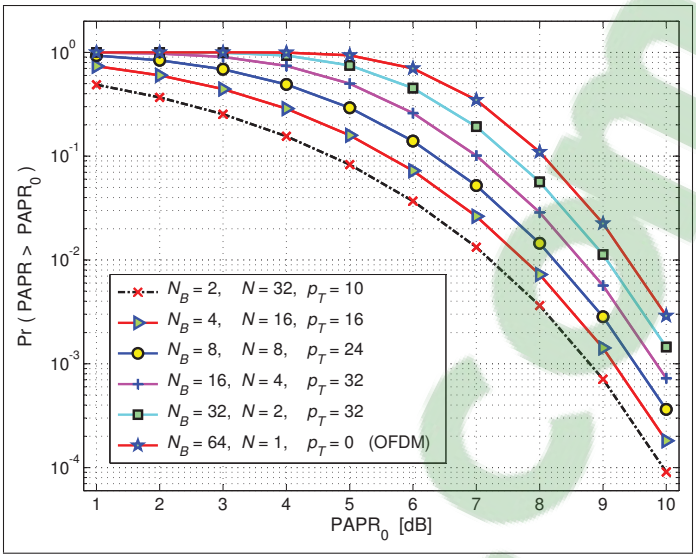

Figure 2.7 CCDFs of the PAPR of the proposed FIM system with complementing N_B and N combinations for $N_{\text{FIM}} = 64$

since there are fewer subcarriers per transmission. But that technique has not been widely employed since the increase in the number of power amplifiers makes their proposal impractical in many applications. However, in our work, we have a single antenna and the implementation of several antennae has been substituted by using a frequency-indexing method. Brief, we reduce PAPR by clustering using various frequency bands instead, to replace the deployment of several antennae.

Regarding the energy efficiency, the proposed FIM system the energy saving is significant as the number of mapped bits increases (see (2.31)). Compared to FH or OFDM systems, the FIM system is competitive in terms of energy efficiency for a given number of bits per transmission. Instead of using a pseudo-random generator to select a frequency as in FH, FIM activates one subcarrier which is selected by the mapper (the index selector). As a result, if $p_n = p_1 + p_2$ bits need to be transmitted, FH systems will use $E_{\text{FH}} = p_n E_b$ whereas FIM system will dispose $E_{\text{FIM}} = p_2 E_b$, where E_b is the energy to transmit one bit. For example, for $p_n = 2$ bits per transmission, it is possible to use one bit for index mapping and another bit for modulation in the FIM system whereas both bits will be transmitted via the activation of various hoppings in the FH. Under this condition, from (2.31), FIM will save 50% of energy compared

to conventional FH. It can be seen that the percentage of energy saving will be reduced as the modulation order increases, i.e as $p_2 \to \infty$.

2.5.3.2 System Complexity

The computational complexity of these systems is considered for evaluation here. We compare the complexity of FIM to that of conventional OFDM, by fixing the the modulation order. As such, we observe that the complexity of the OFDM pertaining to modulation and demodulation parts is $\sim 3N\log_2(M)$ whereas the complexity of the FIM scheme is $\sim N + 3\log_2(M)$. Clearly, as the number of subcarriers increases, $N > 1$, the FIM is the winner in terms of low-complexity. Furthermore, since the OFDM-IM uses the maximum likelihood detection, its computational complexity is higher than the others. In fact we have $\mathscr{O}_{\text{FIM}} \leq \mathscr{O}_{\text{OFDM}} \leq \mathscr{O}_{\text{OFDM-IM}}$. Fig. 2.8 depicts the computational complexity based on (2.36), (2.37) and (2.38) that represent the complexity of these OFDM-like systems, by fixing the modulation order to a 16-PSK modulation. It is clearly observed that higher number of active subcarriers involved in transmission increases the computational complexity, and that FIM has the lowest complexity compared to others.

However, the number of bits per transmission will not be the same in these systems. Indeed, if one single subcarrier is activated per transmission, then the number of bits per transmission will be $p_{n_{\text{FIM}}} = \log_2(M) + \log_2(N)$ whereas $p_{n_{\text{ODFM}}} = N\log_2(M)$ in the conventional OFDM system because every subcarrier is activated. For the OFDM-IM, the number of bits per transmission is $p_{n_{\text{OFDM-IM}}} = k\log_2(M) + \log_2(N)$. Clearly, the FIM scheme has the lowest number of bits per transmission. Table 2.2 depicts the performance of these systems for the conveyance of 3 bits per transmission. In this case, the complexity of the FIM is comparable to the OFDM but we have 66.6% of energy saving. The OFDM-IM saves only 33.3% of the energy and have the highest complexity due to the maximum likelihood decoder. In this condition, the proposed FIM system is competitive to the current state of the art in terms of energy saving and complexity. This renders the proposed system exceptionally adaptable to WSN applications.

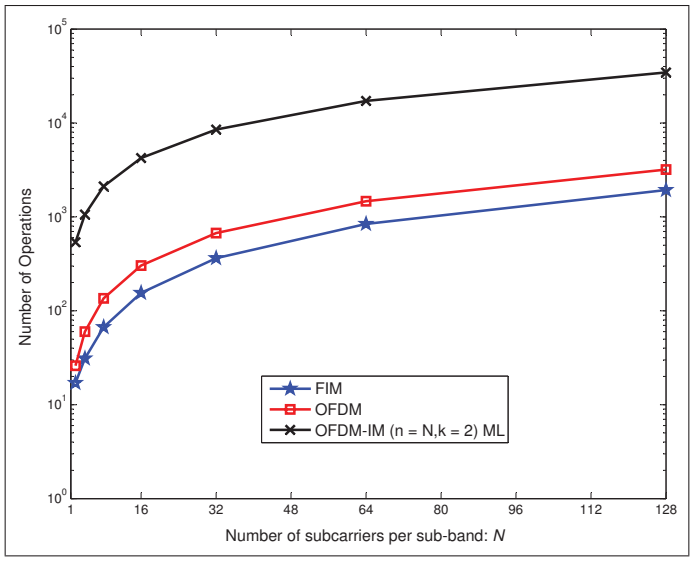

Figure 2.8 Complexity comparison of the proposed FIM, conventional OFDM and OFDM-IM(n,k) systems using a number of subband $N_B = 1$ and FFT-length $N_{\text{FIM}} = NN_B$

Table 2.2 Comparison, OFDM, OFDM-IM and FIM systems for the conveyance of 3 bits per transmission

	OFDM	OFDM-IM(4,2)	FIM $M = 2, N = 4$
Complexity	22	28	22
Energy saving	0%	33.3%	66.6%

2.6 Conclusions

In this paper, we have proposed a frequency-index modulation (FIM) scheme that suits the physical layer of IoT applications. The proposed system uses OFDM waveforms for its ease of implementation and flexibility. Unlike SM and OFDM-IM which are either hardware-demanding or too complex to be implemented based on the *index modulation* technique, the suggested system conveys addition information bits by virtue of the active frequency indices in every sub-band. At the modulator side, the bit stream is divided into two blocks: mapped and modulated. The bits within the mapped block are used to activate the corresponding subcarrier to carry the data of the modulated block, while other subcarriers are nulled out. To recover the transmitted and mapped data, an FFT is performed first, and then the square-law envelope detector is applied to estimate the active frequency index to recover the mapped bits, followed

by a conventional demodulation to demodulate the transmitted bits. Furthermore, energy efficiency and complexity analyses have been carried out and it has been shown that PAPR is decreased in such a structure, which demonstrates the appropriateness of our system for WSN applications, where power and complexity must be kept at low profiles. Moreover, the closed-form expressions of the BER performance over Rayleigh fading channels are derived. The proposed modulation scheme meets the needs of 5G wireless systems to a great extent, reduces PAPR, minimizes the consumed power, operates using a low latency and power profile and shows a promising overall performance.

CHAPTER 3

DESIGN OF AN INITIAL-CONDITION INDEX CHAOS SHIFT KEYING MODULATION

Ebrahim Soujeri[1], Georges Kaddoum[1] and Marijan Herceg[2]

[1] Department of Electrical Engineering, École de Technologie Supérieure,
1100 Notre-Dame West, Montreal, Quebec, Canada H3C 1K3
[2] Department of Communications, Faculty of Electrical Engineering, Computer Science and Information Technology Osijek, Croatia

Paper published in *Electronics Letters*, February 2018.

Abstract

An initial condition index chaos shift keying modulation is proposed. This design aims to increase the spectral and energy efficiencies to unprecedented levels. The proposed scheme exploits the initial conditions to generate different chaotic sequences to convey extra bits per transmission. In the proposed design, the input data stream is formed in blocks of $p_{\text{tot}} = n + 1$ bits. In this architecture, n bits are mapped into $N = 2^n$ predetermined initial conditions that are used to generate unique chaotic sequences at the transmitter. At the receiver side, the predetermined initial conditions are used to generate a set of N chaotic sequences that are correlated with the received signal. The index of the initial condition for which the chaotic sequence produces a maximum correlation with the received signal is selected to recover the mapped bits, and the corresponding sequence is used to despread the transmitted *modulated* bit. To validate the proposed scheme, the bit error rate over fading channels is analyzed and formulated and the proposed system performance is compared with other conventional and index modulation schemes. In comparison to rival modulation schemes, the results obtained in the proposed work show a promising data rate boost and a competitive performance.

3.1 Introduction

During the last decade, a tremendous increase in the number of wireless devices has brought new challenges for the wireless network industry. In particular, low energy consumption and high spectral efficiency are among the most important and essential requirements for the increasing number of wireless devices in wireless sensor networks (WSN), wireless body area networks (WBAN) and internet of things (IoT) systems. Therefore, new technologies in wireless systems design have recently been investigated and developed to meet the needs of increasing network demands. To be specific, WSNs and microsensors require the spread spectrum technology which is adopted by the IEEE 802.15.4 standard that comes under the broader umbrella of the license-free industrial scientific and medical (ISM) bands. Concurrently, index modulation has been proposed to increase data rate by carrying extra bits, at no or minimum additional cost. In this vein, an alternative low energy consumption version of MIMO scheme called spatial modulation (SM) in which the index of the active antenna along with constellation symbols are used for bits mapping is proposed in Mesleh *et al.* (2008). By exploiting the spreading code domain, the code index modulation (CIM) for spread spectrum systems is recently proposed Kaddoum *et al.* (2016b). In the CIM scheme, the indices of spreading codes are used in conjunction with symbol constellation for bits mapping. On the other hand, non-coherent and coherent chaotic modulations have been proposed in the last two decades due to their low complexity, low power consumption, robustness on multipath fading or increased transmission security for coherent modulation schemes Kaddoum (2016b).

Recently, index modulation has been applied to non-coherent chaos-based modulation schemes Xu *et al.* (2017); Cheng *et al.* (2017); Herceg *et al.* (2017). In Xu *et al.* (2017), a code-shifted differential chaos shift keying (CS-DCSK) system exploiting Walsh codes indices to map extra bits is proposed while in Cheng *et al.* (2017) the authors combine index modulation with multicarrier DCSK. In addition, a system named permutation index DCSK (PI-DCSK) modulation that supports multi-user access and secure transmission is proposed in Herceg *et al.* (2017). Nonetheless, to the best of authors' knowledge, index modulation with coherent chaos-based modulation scheme has not been studied before.

In this letter, we apply for the first time the index modulation to a coherent secure chaos-based scheme named chaos shift keying (CSK). This new scheme named initial condition index chaos shift keying (ICI-CSK) aims to enhance the spectral and energy efficiencies. In this vein, the proposed ICI-CSK scheme exploits the chaotic maps sensitivity on initial conditions to generate a large number of uncorrelated chaotic signals from the same chaotic map. In particular, at the transmitter, data stream is formed in blocks of $p_{\text{tot}} = n + 1$ bits where the first n bits selects an initial condition index from a set of N available initial conditions used to generate a chaotic sequence of length β, while the remaining single bit is spread by the selected chaotic sequence. At the receiver side, the received signal is correlated with a set of N chaotic signals that are generated using each of the initial conditions described at the transmitter. First, the output of each correlator is squared to compute the received energy in order to allow the identification of the correct initial condition used at the transmitter, by examining the maximum squared correlation value. The index of chaotic sequence that produces the maximum correlation with the received signal is selected to recover the n mapped bits and then sign of the correlator output is utilized to recover the modulated bit. Note that increasing the number of mapped bits per transmission to very large values would necessitate the use of more correlators at the receiver which could lead to more reception complexity. Furthermore, the limit of allowed mapped bits is disclosed in Kaddoum *et al.* (2016b) and has been respected in the proposed ICI-CSK scheme to keep this system low complex. On the other hand, it was demonstrated in Kaddoum (2016b) that the application of code synchronization techniques based on acquisition and tracking algorithms to CSK schemes yield robust and reliable performance. Hence, these techniques can be used in ICI-CSK to tackle the synchronization problem. In addition, large spreading factors are considered to avoid the bit energy variation in the ICI-CSK system Kaddoum (2016b). In the sequel, analytical bite error rate (BER) expressions over flat Rayleigh fading channel is formulated and validated via Monte Carlo simulations. Finally, the performance of ICI-CSK is analyzed and compared to conventional schemes like spread spectrum M-PSK, and index-based schemes like SM.

3.2 ICI-CSK system model

A block diagram of the proposed ICI-DCSK system is illustrated in Fig. 3.1. As shown, the information bits of the outgoing data frame at the transmitter are arranged in blocks of $p_{\text{tot}} = n+1$ bits per transmission. For an i^{th} block $\mathbf{B}_i = [\mathbf{s}_i, b_i] \in \{1,-1\}^{1\times p_{\text{tot}}}$, $\mathbf{s}_i$ represents n mapped bits and b_i is the transmitted bit with CSK modulation. In addition, a corresponding initial condition vector of N predefined initial conditions given in the vector $\mathbf{x}_0 = [x_{1,0}, \cdots, x_{N,0}]^T$, shared with the receiver, is used to generate the chaotic sequence to map the n bits of $\mathbf{s}_i$. In this vein, a selected initial condition $x_{j,0}$ from the codebook, $\mathbf{x}_0$, corresponding to a given set of mapped bits $\mathbf{s}_i$ is used to generate the chaotic sequence in order to spread the bit b_i. As such, the transmitted baseband signal $\mathbf{e}_i$ takes the following form

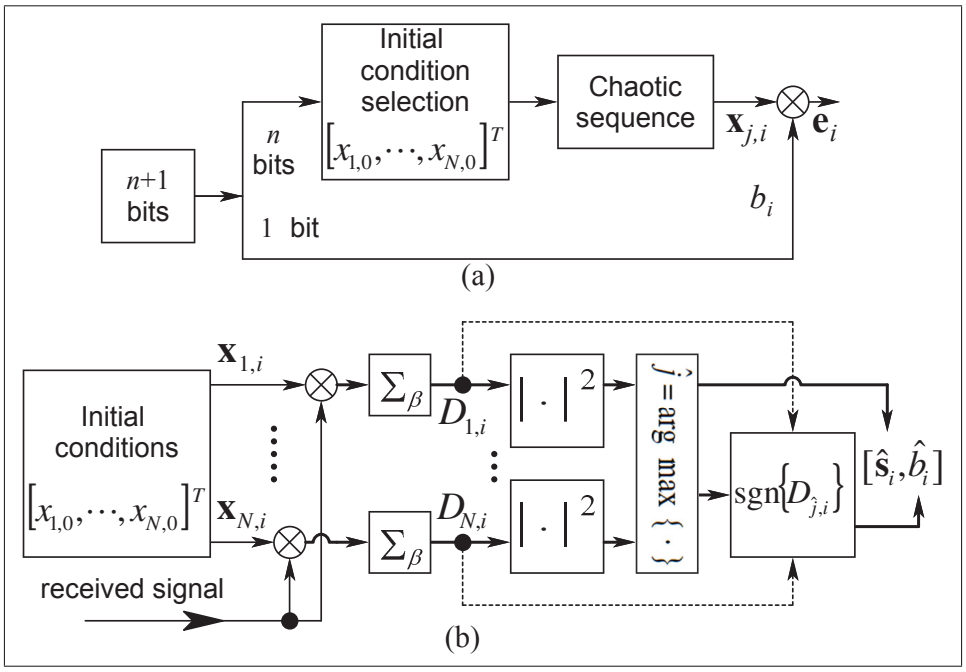

Figure 3.1 A general scheme of the proposed ICI-CSK architecture: (a) transmitter and (b) receiver

$$\mathbf{e}_i = \sqrt{E_b}\, b_i \cdot \mathbf{x}_{j,i}, \tag{3.1}$$

where $\mathbf{x}_{j,i} = [x_{j,1,i}, \cdots, x_{j,\beta,i}]$ is the chaotic sequence of β chips generated using the j^{th} initial condition, and E_b is the transmitted bit energy. Since the spreading length of the chaotic sequence is β, the length of the ICI-CSK bit is $T_b = \beta T_c$, where T_c is the duration of one chip and is set to unity in this letter. Moreover, the second-order Chebyshev polynomial function $x_{j,\kappa+1} = 1 - 2x_{j,\kappa}^2$ is used to generate chaotic sequences due to simplicity and reasonable performance Kaddoum (2016b). The baseband received signal over quasi-static flat fading Rayleigh channel is expressed as

$$\mathbf{r}_i = \lambda_i \mathbf{e}_i + \mathbf{n}_i, \tag{3.2}$$

where λ_i is the quasi static fading channel coefficient over the i^{th} ICI-CSK symbol duration, and $\mathbf{n}_i$ is a β-samples additive white Gaussian noise (AWGN) with zero mean and variance $N_0/2$. At the receiver, the received signal is correlated with N replicas of chaotic signals generated with the same initial conditions from the set $\mathbf{x}_0$ used at the transmitter. Subsequently, N correlator output variables are formed

$$D_{m,i} = < \lambda_i \sqrt{E_b}\, b_i\, \mathbf{x}_{j,i} + \mathbf{n}_i, \lambda_i \mathbf{x}_{m,i} > \quad \text{for } m = 1, \cdots, N \tag{3.3}$$

where $< \cdot, \cdot >$ stands for the inner product operator. To determine the corresponding initial condition index, the square magnitudes of the N correlators are compared in order to find the largest value

$$\hat{j} = \arg\max_{m} \left\{ |D_{m,i}|^2 \right\}, m \in \{1, 2, \cdots, N\}. \tag{3.4}$$

By estimating the index $\hat{j}$ of the correlator with the largest energy output, the receiver knows which initial condition is used for chaotic sequence generation at the transmitter side and hence, the implicitly transmitted n number of mapped bits can be estimated. Furthermore, the modulated bit can be recovered by computing the *sign* of the correlator with maximum output as $\hat{b}_i = \text{sgn}(D_{\hat{j},i})$.

3.3 Probability of Error for Mapped Bits

In this part we will analyze the erroneous detection of the desired chaotic sequence. In fact, provided that the j^{th} initial condition $x_{j,0}$ has been used for the generation of the chaotic sequence used in transmission, an error occurs in detecting the mapped bits if the largest square absolute value of the m^{th} correlator output is larger than the square absolute value of the j^{th} desired correlator output for any $m \neq j$. Therefore, the probability that an erroneous correlator output will be selected P_{ed} would fit the description

$$\begin{aligned} P_{\text{ed}} = P\left(\left|D_{j,i}\right|^2 < \max\left(\left|D_{m,i}\right|^2\right) \mid x_{j,0}\right), \\ \text{for} \quad 1 \leq \underset{m\neq j}{m} \leq N. \end{aligned} \tag{3.5}$$

Since all correlator output variables are statistically mutually independent Kaddoum *et al.* (2016b), the erroneous detection probability over fading channel is similar to $M-$ary orthogonal signalling Proakis (1995) and the work of Soujeri *et al.* (2017). Therefore, the final form of (3.5) and considering $\bar{\gamma}_s = \mathbb{E}(\left|\lambda^2\right|)E_b/N_0$ where $\mathbb{E}(\cdot)$ is the expectation operator, will be expressed as

$$P_{\text{ed}} = \sum_{k=1}^{N-1} \frac{(-1)^{1+k}}{1+k+k\bar{\gamma}_s} \binom{N-1}{k}. \tag{3.6}$$

Since n bits are mapped into a given sequence, the mapped bit error rate probability is given by Proakis (1995)

$$P_{\text{map}} = \frac{2^{(n-1)}}{2^n - 1} \cdot P_{\text{ed}}. \tag{3.7}$$

3.4 BER Performance Analysis of the ICI-CSK System

In this section, we examine the performance of the ICI-CSK scheme. First, the probability of error of transmitted modulated bit, b, for the ICI-CSK system depends on the detection probability of the initial condition given in (3.6). That is to say, if the initial condition is

correctly identified, then the error will be that associated with bit error rate demodulation of CSK scheme P_{csk}, if not, the output is guessed with 50% chance of estimation error. Then, the probability of error of the transmitted modulated bit, P_{mod} is expressed as

$$P_{\text{mod}} = (1 - P_{\text{ed}}) \cdot P_{\text{csk}} + 0.5 \cdot P_{\text{ed}} \tag{3.8}$$

where P_{csk} is the bit erorr rate probability of the coherent chaotic shift keying system that does not involve any indexing Kaddoum (2016b)

$$P_{\text{csk}} = \frac{1}{2}\left(1 - \sqrt{\frac{\bar{\gamma}_s}{1+\bar{\gamma}_s}}\right). \tag{3.9}$$

Once the probability of error of modulated bits P_{mod} and mapped bits P_{map} are determined as in equations (3.8) and (3.7) respectively, the overall bit error rate probability of the proposed ICI-PSK system, $P_{\text{ICI-CSK}}$, can be formulated as

$$P_{\text{ICI-CSK}} = \frac{n}{p_{\text{tot}}} P_{\text{map}} + \frac{1}{p_{\text{tot}}} P_{\text{mod}}. \tag{3.10}$$

Furthermore, since part of the transmitted bits are conveyed by the initial condition index, and to have a fair comparison with other conventional systems, we define an equivalent system bit energy E_{b_s} which represents the effective energy consumed per transmitted bit and is related to the physically modulated bit energy by the relationship $E_{b_s} = p_{\text{tot}} \cdot E_b$.

3.5 Simulation and Evaluation

The overall bit error probability of error of the proposed ICI-CSK system is evaluated according to (3.10). Fig. 3.2 shows the BER performance of the proposed system for the transmission of $p_{\text{tot}} = 4$ and $p_{\text{tot}} = 6$ bits for $\beta = 128$ over a flat fading channel, where a perfect match between analytical and simulation results is revealed. As witnessed in Fig. 3.2, a marginal BER performance improvement is observed as N increases from 8 to 32 in the ICI-CSK system. This returns to the fact that increasing n contributes to transmit more bits with a similar bit energy

E_b. Note that without the contribution of the energy contained in the mapped bits, the BER performance would deteriorate as the receiver is challenged to pick up an initial condition from a larger set. This evidence affirms that while the BER performance is minimally improved, the only price paid for conveying more mapped bits is added complexity. Moreover, for fair comparison, the performance of our proposed scheme is compared to SM and conventional M-PSK schemes transmitting the same number of bits p_{tot} as ICI-CSK and over flat fading channel. In this vein, SM scheme using BPSK modulation for $N_t = 8$ and $N_t = 32$ transmitted antennas respectively, and PSK 16-ary and 64-ary are used. It is clearly shown that the proposed system outperforms M-PSK and SM while maintaining a much simpler hardware architecture compared to SM. This is because SM relies on channel state information to detect the active antenna which leads to a higher probability of error compared to ICI-CSK. Finally, in the case of M-PSK, the Euclidean distance between symbols is decreased as M increases while in the ICI-CSK structure, augmenting p_{tot} only increases the number of mapped bits as the Euclidean distance is preserved at maximum and maintained constant since BPSK modulation is used in the proposed ICI-CSK scheme.

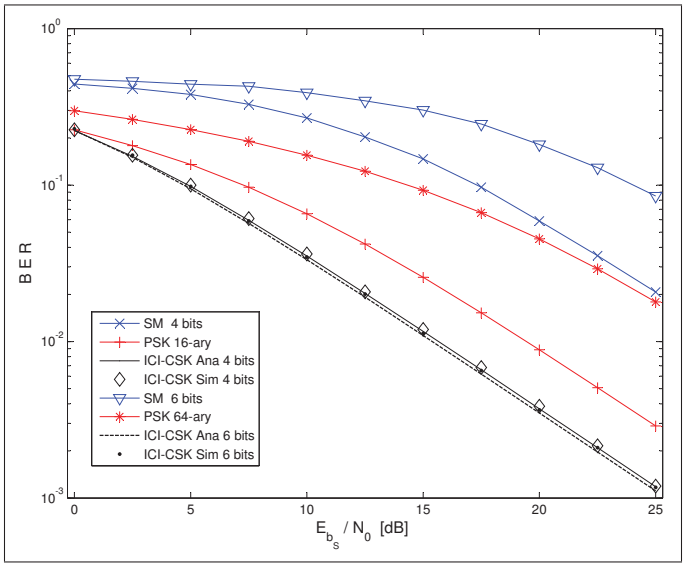

Figure 3.2 BER performance of ICI-CSK compared to SM and M-ary PSK for the transmission of $p_{\text{tot}} = 4, 6$ bits. CSK sequence length $\beta = 128$

3.6 Conclusions

A new, simple, energy and spectral efficient coherent chaos-based communication system named ICI-CSK is presented in this letter, where the initial condition of the chaotic sequence is used as a new dimension to map information and carry extra bits. The proposed system achieves high throughput and energy efficiency considering that a single information bit out of p_{tot} bits per transmission is physically transmitted. Judging by the results obtained, this system will have a remarkable place in futuristic 5G sensor nodes and IoT applications where size, simplicity and efficiency say the final word.

CONCLUSION AND RECOMMENDATIONS

Concluding Remarks

The futuristic 5G wireless communications is very ambitious in terms of high bandwidth and large energy saving requirements. This fact has driven innovative research to be undertaken in this direction. As index modulation is becoming one of the pioneer techniques to be used in order to enhance the spectral and energy efficiencies of 5G communication systems, we have considered this technique in this Ph.D study.

The work of Mesleh *et al.* (2008) is in fact the first in this contention that has received considerable attention from researchers in the field. However, SM modulation faces serious challenges in terms of capacity achievement, effective data rate and overall efficiency. This is because SM is too channel-dependent and its implementation relies on imperfect RF switches that practically slow down transmission speed.

Providing other indexing techniques, therefore, is deemed necessary to assure the expectations from the next generation of wireless systems are met.

In this context, in the the research study carried out in this Ph.D work, we have shed light on the weaknesses of SM and we have proposed alternative index modulation schemes.

The results we have obtained in our research with respect to SM drawbacks indicate that given the speed limitation of practical RF switches in performing transitions, antenna transition-based technologies like SM schemes are capped in terms of data rate performance. In fact, the effective data rate of SM will remain hostage to developments in industrial RF switches. This brings restrictions to the implementation and operation issues when extremely high data rates become a necessity. Since the technology marches towards emerging systems where bandwidth efficiency and data rate are both essential requirements, it is necessary to develop

new SM techniques based on minimum transition of antennas, or on the transition of a group of antennas at a time rather than schemes that require a transition at every transmission instant. It is shown by the assemblage of our results that the switching time T_{sw} which is a requirement for transitions between antennas to happen, dictates restrictions on data rate, capacity and spectral efficiency of SM systems.

The BER performance of SM detectors deteriorate with channel imperfections especially in low SNR regions. The performance of the SM is very fragile and sensitive to either correlated or imperfect channel coefficients. Channel impairments cause the SM system capacity to drop as a reasonable and logical aftermath of the rise in the probability of error, noting that CSI is a phenomenon that can not always be assumed to be perfect because of the serious impacts it has on the BER performance and on the capacity of the SM system.

Furthermore, the deployment of SM to WSN and IoT applications are almost impossible as these applications are either composed of or involve tiny modules and sensors that may not handle multiple antennas on board.

The results we have obtained with respect to suggesting alternative index modulation schemes assert the following:

The proposed frequency-index modulation (FIM) scheme uses OFDM waveforms for its ease of implementation and flexibility. This technique which suits the physical layer of IoT applications is presented in Chapter 2. Unlike SM and OFDM-IM which are either hardware-demanding or too complex to be implemented based on the *index modulation* technique, the suggested system conveys additional information bits by the virtue of the active frequency indices in every sub-band. Furthermore, energy efficiency and complexity analyses have been carried out and it has been shown that PAPR is decreased in such a structure, which demonstrates the appropriateness of our system for WSN and IoT applications, where power and

complexity must be kept at low profiles. The proposed modulation scheme meets the needs of 5G wireless systems to a great extent, reduces PAPR, minimizes the consumed power, operates using a low latency and power profile and shows a promising overall performance.

Realizing the attractive features of chaotic codes in terms of security and SS gains, the next indexing method that we eye in this study is initial condition-index CSK. In the ICI-CSK article which is presented in Chapter 3, we propose a new, simple, energy and spectral efficient coherent chaos-based communication system, where the initial condition of the chaotic sequence is used as a new dimension to map information and ferry extra bits. The proposed system achieves high throughput and energy efficiency considering that a single information bit out of p_{tot} bits is physically transmitted. Judging by the results obtained, this system will have a remarkable place in futuristic 5G sensor nodes and IoT applications where size, simplicity and efficiency are of vital importance.

In the same vein, we consider differential CSK and index modulation related to this evolving technique. In the PI-DCSK article that is placed in Appendix II, we suggest a new multi-user multi-level non-coherent PI-DCSK scheme for chaos-based communication systems. In the proposed design, time-multiplexing is used to separate reference and data bearing sequences, as in conventional DCSK. In PI-DCSK, multiple quasi-orthogonal data sequences are formed as a consequence of permuting the reference sequence so the PI-DCSK energy and spectral efficiencies are significantly boosted compared to its competitors.

In addition, the utilisation of different permutations eradicates the similarity between reference sequences and data bearing sequences, which in turn significantly increases the PI-DCSK transmitted data security. Moreover, an efficient multiple access method is proposed for adoption in the PI-DCSK system, by granting absolute access to a distinct set of $M/2$ permutations out of $\beta! - 1$ possible, for each user.

In light of the obtained results, the proposed novel PI-DCSK system is expected to be quite competitive and promising in the field of index modulation.

In conclusion, we have explored other indexing schemes in which extra bits are transmitted without the involvement of additional heavy and bulky hardware like transmitter antennas, where the indexing mechanism is taken from the hard zone, i.e. antennae and RF switching, to the soft zone where the implementation is possible by FPGA or logical circuits.

Future Work: Hybrid Index Modulation Mechanisms

In large infrastructures like base stations, where space is abundant, the implementation of numerous antennas could make it a possibility to apply a hybrid modulation scheme that considers antenna indexing along with any other soft indexing scheme. For example, CIM and SM could be merged together to constitute a hybrid CIM-SM modulation system. We expect this to increase the data rate and achieve a higher throughput without adding extra computation complexity to the system. This hybrid CIM-SM might constitute an example of a future work. To provide an idea in advance, consider the simple transmission scheme shown in the figure below in which the outgoing stream is divided into $7-$bit parcels, where 3 bits decide on a code index to choose a code from a rack that contains 8 spreading codes, 2 bits choose an antenna in a system that has $N_t = 4$ transmitter antennas and 2 bits designate a symbol from a signal constellation map. In fact, this structure is expected to be very efficient, because while the data rate is increased from 2 bpcu to $2+2+3 = 7$ bpcu, the consumed energy is dropped from $\sqrt{7E_b}$ to only $\sqrt{2E_b}$, i.e. 5 bits are transmitted free of charge.

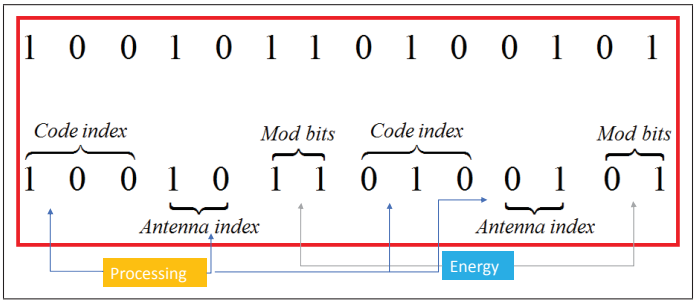

The hybrid CIM-SM system is a multiantenna high bandwidth system, proposed as an example of a possible future work

APPENDIX I

PERFORMANCE COMPARISON OF SPATIAL MODULATION DETECTORS UNDER CHANNEL IMPAIRMENTS

Ebrahim Soujeri[1] and Georges Kaddoum[1]

[1] Department of Electrical Engineering, École de Technologie Supérieure,
1100 Notre-Dame West, Montreal, Quebec, Canada H3C 1K3

Paper published in *IEEE International Conference on Ubiquitous Wireless Broadband (ICUWB)*, October 2015.

Abstract

Spatial modulation (SM) is a multiple antenna transmission approach that uses the index of the transmitting antenna for delivering information data. The choice on the transmitting antenna depends on the incoming bit sequence and has a random nature. The receiver estimates the transmitted symbol and the active transmit antenna index and uses both estimations to retrieve the original information bits. For best reception, individual channel links between transmit and receive antenna pairs must be unique. In fact, correct reception totally depends on the uniqueness of channel coefficients. Incorrectly interpreting channel state information at the receiver causes the BER performance to degrade and the detection to fall short. In this paper, we develop a channel model that incorporates both correlated and imperfect channel state information and use this model to study the bit-error-ratio (BER) performance of most widely used SM detectors, namely the minimum mean square error, the maximum likelihood and the optimum detector in flat Rayleigh fading channels to examine the sensitivity these detectors exhibit to the presence of either channel correlation or imperfect channel state information. The capacity of SM system is studied in comparison to other multiple-input multiple-output techniques and the influence of channel impairments on the overall system capacity is observed.

1. Introduction

Spatial Modulation (SM) is a recently developed low-complexity Multiple-Input Multiple-Output (MIMO) scheme where the information bitstream is divided into blocks of length $(n_t + m) = \log_2(N_t M)$ bits, where N_t is the number of transmit antennae and M is the size of the signal set Mesleh *et al.* (2006a, 2008). In SM, only one antenna out of N_t antennae is active during a transmission time. In each block of $(n_t + m)$ bits, $m = \log_2(M)$ bits select a symbol from an M-ary signal set (such as M-QAM or -PSK) and $n_t = \log_2(N_t)$ bits select an antenna out of N_t transmit antennae to accomplish transmission. In this configuration, transmit antenna indices will be $j = 1, 2, 3, ..., N_t$.

The throughput achieved by this scheme is $R = \log_2(N_t M)$ bpcu. Therefore, the SM scheme achieves an increase in the spectral efficiency of $\log_2(M)$ bits over single-antenna systems. In order to achieve higher throughputs, either N_t or M, or both need to be increased which renders this scheme suitable for low and moderately high spectral efficiencies. One of the important benefits of this scheme is that it is free from inter-channel interference (ICI) by virtue of activating a single transmit antenna at a time. In the context of the scope of this paper, the impact of imperfect CSI on a multiple-input multiple-output (MIMO) system with interference has been studied in Lee *et al.* (2012), the performance of a MISO system with maximum likelihood (ML) detection and full CSI at the receiver is considered in Di Renzo & Haas (2010) and the effect of channel estimation errors on the performance of SM with ML detection is examined in Mesleh & Ikki (2012). Since the uniqueness of channel coefficients is a requirement for correct detection in SM system and because the system performance entirely depends on the peculiarity of channel coefficients, inaccurately depicting channel state information at the receiver leads to BER performance degradation.

In this paper, a channel model that incorporates both correlated and imperfect channel state information at the receiver is developed. The developed model is then used to study the bit-error-ratio (BER) performance of three most widely used SM detectors, namely the minimum

mean square error (MMSE), the ML and the optimum detector (OD) in flat Rayleigh fading channels to ponder the extent to which the BER performance deviates from the ideal case with perfect knowledge of channel state information (CSI). The influence of channel impairments on the capacity of the SM system under the developed model is also investigated. The rest of this paper is organized as follows: In Section 2, SM system model is presented. In Section 3, an explanation regarding the SM detectors on which this study focuses is presented. Section 4 studies channel impairments. Capacity of SM is provided in Section 5. Simulation results are presented in Section 6 and discussions and conclusions are given in Section 7.

2. SM System Model

The SM system consists of a MIMO wireless link with N_t transmit and N_r receive antennae, and a random sequence of independent bits $\mathbf{b} = \begin{bmatrix} b_1 & b_2 & \cdots & b_{N_t} \end{bmatrix}$ that enter an SM mapper or interleaver encoder, where groups of $m + n_t$ bits are mapped into a constellation vector $\mathbf{x} = \begin{bmatrix} x_1 & x_2 & \cdots & x_{N_t} \end{bmatrix}^T$ and are transmitted at a time. In SM, only one antenna is active during transmission and only one single entry is non-zero in $\mathbf{x}$, i.e. the entry (or index) of the chosen antenna will be nonzero. Fig. I-1 gives a pictorial representation of this scheme. Note that the mapping table in Fig. I-1 is for the binary transmission case and is put there for illustration simplicity.

2.1 The Wireless Channel

The SM signal is transmitted over an $N_r \times N_t$ wireless channel $\mathbf{H}$ and experiences an N_r-dim additive white Gaussian noise (AWGN) $\mathbf{n} = \begin{bmatrix} n_1 & n_2 & \cdots & n_{N_r} \end{bmatrix}^T$. The channel matrix $\mathbf{H} \in \mathbb{C}^{N_r \times N_t}$ has entries given by

$$\mathbf{H} = \begin{bmatrix} h_{11} & h_{12} & \cdots & h_{1N_t} \\ h_{21} & h_{22} & \cdots & h_{2N_t} \\ \vdots & \vdots & \ddots & \vdots \\ h_{N_r1} & h_{N_r2} & \cdots & h_{N_rN_t} \end{bmatrix} \quad \text{(A I-1)}$$

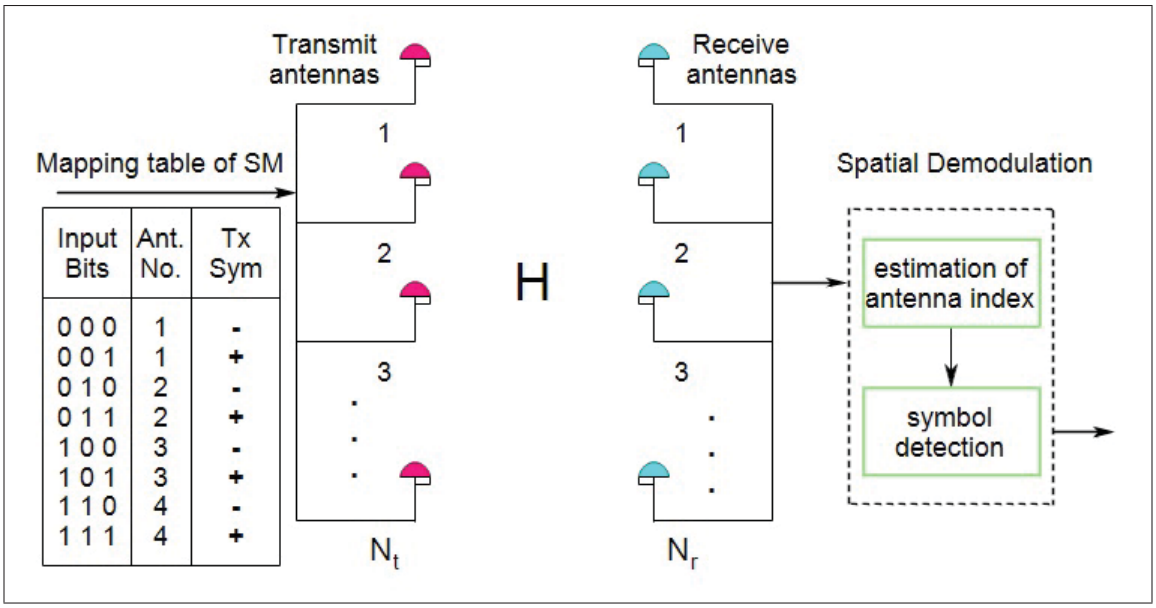

Figure-A I-1 The spatial modulation system

where h_{ji} is a complex fading coefficient that connects the i^{th} transmit antenna to the j^{th} receive antenna and is modelled as independent and identically distributed (iid) zero-mean complex Gaussian (ZMCG) random variables with unit variance. Knowing that SM uses symbol indices as well as antenna indices as means to send information, the symbol index combined with the antenna index make up the SM mapper which outputs a constellation vector that has the following form

$$\mathbf{x}_{jq} = \begin{bmatrix} 0 & 0 & \cdots & \underset{\substack{\uparrow \\ j^{th}\,position}}{x_q} & \cdots & 0 & 0 \end{bmatrix}^T \tag{A I-2}$$

where x_q is the q^{th} symbol from the M-ary constellation $\mathscr{X}$ and j is the index of the activated antenna. Therefore, only the j^{th} antenna remains active transmitting the q^{th} symbol. The output of the SM channel when the q^{th} symbol is transmitted on the j^{th} antenna is expressed as

$$\mathbf{y} = \sqrt{E_s}\,\mathbf{h}_j x_q + \mathbf{n} \tag{A I-3}$$

where E_s is the symbol energy defined as $E_s \triangleq mE_b$, $\mathbf{h}_j$ denotes the activation of the j^{th} column of $\mathbf{H}$ for a randomly chosen j during each transmission period, $\mathbf{y} \in \mathbb{C}^{N_r \times 1}$ is the received

samples vector and $\mathbf{n} \in \mathbb{C}^{N_r \times 1}$ is the additive noise vector, where each element is assumed to be iid ZMCG random variable with variance σ_n^2. From this point onwards and for the sake of simplicity, we assume that the symbol energy $\sqrt{E_s}$ is embedded in the transmitted symbol x_q such that the expression $\sqrt{E_s}\, x_q$ reduces to x_q.

3. SM Detector Types

As indicated earlier, we consider the performance of the most widely used three types of SM detectors, namely the MMSE, the ML and the OD receivers. In MMSE, the antenna index is estimated first, then the transmitted symbol is detected Mesleh *et al.* (2006a). In both ML and OD, a joint detection of antenna index and transmitted symbol is carried out. The size of the search space in MMSE is $N_t + M$ while it is $N_t M$ in ML and OD.

3.1 Minimum Mean Square Error Detection

The MMSE detector carries out detection at two consecutive stages; first, the antenna index is estimated, then the transmitted symbol is detected Mesleh *et al.* (2006a). The transmitted signal is received by N_r receive antennae. After demodulation at the k^{th} antenna, the complex conjugate of the k^{th} row of $\mathbf{H}$ is multiplied by $\mathbf{y}$ resulting in

$$g_k = \mathbf{h}_k^H \mathbf{y} \tag{A I-4}$$

for $k = 1, 2, \cdots, N_t$. Placing the outcome for all transmit antennae coefficients in a complex vector such that

$$\mathbf{g} = \begin{bmatrix} g_1 & g_2 & \cdots & g_{N_t} \end{bmatrix} \tag{A I-5}$$

The transmit antenna number $\hat{j}$ is the index (position) of the element in $\mathbf{g}$ whose absolute value is maximum Mesleh *et al.* (2006a)

$$\hat{j} = \arg\max_j |\mathbf{g}| \tag{A I-6}$$

The antenna index (number) estimate is the position of the maximum absolute value of all elements in the vector $\mathbf{g}$. As can be noticed in the SM transmission, $\mathbf{H}$ reduces to $\mathbf{h}_j$ by virtue

of having only one active antenna at a time, i.e. the j^{th} antenna. The search argued in Eq. (A I-6) corresponds to finding the element of greatest magnitude in the spatial domain among a set of N_t elements. Assuming that the estimate of the transmit antenna number is correct, the transmitted symbol at this instant can be estimated by finding the distance between g_j and each signal constellation point. That is to say, the constellation point that has minimum distance to g_j is considered to be the winner.

$$\hat{q} = \arg\min_{q} |g_j - x_q| \tag{A I-7}$$

3.2 Maximum Likelihood Detection

The ML detection which is based on maximum likelihood sequence estimation (MLSE) is a detection scheme that calculates the minimum Euclidean distance between the received signal and all possibly transmitted sequences. An example of such a detection scheme and the search for the closest lattice point for MIMO is performed in Damen *et al.* (2003) and for SM-MIMO is carried out in Legnain *et al.* (2013). ML estimates the combination of antenna index and transmit symbol at one shot, given by the expression

$$\left[\hat{j}, \hat{q}\right] = \arg\min_{j,q} \|\mathbf{y} - \mathbf{h}_j x_q\|^2 \tag{A I-8}$$

where $||\cdot||_{\text{F}}$ denotes the Frobenius norm which is defined as the sum of the absolute squares of its argument Golub & Van Loan (2012). The ML detector jointly estimates the antenna index and the transmitted symbols by searching over all possible values of the constellation vector space $\mathscr{X}$ and channel matrix $\mathbf{H}$. It must be noted, however, that the complexity of this detector increases exponentially with the modulation order M and number of transmit antennae N_t as a natural consequence for the expansion of the search space given by $N_t M$.

3.3 Optimal Detection

Like the ML detector, the optimum detector (OD) also performs a joint detection of antenna indices and transmitted symbols, however, it follows slightly a different rule than the ML detector and is given by

$$[\hat{j},\hat{q}] = \arg\min_{j,q} \left(||\mathbf{h}_j||_{\mathrm{F}}^2 \, |x_q|^2 - 2\mathrm{Re}\{\mathbf{y}^H \mathbf{h}_j \, x_q\} \right) \tag{A I-9}$$

where the optimal detection is based on the maximum likelihood detection parameters excluding the term $\mathbf{y}^H\mathbf{y}$.

4. Channel Impairments

The channel impairments we attempt to study in this work are classified in two categories. First we study the effect of channel estimation errors (imperfections) on the performance of SM detectors, then we investigate the influence of channel correlation. The former is the case in which the estimated channel coefficients are contaminated with noise. The latter is the case where channel coefficients are correlated.

4.1 Erroneous Channel

Channel estimation is the most crucial and important part of SM detection process. We assume the presence of either error-free (perfect) or erroneous (imperfect) channel estimations. Since avoiding CSI errors is difficult in practical systems, we assume the existence of both amplitude and phase errors in the estimated CSI. We define erroneous CSI such that the following relationship between the estimated and the correct channel coefficients at the k^{th} receiver holds

$$\hat{\mathbf{h}}_k = \rho \; \mathbf{h}_k + (1-\rho) \; \boldsymbol{\varepsilon}^{1\times N_t} \tag{A I-10}$$

where ε is a normal distributed random variable with zero mean and unit variance. The coefficient $0<\rho<1$ is a correspondence factor that determines the resemblance of the estimated CSI to the actual one. Perfect CSI estimation is achieved when $\rho = 1$, i.e. when $1-\rho = 0$.

4.2 Correlated Channel

In the context of our work, we define channel correlation to be the interference of the entries of the channel matrix with each other such that the correlated channel becomes

$$\widehat{\mathbf{H}} = \mathbf{H}\Delta, \tag{A I-11}$$

where

$$\Delta \in \mathbb{R}^{N_t \times N_t}$$

is a Toepltiz matrix with the value $1-\delta$ in the diagonal elements and the value δ in the super-diagonal and sub-diagonal elements. The Δ matrix takes the form given below for $N_t = 4$

$$\Delta = \begin{bmatrix} (1-\delta) & \delta & 0 & 0 \\ \delta & (1-\delta) & \delta & 0 \\ 0 & \delta & (1-\delta) & \delta \\ 0 & 0 & \delta & (1-\delta) \end{bmatrix} \tag{A I-12}$$

where $0 < \delta \ll 1$. Channel coefficients are said to be perfectly uncorrelated when $\delta = 0$, i.e. when $1-\delta = 1$.

4.3 Erroneous and Correlated Channel

We consider the generalized case where the channel coefficients are first correlated with each other, then undergo certain amount of contamination with noise. We have used the following model to incorporate both correlation and contamination with noise

$$\widetilde{\mathbf{H}} = \rho\,\mathbf{H}\Delta + (1-\rho)\,\varepsilon^{N_r \times N_t}. \tag{A I-13}$$

It is clear that the overall channel model $\widetilde{\mathbf{H}}$ depicted in Eq. (A I-13) is governed by the two parameters δ and ρ each with the properties described aforetime and is the the result of having $\mathbf{H}$ be first correlated by Δ in the fashion expressed in Eq. (A I-12) and then contaminated by noise in a similar manner to Eq. (A I-10).

5. Capacity of SM

The capacity of MIMO, single-input multiple-output (SIMO) and multiple-input single-output (MISO) systems are well discussed in Chapter 8 of David & Pramod (2005) where the capacities of these systems are compared and graphically presented for $n = 1, 2, \cdots, 16$ for the $n \times n$ MIMO, $n \times 1$ SIMO and $1 \times n$ MISO cases where $n = N_t = N_r$. In this work, we reproduce the capacities described and shown in Fig. 8.6 on page 345 of David & Pramod (2005) and we base our argument on capacity by adding the capacity of SM to this collection in order to have a better outlook on the location of SM, in terms of capacity, among the other MIMO technologies mentioned here.

5.1 Capacity Calculation

In order to calculate the capacity of the SM system, the MIMO capacity approach will not apply because the antenna number represents added information. Furthermore, the antenna pattern is considered as spatial constellation and not as source of information. Thus, concerning computing the SM capacity, the conventional information theory approach will be used Prisecaru

(2010)

$$C_{SM} = (m+n_t)[1+p_e\log_2(p_e)+(1-p_e)\log_2(1-p_e)] \quad \text{(A I-14)}$$

where p_e is the probability of error of SM detection at a given SNR value and $m+n_t$ represents the total number of bits conveyed by the SM system. Since N_t has to be a power of 2 in SM systems, the number of antennae n must be set to 2, 4, 8 or 16 and the SM capacity must be calculated based on the probability of error for the 2×2, 4×4, 8×8, and 16×16 configurations which correspond to number of antenna indexing bits n_t to be 1, 2, 3 and 4 respectively. Note that the configuration size follows from $n = N_t = N_r$ as indicated earlier. A flashback on the capacity issue along with the obtained capacity results are presented in Section 6.

6. Simulation Results

In this section we provide simulation results for the SM scheme in Rayleigh fading channels using Monte Carlo simulation for the MMSE, ML and Optimum detectors. Various values for modulation order M has been used but the antenna configuration has been restricted to 4×1 and 4×4. The case of perfect and imperfect CSI has been studied first, then the effect of channel correlation is investigated. The destructive effects of CSI imperfection and correlation on the BER performance and on the capacity of SM systems is explored. The partially estimated CSI case comprises two situations, the first is when the CSI estimation is erroneous (imperfect) and is contaminated with noise, the second is when channel coefficients are correlated CSI, i.e. the coefficients do interfere among themselves. In this work, we study the consequences of erroneous and correlated CSI on the BER performance and on the capacity of SM system. The noise at each antenna is assumed to be independent zero-mean complex Gaussian random variable with variance σ.

6.1 The Perfect CSI case

To have a clear vision on the performance of SM detectors presented in this paper, we first have a look at the perfect CSI case where channel coefficients are perfectly estimated. Fig. I-2 demonstrates the BER performance of the system for the 4×1 and 4×4 cases, both with a

modulation order $M = 8$. As expected and observed in Fig. I-2, the optimum detector shows superior performance in comparison to its rivals in this scenario and antenna diversity plays its BER enhancement role as expected.

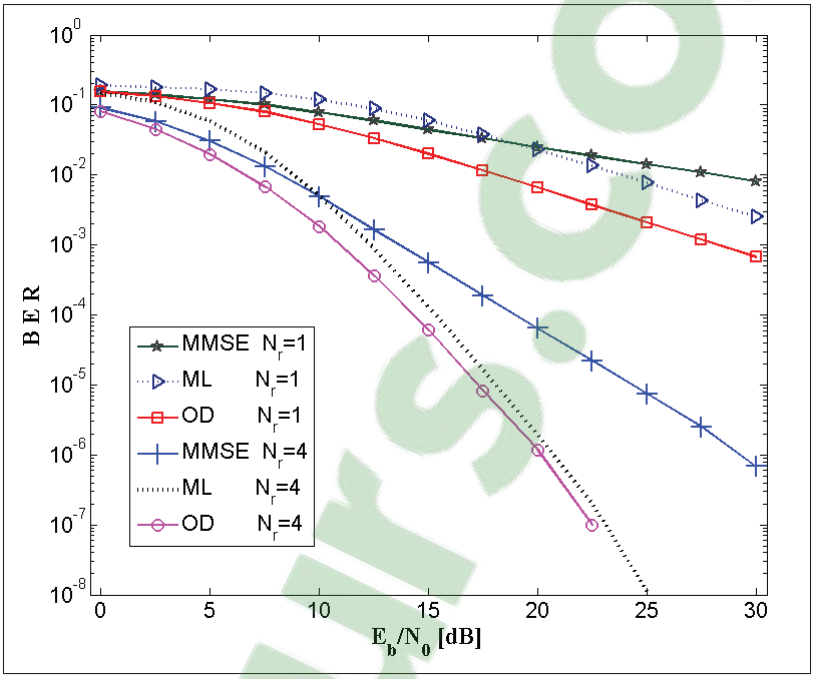

Figure-A I-2 BER performance of SM with perfectly estimated CSI for 4×1 and 4×4 configurations

6.2 The Imperfect CSI case

In this section, we study the performance of SM detectors with imperfect channel coefficients as narrated in Eq. (A I-10). The BER performance of SM detectors for $\rho = 0.85$ and $\rho = 0.7$ is shown in Fig. I-3. As obsreved, the BER performance deteriorates with decreased value of the correspondence factor ρ. The ML detector seems to be more susceptible to noise since it contains more noisy terms that challenge the minimum Euclidean distance.

6.3 The Correlated CSI case

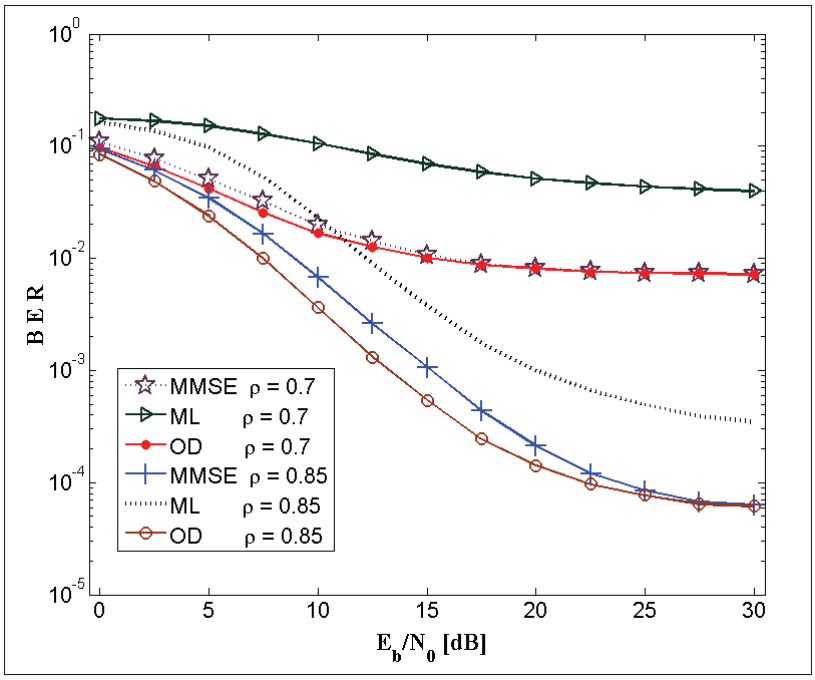

Figure-A I-3 BER performance of SM with imperfect CSI for a 4×4 configuration with $M = 8$

The BER performance of the SM system with correlated channel coefficients as described by the Δ matrix in Eq. (A I-12) is considered here. The performance of SM detectors for $\delta = 0.15$ and $\delta = 0.3$ is shown in Fig. I-4. As can be observed in this figure, the BER performance deteriorates as the correlation value increases.

6.4 Correlated and Imperfect CSI

The system has been tested in accordance with the inclusive model we propose in Eq. (A I-13) with $M = 8$, $N_t = N_r = 4$. A 3-D view of the BER using OD SM versus δ and $1 - \rho$ is shown in Fig. I-5 for $0 \leq \delta \leq 0.5$ and $0 \leq 1 - \rho \leq 0.5$. The reason why we chose the optimum detector is because this detector proved to outperform the rival detectors while it maintained more robustness against both imperfection and correlation. As observed here, both factors ρ and δ exhibit a similar destructive trend. The relationship between ρ, δ and the noise variance is left for future analysis.

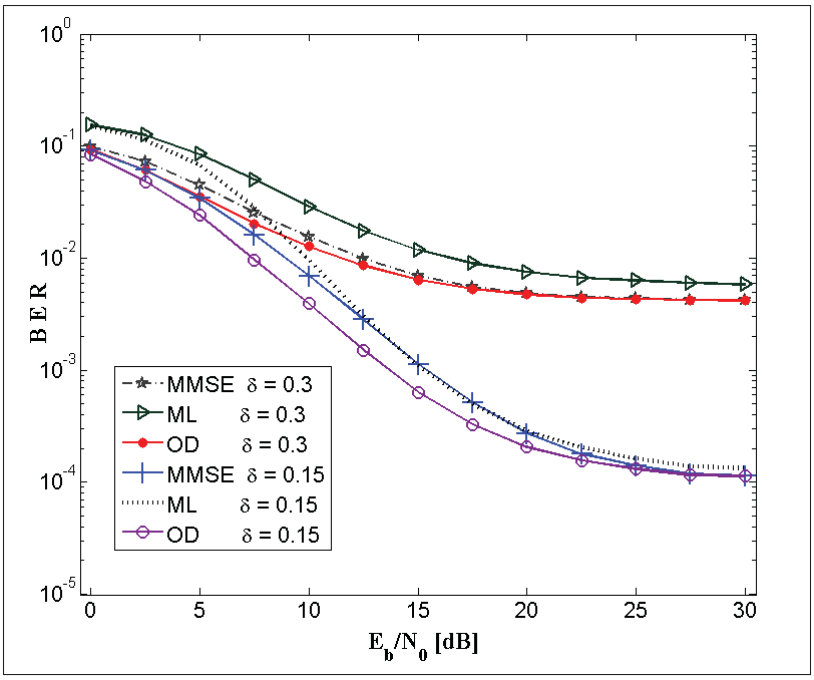

Figure-A I-4 BER performance of SM with correlated CSI for a 4×4 configuration with $M = 8$

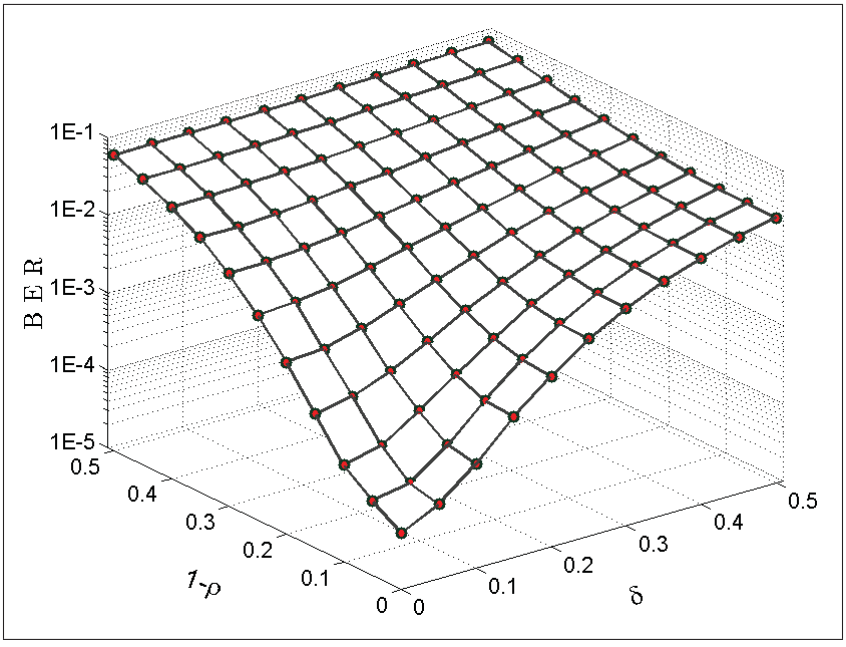

Figure-A I-5 BER performance of SM vs. correlated and imperfect CSI estimation at $E_b/N_0 = 15$ dB

6.5 Capacity Issues

Having studied the influence of imperfect and correlated CSI on the system performance, we will have a look at the capacity degradation under the presence of ρ and δ. Based on our results, the OD has proved to achieve the best BER performance while it exhibits most robustness against channel imperfections and correlation, so the probability of error in Eq. (A I-14) will be based on optimal detection. Furthermore, the signal to noise ratio will be fixed at 0 dB since the MIMO, MISO and SIMO systems of Prisecaru (2010) are evaluated at this value. In Fig. I-6 the capacities originally given in David & Pramod (2005) were reproduced and the capacity of SM was then calculated and added in the described fashion. Since MIMO, SIMO and MISO evaluations are done at perfect CSI, i.e. $\rho = 1, \delta = 0$, the capacity of SM at these values corresponds to the perfect CSI case and represents the capacity of SM in comparison with other MIMO technologies. As seen in Fig. I-6, with imperfect and correlated coefficients, capacity of the SM system drops as a consequence of the BER performance decline at no surprise. The capacity of SM deteriorates even more as ρ and δ take farther distances from the ideal values. More on MIMO capacity issues may be looked up in Foschini (1996) and Kalis *et al.* (2008).

7. Discussions and Conclusions

In this work, we have developed a general model for channel impairments that incorporates channel imperfection and channel correlation. The developed model is then used to study the effects of channel impairments on the BER performance of three most widely used SM receivers, namely the MMSE, ML and OD receivers. Moreover, the influence of channel impairments on the capacity of the SM system has also been investigated. Even though numerical calculations are mainly based on a 4×4 SM system configuration, the results obtained may be generalized to any accommodating configuration. Furthermore, our results reveal that the BER performance of SM detectors under study deteriorate with channel imperfections especially in high SNR regions. In fact, the performance of the ML is very fragile and sensitive to either correlated or imperfect channel coefficients while MMSE and OD do better in such situations.

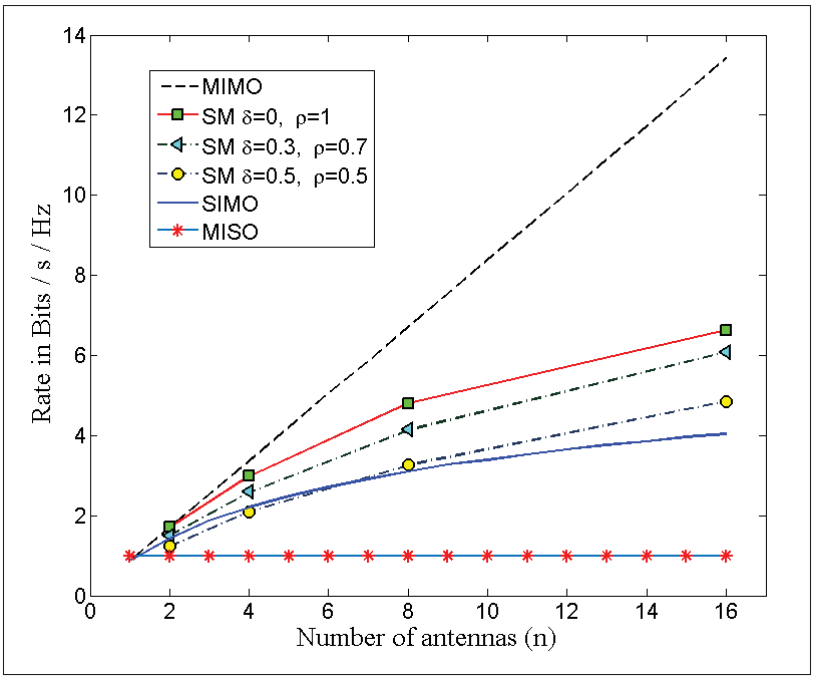

Figure-A I-6 Capacities of MIMO, SM, SIMO and MISO channels

Given the lower complexity of MMSE compared to OD and the convergence of their BER performance at high SNR values, the MMSE might be a preferred candidate for higher power scenarios where simplicity matters. However, at lower SNR, the OD becomes a more suitable choice. Fundamental complexity concepts are provided in Bai *et al.* (2014) while more related complexity discussions are found in Mesleh *et al.* (2006a, 2008); Kaddoum & Soujeri (2015) and is not repeated here. The information theory-based calculation of the SM capacity carried out in this work confirms and approves this fact. Consequently, channel impairments cause the SM system capacity to drop as a reasonable and logical aftermath of the rise in the probability of error. Therefore, CSI is a phenomenon that can not be always assumed to be perfect because of the serious impacts it has on the BER performance and on the capacity of the SM system. Finally, we observe that SM is sensitive to both imperfect and correlated channels.

APPENDIX II

PERMUTATION INDEX DCSK MODULATION TECHNIQUE FOR SECURE MULTI-USER HIGH-DATA-RATE COMMUNICATION SYSTEMS

Marijan Herceg[2], Georges Kaddoum[1], Denis Vranješ[2] and Ebrahim Soujeri[1]

[1] Department of Electrical Engineering, École de Technologie Supérieure,
1100 Notre-Dame West, Montreal, Quebec, Canada H3C 1K3
[2] Department of Communications, Faculty of Electrical Engineering, Computer Science and Information Technology Osijek, Croatia

Paper published in *IEEE Transactions on Vehicular Technology*, November 2017.

Abstract

A new non-coherent scheme called Permutation Index Differential Chaos Shift Keying (PI-DCSK) modulation is proposed in this paper. This original design aims to enhance data security, energy and spectral efficiencies, compared to its rivals. In the proposed PI-DCSK scheme, each data frame is divided into two time slots in which the reference chaotic signal is sent in the first time slot and a permuted replica of the reference signal multiplied by the modulating bit is sent in the second time slot. In particular, the bit stream is divided at the transmitter into blocks of $n+1$ bits, where n mapped bits are used to select one of the predefined reference sequence permutations, while a single modulated bit is spread by the permuted reference signal just mentioned. At the receiver side, the reference signal is recovered first, then all permuted versions of it are correlated with the data-bearing signal. The index of the correlator output with maximum magnitude will estimate the mapped bits, while the output content of the corresponding correlator is compared to a zero threshold to recover the modulated bit. Moreover, a new multiple access (MA) method based on the proposed scheme is described and analysed. Analytical expressions for the error performance in single-user and multi-user environments are derived for additive white Gaussian noise (AWGN) and multipath Rayleigh fading channels, respectively. Furthermore, the performance of the proposed PI-DCSK system

is analysed and compared with other non-coherent chaotic modulation schemes and is found to be promising.

1. Introduction

Chaotic signals have gained increasing popularity for usage in spread spectrum communication systems in the last two decades. The main reason is that such signals can be easily generated and have properties like wideband spectrum, impulse-like auto-correlation and low cross-correlation values Lau & Tse (2003). These properties are very important for better multiple access performance, higher resistance to jamming or interference and more immunity against multipath effects. Besides, its non-periodic nature reinforces the transmission security when, this latter, is used in a coherent fashion.

During previous researches numerous coherent and non-coherent chaos-based communication schemes have been proposed. The main drawback of coherent systems like chaos-shift-keying (CSK) Dedieu & Kennedy (1993) is the synchronization of chaotic signals at the receiver, which is a challenging task in noisy channels.

Enjoying excellent correlation properties of chaotic signals, non-coherent modulation schemes based on transmitted reference (TR) Rushforth (1964) method have been increasingly studied by the scientific community. The first non-coherent modulation based chaotic scheme is the differential chaos shift keying (DCSK) Kolumbán *et al.* (1996) and its constant power frequency-modulated DCSK version (FM-DCSK) Kolumbán *et al.* (1997a). In DCSK, every bit duration is split into two time slots. In the first slot, a reference chaotic sequence is sent, while in the second slot, a data-modulated time-delayed reference chaotic sequence is sent. At the receiver, the reference sequence is correlated with the data modulated sequence in order to recover the transmitted bit. The main advantages of such an approach are avoidance of chaotic sequence recovery, inexistence of a channel state estimator at the receiver, resistance to multi-path interferences and simple implementation. However, the main drawbacks of such an approach are low data rate, high energy consumption as well as the usage of wideband RF

delay lines, which are not easy to implement in CMOS technologyXu *et al.* (2011). It should also be mentioned that the RF delay line is an issue only in analogue implementations, while in digital implementations, such as FPGA or system-on-chip (SoC), is no longer an issue.

Recently, some DCSK improvements on energy efficiency and data rate have been addressed in many works. In this vein, high-efficiency DCSK (HE-DCSK) is proposed in Yang & Jiang (2012). In HE-DCSK, bandwidth efficiency is doubled and chaotic signal re-transmission is reduced, which adds to the transmitted signal data security in comparison with DCSK. However, it needs four delay lines and is thus not suitable for fast fading channels. In order to reduce the number of needed delay lines in HE-DCSK, reference-modulated DCSK (RM-DCSK) has been proposed in Yang & Jiang (2013). In RM-DCSK, the reference chaotic signal also serves as a data bearer, which enhances bandwidth efficiency. To reduce the noise variance at the receiver, a noise-reduction DCSK (NR-DCSK) is proposed in Kaddoum & Soujeri (2016). In NR-DCSK, multiple replicas of the reference chaotic signal are sent and averaged at the receiver in order to reduce the noise interference prior to correlation with the data bearing chaotic sequence. Short-reference DCSK (SR-DCSK) is proposed in Kaddoum *et al.* (2016a) with the target of reducing delay lines. In SR-DCSK, a reference chaotic signal is shortened to less than a half of the bit duration and multiple replicas of the reference signal are used to spread the data. Such an approach improves energy efficiency and boosts data rate without adding hardware complexity. To improve spectral efficiency, quadrature chaos-shift keying (QCSK) is proposed in Galias & Maggio (2001). In QCSK, the reference chaotic signal is sent in the first slot, while a linear combination of the Hilbert transform of the reference signal and a delayed version of the reference signal are used to map two bits in the second slot. The non-coherent chaos-based permuted sequence technique is introduced in Lau & Tse (2009), in which permutations of the reference signal are used for mapping additional bits per transmitted symbol. Furthermore, to mitigate the effect of multipath fading and to achieve a full-scale diversity gain without the need to channel state information, space-time block codes (STBC) are used in combination with DCSK in Chen *et al.* (2013).

To avoid the usage of wideband RF delay lines and double the data rate, the authors in Kaddoum *et al.* (2015a) have proposed an improved DCSK (I-DCSK) in which a time-reversal operation on the reference sequence is used to separate the data and reference sequences, and the resultant symbol is transmitted in one time slot rather than two. Furthermore, the binary code-shifted DCSK (CS-DCSK) in which reference and data chaotic sequences are separated by Walsh codes instead of time delay multiplexing, is presented in Xu *et al.* (2011). Two multi-level versions of CS-DCSK, called generalized CS-DCSK (GCS-DCSK) and its improved version multi-level CS-DCSK (MCS-DCSK) are presented in Xu *et al.* (2012) and Huang *et al.* (2016), respectively. In high-data rate CS-DCSK (HCS-DCSK) Kaddoum & Gagnon (2012), different chaotic sequences are used instead of Walsh codes in order to separate the reference and data sequences. However, such approaches need chaotic sequence synchronization at the receiver side. The implementation of DCSK-based communication systems in ultra-wideband (UWB) applications and cooperative communications (CC) is analysed in Fang *et al.* (2016) and Chen *et al.* (2016), respectively.

Multi-level, multi-carrier DCSK (MC-DCSK) in which the reference chaotic signal is sent over a predefined subcarrier frequency, while multiple modulated data streams are sent over the remaining orthogonal subcarriers was introduced in Kaddoum *et al.* (2013a). Despite the improvements achieved by such an approach with respect to energy efficiency and data rate, it demands large bandwidth.

Recently, the combination of index modulation (IM) and MC-DCSK, named carrier index DCSK (CI-DCSK) is proposed in Cheng *et al.* (2016). In CI-DCSK, energy and spectral efficiency are enhanced by mapping a part of the bits in the subcarrier indices, i.e. to determine the subcarriers that will be active, while the remaining bits are conveyed by DCSK through these active carriers. To allow multiple-access and reduce bandwidth demands of MC-DCSK, a multi-user orthogonal-frequency-division-multiplexing DCSK (MU-OFDM-DCSK) is proposed in Kaddoum (2016a). In MU-OFDM-DCSK, the spreading operation is performed in the time domain over multiple orthogonal frequencies. Each user is dedicated a set of predefined frequencies from multiple available frequencies, to transmit reference chaotic signals,

while the remaining frequencies are shared with the other users to transmit multiple bits. In Kaddoum *et al.* (2013a) and Cheng *et al.* (2016), the reference and data chaotic sequences are orthogonal over a chip time (the time duration of one chaotic sample), which requires the carrier time period to be less than the chip period. To reduce the demand on carrier frequencies, the frequency-translated DCSK (FT-DCSK) is proposed in Herceg *et al.* (2016). In FT-DCSK, the orthogonality between reference and data chaotic sequences is sustained over a symbol duration, using an orthogonal sinusoid carrier. FT-DCSK has a lower demand on carrier frequencies compared to the methods proposed in Kaddoum *et al.* (2013a) and Cheng *et al.* (2016), but is very sensitive to multipath time delays.

Recently, a novel $M-$ary modulation scheme called orthogonal multi-level DCSK (OM-DCSK) is proposed Yang *et al.* (2016). In this configuration, each data-bearing signal is chosen from a set of orthogonal chaotic sequences constructed from a reference signal. In order to increase the number of signals contained in the orthogonal signal set, chaotic sequences and their Hilbert transforms along with Walsh codes are used. The new scheme achieves a higher data rate, has an augmented energy efficiency and scores a better bit error rate (BER) performance.

Inspired by the works of Lau & Tse (2009), Kaddoum *et al.* (2015a) and Yang *et al.* (2016), we propose in this paper a multi-level permutation index DCSK (PI-DCSK) architecture. In the PI-DCSK scheme proposed here, the input bit stream is divided into blocks of $n+1$ bits transmitted at a time, where n bits are mapped in distinct permuted reference sequences and a single bit is physically transmitted.

Here, the n mapped bits are used to select one of the predefined reference sequence permutations while a single bit called the *modulated bit* is spread by the selected permuted sequence. This approach engages $n+1$ bits into each transmission instant. The remaining procedure in PI-DCSK has a similar structure to the conventional DCSK, where each data frame is separated into two time slots. In the first slot, the reference chaotic signal is sent and in the second slot, the modulated bit is transmitted after being spread by the selected permuted sequence.

At the receiver side, the reference signal is first recovered, then all possible permuted versions of it are correlated with the data bearing signal in order to find a maximum winner. The index of the winner correlator will estimate the mapped bits, while its content is used to provide an estimation of the modulated bit, after being compared to a zero threshold.

In the proposed design, the utilisation of 2^n quasi-orthogonal signals achieves a modulation order of $M = 2^{n+1}$. This fact enhances data rate and energy efficiency while it keeps hardware complexity relatively low. Furthermore, by eradicating the similarity between reference and data bearing signals through using different permutations, the transmitted data security of the proposed scheme is enhanced.

Furthermore, by exploiting the possible permutation set size, a new multiple access (MA) method is proposed. Namely, for a given chaotic sequence length β, there is $\beta! - 1$ possible permutations. In order to allow the MA in PI-DCSK, a distinct set of 2^n permutations is used for each user.

Compared to OM-DCSK, PI-DCSK avoids the usage of repeated chaotic generators (RCG), Hilbert transforms or Walsh codes at the transmitter and receiver sides. The fact that we put aside Walsh codes in PI-DCSK equips the proposed system with all properties of non-coherent modulation.

To complete the proposed scheme, analytical bit error rate (BER) expressions over Rayleigh multipath fading and additive white Gaussian noise (AWGN) channels, in both single-user and multi-user environments are derived and validated versus simulation results. This is to show the extent and level of accuracy of our analytical expressions. Finally, the performance of PI-DCSK is analysed and compared with rival modulation techniques to show its superiority.

The remainder of this paper is organized as follows: In Section 2, the PI-DCSK system model is briefly described. System analysis is provided in section 3. Performance analysis of PI-DCSK system over AWGN and multipath Rayleigh channels is provided in section 4. Simulation results and discussions are presented in Section 5 while conclusions are given in section 6.

2. PI-DCSK System Model

In this section, the transmitter and receiver architectures of the proposed system will be described in detail.

2.1 The transmitter

The block diagrams of the proposed PI-DCSK system are presented in Figs. -II-1II-3, where the transmitter is shown in Fig. II-1, the permutation process in Fig. II-2 and the receiver in Fig. II-3. At the transmitter, the chaotic generator generates a chaotic sequence of β samples that is used as a reference signal and is placed in the first time slot. This reference signal is simultaneously loaded into a permutation block in order to generate different permuted replicas of the original reference signal in the second time slot. Permutations are chosen in a way such that it provides quasi-orthogonality between the generated permuted reference signal replicas. An efficient method for generating a suitable set of permuted sequences with the aforementioned properties from the reference sequence is proposed in Lau *et al.* (2003). Moreover, it is demonstrated that for a large spreading factor, permuted replicas of a chaotic signal are quasi-orthogonal to each other Lau *et al.* (2003) such that

$$\mathbf{x}P_j(\mathbf{x})^T \approx 0, \tag{A II-1}$$

$$P_i(\mathbf{x})P_j(\mathbf{x})^T \approx 0, \text{ for } i \neq j, \tag{A II-2}$$

where $\mathbf{x}$ is a vector that contains β number of chaotic samples, $P_j(\cdot)$ represents the j^{th} permutation operator and $(\cdot)^T$ denotes transposition. Therefore, to carry n mapped bits, each transmitter will generate 2^n distinct permutations. By using a method described in Lau *et al.* (2003), the $\beta - 1$ permutations can be easily generated.

In particular, the input signed bit stream is divided at the PI-DCSK modulator into blocks of $n+1$ bits. The i^{th} block of bits of the k^{th} user can be written as $\left[a_{i,1}^{(k)}, a_{i,2}^{(k)}, \cdots, a_{i,n+1}^{(k)}\right] = \left[\mathbf{s}_i^{(k)}, a_{i,n+1}^{(k)}\right]$, where $\mathbf{s}_i^{(k)} = \left[a_{i,1}^{(k)}, a_{i,2}^{(k)}, \cdots, a_{i,n}^{(k)}\right]$ is the vector of n mapped bits.

The mapped bits $\mathbf{s}_i^{(k)}$ select one of the 2^n predefined permutations $\mathbf{P}^{(k)} = \{P_1^{(k)}, P_2^{(k)}, \cdots, P_{2^n}^{(k)}\}$. Each element in $\mathbf{s}_i^{(k)}$ is a code vector generated by introducing a permutation of the original reference sequence, as indicated earlier, while the modulated bit denoted by $a_{i,n+1}^{(k)}$ is spread by the selected permuted sequence. Note that by using this mapping approach, the overall PI-DCSK modulation order becomes equal to $M = 2^{n+1}$ by using only $M/2 = 2^n$ quasi-orthogonal signals.

Furthermore, asynchronous data transmission of different users is assumed in this paper. In addition, in the PI-DCSK system, each user uses a distinct set of $M/2$ permutations, such that $\mathbf{P}^{(k)} \cap \mathbf{P}^{(u)} = \emptyset$, for $k \neq u$. In general, the overall number of possible permutations that can be performed on a reference chaotic sequence of length β is equal to $\beta! - 1$. This allows us to assign different sets of chaotic codes to a large number of users without having scarcity of spreading sequences. In this vein, by permuting a reference signal of length β, the number of users N_u in the PI-DCSK system is theoretically very large and is bound to

$$N_u \leq (\beta! - 1)/(M/2). \tag{A II-3}$$

By using the proposed MA method, even for moderate spreading factors β, the possible number of users grows to large values because the number of users in PI-DCSK system is proportional to the different permutation that can be performed on the reference signal. This fact constitutes a great advantage for multi-user scenarios. For example, for $\beta = 50$, the total number of users turns to be $N_u \approx 1.52 \times 10^{64}$ users, for $M = 4$. However, it should be stated that not all permutations, out from set of $\beta! - 1$ permutations, have a low cross-correlation property and therefore, the system performance may degrade if permutations are not properly chosen.

The discrete baseband vector representation of the k^{th} user, i^{th} PI-DCSK symbol that contains $n+1$ bits, can be expressed as

$$\mathbf{e}_i^{(k)} = \left[\mathbf{x}_{i,0}^{(k)} \;\; a_{i,n+1}^{(k)} P_j^{(k)}\left(\mathbf{x}_{i,\beta}^{(k)}\right)\right], \tag{A II-4}$$

where $\mathbf{x}_{i,v}^{(k)}$ is the k^{th} user, i^{th} vector of β chaotic samples, with time delay v, defined as

$$\mathbf{x}_{i,v}^{(k)} = \left[x_{i,1-v}^{(k)}, x_{i,2-v}^{(k)}, \cdots, x_{i,\beta-v}^{(k)}\right]. \tag{A II-5}$$

In (A II-4), $\mathbf{x}_{i,0}^{(k)}$ is the reference signal vector of β delay-free chaotic samples while $\mathbf{x}_{i,\beta}^{(k)}$ is a replica of the reference signal delayed by β samples. Moreover, $P_j^{(k)}(\cdot)$ represents the permutation operation of the k^{th} user, for the i^{th} block of mapped bits $\mathbf{s}_i^{(k)}$, while $j \in \{1, 2, \cdots, M/2\}$ represents the index of the selected permutation. The PI-DCSK frame architecture is shown in Fig II-2. Furthermore, it is clear from (A II-4) that the symbol duration in PI-DCSK is equal to $T_s = 2\beta T_c$, where T_c is the chip duration and 2β is the spreading factor.

2.2 The receiver

In this paper, a commonly used channel model in wireless communications Kaddoum *et al.* (2013a); Xia *et al.* (2004) is considered. In this model, the k^{th} user, l^{th} path channel coefficient and time delay are denoted as $\lambda_{l,k}$ and $\tau_{l,k}$, respectively. It should be noted that in this work, all L_k channel coefficients are considered to be flat and quasi-static over the transmission period of one frame and that they are i.i.d. random variables that follow a Rayleigh distribution. The Rayleigh probability density function (PDF) of the channel coefficients is given by

$$f_\lambda(z) = \frac{z}{\sigma^2}\; e^{-z^2/2\sigma^2}, \tag{A II-6}$$

where $\sigma > 0$ is the distribution scale parameter representing the root mean square value of the received signal before envelope detection.

Therefore, when the transmitted signal passes through the Rayleigh fading channel, the received signal of the k^{th} user, i^{th} symbol can be stated as

$$\begin{aligned}\mathbf{r}_i^{(k)} &= \sum_{l=1}^{L_k} \lambda_{l,k} \left[\mathbf{x}_{i,\tau_{l,k}}^{(k)} \;\; a_{i,n+1}^{(k)} P_j^{(k)} \left(\mathbf{x}_{i,\beta+\tau_{l,k}}^{(k)} \right) \right] \\ &+ \sum_{\substack{u=1 \\ u\neq k}}^{N_u} \sum_{l=1}^{L_u} \lambda_{l,u} \left[\mathbf{R}_{i,\tau_{l,u}}^{(u)} \;\; \mathbf{D}_{i,\tau_{l,u}}^{(u)} \right] + \left[\mathbf{n}_{i,0,k}^{R} \;\; \mathbf{n}_{i,0,k}^{D} \right],\end{aligned} \tag{A II-7}$$

where the vector $\mathbf{R}_{i,\tau_{l,u}}^{(u)}$ is the u^{th} user transmitted signal of β chaotic samples, which describes the k^{th} user reference time slot, while the vector $\mathbf{D}_{i,\tau_{l,u}}^{(u)}$ is the u^{th} user signal of β chaotic samples, which characterizes the k^{th} user data time slot, respectively. More, L_u is the number of paths for the u^{th} user, while the vectors $\mathbf{n}_{i,0,k}^{R}$ and $\mathbf{n}_{i,0,k}^{D}$ are the noise components of the k^{th} user, i^{th} data frame that occur during the reference and data time slots, respectively. These noise vectors are respectively defined as

$$\mathbf{n}_{i,0,k}^{R} = [n_{i,1,k}, \cdots, n_{i,\beta,k}], \tag{A II-8}$$

$$\mathbf{n}_{i,0,k}^{D} = [n_{i,\beta+1,k}, \cdots, n_{i,2\beta,k}], \tag{A II-9}$$

where $n_{i,v,k}$ is an AWGN sample with zero mean and a variance $N_0/2$.

At the receiver, as shown in Fig. II-3, the reference signal is loaded in the permutation block during the first time slot i.e., $[iT_s, (2i+1)T_s/2]$. Then, $M/2$ permutations $\{P_1^{(k)}, P_2^{(k)}, \cdots, P_{M/2}^{(k)}\}$ of the reference sequence are performed and stored. Furthermore, all permuted reference sequences are simultaneously correlated with the data bearing sequence during the second time slot of duration $[(2i+1)T_s/2, (i+1)T_s,]$, forming $M/2$ decision variables.

The corresponding decision variable at the output of the k^{th} user, i^{th} time slot, m^{th} correlator may be stated as

$$
\begin{aligned}
D_{i,m}^{(k)} = P_m^{(k)} \Bigg(& \sum_{l=1}^{L_k} \lambda_{l,k} \mathbf{x}_{i,\beta+\tau_{l,k}}^{(k)} \\
& + \sum_{\substack{u=1 \\ u\neq k}}^{N_u} \sum_{l=1}^{L_u} \lambda_{l,u} \mathbf{R}_{i,\beta+\tau_{l,u}}^{(u)} + \mathbf{n}_{i,\beta,k}^{R} \Bigg) \\
\times \Bigg(& \sum_{l=1}^{L_k} \lambda_{l,k} a_{i,n+1}^{(k)} P_j^{(k)} (\mathbf{x}_{i,\beta+\tau_{l,k}}^{(k)}) \\
& + \sum_{\substack{u=1 \\ u\neq k}}^{N_u} \sum_{l=1}^{L_u} \lambda_{l,u} \mathbf{D}_{i,\tau_{l,u}}^{(u)} + \mathbf{n}_{i,0,k}^{D} \Bigg)^{T}, 1 \le m \le M/2.
\end{aligned}
\tag{A II-10}
$$

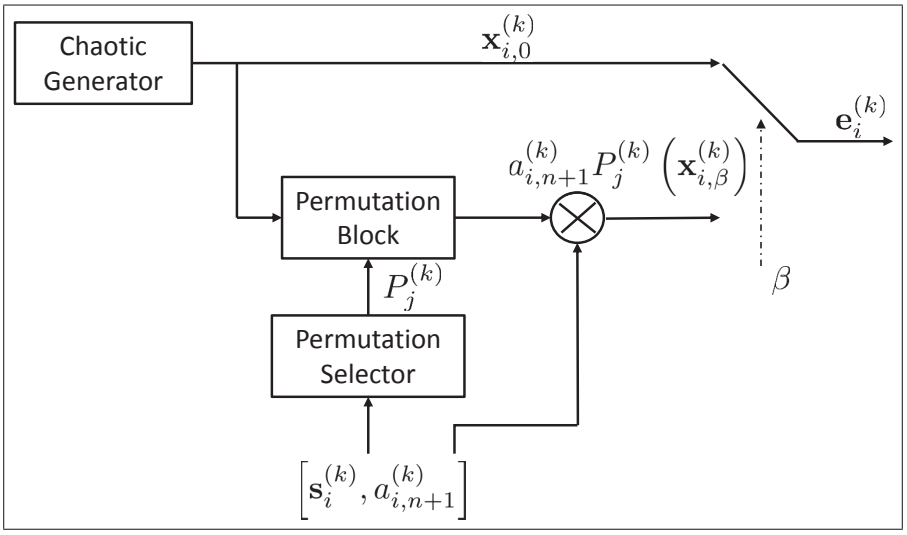

Figure-A II-1 A block diagram of the PI-DCSK communication system transmitter

In order to determinate the matching permutation index, in the detector and decision logic circuit, the magnitude of $M/2$ correlator outputs, are compared in order to find the largest value

$$
\hat{j} = \arg\max_{m} \left\{ \left| D_{i,m}^{(k)} \right| \right\}, m \in \{1, 2, \cdots, M/2\}. \tag{A II-11}
$$

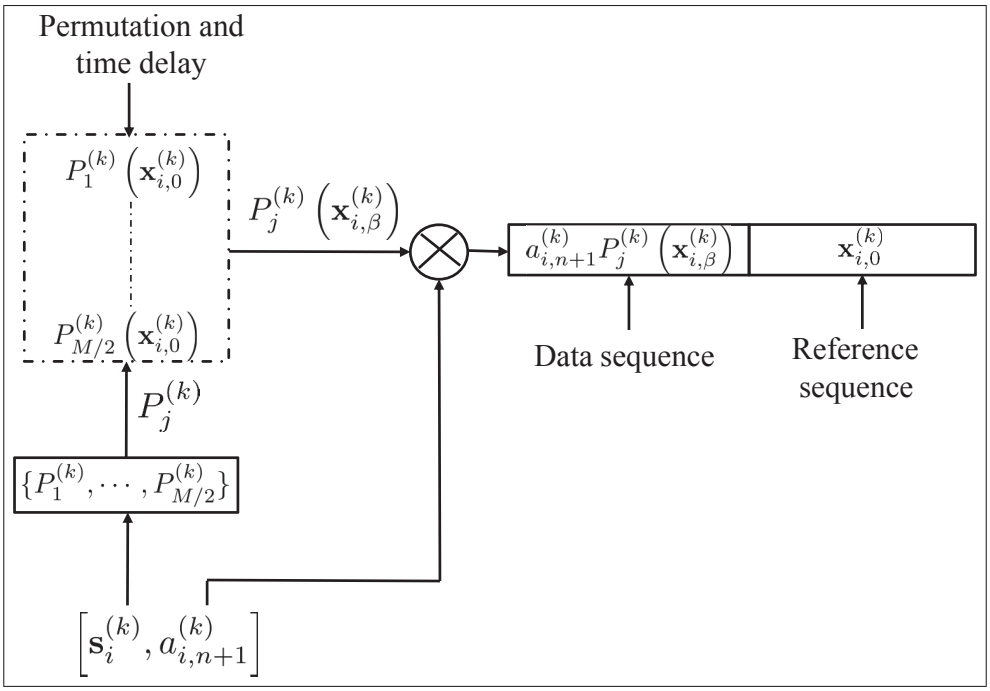

Figure-A II-2 A block diagram of the PI-DCSK communication frame architecture

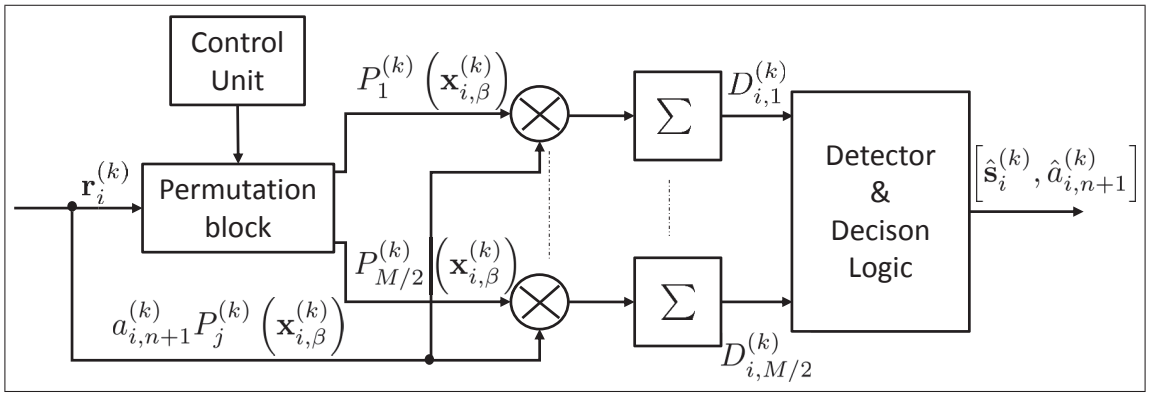

Figure-A II-3 A block diagram of the PI-DCSK communication system receiver

By estimating the index of the largest correlator's output $\hat{j}$, the receiver knows which permutation is used and uses the index of that permutation to provide an estimation of the n mapped bits. The physically modulated bit can then be recovered by computing the sign of the selected correlator

$$\hat{a}_{i,n+1}^{(k)} = \mathrm{sgn}(D_{i,\hat{j}}^{(k)}). \qquad \text{(A II-12)}$$

In our analysis, we assume that the largest delay, over all possible user and path combinations $\tau_{\max}$ is much shorter than duration of the reference signal, i.e.

$$0 < \tau_{\max} << \beta T_c. \tag{A II-13}$$

where $\tau_{\max} = \max(\tau_{l,k})$ for all k, l. With this assumption in hand, the inter symbol interference (ISI) may be neglected.

3. System Analysis

In this section, a PI-DCSK system analysis regarding energy efficiency and data security is provided. Furthermore, hardware complexity comparison with OM-DCSK is performed as the two systems share similar hardware functionalities and properties.

3.1 Energy efficiency

Besides its simplicity and high spectral efficiency, another major advantage of the PI-DCSK is its energy efficiency. In Kaddoum *et al.* (2013a), the authors have introduced the data-energy-to-bit-energy ratio (DBR) as

$$\text{DBR} = \frac{E_{\text{data}}}{E_b}, \tag{A II-14}$$

where E_{data} is the energy of data bearing signal, while E_b is the required total energy to carry each bit. In the proposed PI-DCSK scheme, the symbol energy E_s is expressed as

$$E_s = E_{\text{data}} + E_{\text{ref}}, \tag{A II-15}$$

where E_{ref} is the energy of the reference sequence. Since the data sequence is a permuted version of the reference sequence, the reference and data energies are equal

$$E_{\text{data}} = E_{\text{ref}} = T_c \sum_{k=1}^{\beta} x_{i,k}^2. \tag{A II-16}$$

Thus, the PI-DCSK symbol energy is equal to

$$E_s = 2T_c \sum_{k=1}^{\beta} x_{i,k}^2. \tag{A II-17}$$

In fact, E_s is used to transmit $\log_2(M) = n+1$ bits while E_{ref} is used to carry the reference signal. Therefore, in comparison to the conventional transmit reference scheme, the energy required to transmit one bit would be

$$E_b = \frac{E_s}{\log_2(M)} = \frac{2T_c}{\log_2(M)} \sum_{k=1}^{\beta} x_{i,k}^2. \tag{A II-18}$$

Subsequently, by using (A II-15), (A II-16), (A II-17) and (A II-18), the DBR in (A II-14) can be rewritten as

$$\text{DBR} = \frac{E_{\text{data}}}{E_b} = \frac{\log_2(M)}{2}. \tag{A II-19}$$

Table II-1 shows the DBR of different chaotic modulations. As clearly indicated in (A II-14),

Table-A II-1 DBR comparison of different chaotic modulation techniques

Modulation	**DBR**
DCSK, CS-DCSK	$1/2$
HE-DCSK, RM-DCSK, QCSK, FT-DCSK	$2/3$
MCS-DCSK	$(M-2)/M$
MC-DCSK	$(M-1)/M$
OM-DCSK, PI-DCSK	$\log_2(M)/2$

the DBR can be simply denoted as the ratio of the number of bits per symbol to the number of chaotic sequences needed to transmit that symbol. For example, in DCSK, two chaotic sequences (reference and data) are used to transmit one bit. It can be seen from Table I that the DBR values of both MC-DCSK and MCS-DCSK converge to unity for higher values of M, while this ratio is logarithmic in the order of M for PI-DCSK and OM-DCSK, which is advantageous. Further, in the proposed PI-DCSK system, the DBR is higher than unity because

n bits are mapped in the permutation, while only one bit is physically transmitted. Therefore, with only one reference and one data sequence, $n+1$ bits are transmitted. Note that a higher DBR value is an indication of a higher non-coherent modulation energy efficiency.

3.2 Data security

In conventional DCSK systems, bit rate can be easily detected by analyzing the frequency spectrum of the squared DCSK signal. This arises from the fact that when squaring the DCSK signal, both reference and data bearing signals become equal. This equality is translated into the frequency spectrum as zero values at *odd* multiple frequencies of the bit rate Lau *et al.* (2003). However, when a data-bearing signal is constructed from different reference signal permutations, the similarity between reference and data bearing signals is eradicated and, therefore, the frequency spectrum of the squared PI-DCSK signal remains white. Furthermore, in order to properly demodulate the PI-DCSK signal, $M/2$ permutations should be known at the receiver. Therefore, if some unintended receiver, i.e., a fraudulent one, tries to demodulate the signal, it should first find these $M/2$ permutations from the set of $\beta! - 1$ possible permutations. In fact, according to the security standard described in Daemen & Rijme (2002), a system is deemed secure if a fraudulent receiver needs to perform at least 128! trials in order to find the appropriate permutation set. Therefore, the proposed PI-DCSK can be considered secure for $\beta > 128$.

3.3 Hardware complexity comparison with OM-DCSK

In this section, the PI-DCSK hardware complexity is compared with the OM-DCSK for the same modulation order M, as they share similar modulation properties. Table II-2 and Table II-3 show the elements that are needed to construct PI-DCSK and OM-DCSK transmitters and receivers, respectively. In summary, PI-DCSK avoids the usage of Walsh code generators, Hilbert transforms and repeated chaotic generators (RCG). As observed in Table II-2, the spectral efficiency of the OM-DCSK seems to be double that of the PI-DCSK. This is because OM-DCSK is using I/Q channels for transmitting reference and data bearing signals. How-

Table-A II-2 Transmitter complexity comparison of PI-DCSK and OM-DCSK

Transmitter	**PI-DCSK**	**OM-DCSK**
Adders	0	1
Multipliers	1	$2M$
Spectral efficiency	$\log_2(M)/(2\beta)$	$\log_2(M)/\beta$
Additional blocks	Permutation block, single switch	Walsh code generator, Hilbert transformer, RCG

Table-A II-3 Receiver complexity comparison of PI-DCSK and OM-DCSK

Receiver	**PI-DCSK**	**OM-DCSK**
Adders	$M/2$	M
Multipliers	$M/2$	$2M$
Additional blocks	Permutation block	Walsh code generator, Hilbert transformer

ever, PI-DCSK may also transmit using I/Q channels and achieve a similar spectral efficiency. Furthermore, PI-DCSK transmitters do not need any adders at all and need a single multiplier while OM-DCSK transmitters need an adder and $2M$ multipliers. Therefore, the complexity of the proposed PI-DCSK is reduced to a great extent in comparison with OM-DCSK.

Similarly, the PI-DCSK receiver needs only half the number of adders and quarter the number of multipliers needed by OM-DCSK, regardless of M. By the same token, permutation blocks remain the only additional instrument needed on both sides of the PI-DCSK system.

4. Performance Analysis

In this section, the performance of PI-DCSK is evaluated, and analytical BER expressions are derived for AWGN and multipath Rayleigh fading channels. We employ the Chebyshev polynomial function in this work because of its simplicity and excellent statistical properties Kaddoum *et al.* (2009a). For simplicity, the chip time T_c is set to unity. This polynomial is known to proceed as

$$x_{i,k} = 1 - 2x_{i,k-1}^2. \qquad \text{(A II-20)}$$

In addtion, the chaotic samples are normalized such that their mean values are all zero and their variance is unity i.e., $E(x_{i,k}) = 0$, and $E(x_{i,k}^2) = 1$, where $E(\cdot)$ is the expectation operator. To obtain the system performance analysis, the Gaussian approximation (GA) method has been used. GA is accurate for large spreading factors but shows some inaccuracy for smaller spreading factors Sushchik *et al.* (2000). However, large spreading factors are the basic property of spread-spectrum communication systems, which makes GA suitable for analysis in chaos-based communication systems.

4.1 BER analysis of PI-DCSK

In every PI-DCSK transmission, $\log_2(M) = n+1$ bits are sent, where n bits map into permutation indices and a single bit is modulated. Hence, the BER of the PI-DCSK system is composed of the BER of the mapped bits Pr_{map} and the BER of the modulated bit Pr_{mod}. Therefore, the total BER Pr_M would be expressed as Kaddoum *et al.* (2016b)

$$Pr_M = \frac{n}{\log_2(M)} Pr_{\text{map}} + \frac{1}{\log_2(M)} Pr_{\text{mod}}. \tag{A II-21}$$

The probability of BER for mapped bits Pr_{map} is dependent upon the number of mapped bits n and the probability of erroneous permutation index detection Pr_{ed}. Furthermore, if the permutation is erroneously detected, a wrong combination of mapped bits will be estimated. Each wrong combination may contain a different number of incorrect bits, compared to the correct combination. Thereupon, the probability of erroneous permutation detection can be converted into a corresponding mapped bits BER by using Proakis (1995)

$$Pr_{\text{map}} = \frac{2^{(n-1)}}{2^n - 1} Pr_{\text{ed}}. \tag{A II-22}$$

The correct estimation of the modulated bit depends on the correct permutation index detection and the correct despreading process. Accordingly, two different cases cause an error to occur. In the first case, the permutation index is correctly detected but an error occurs while despreading the modulated bit. Note that the despreading process in PI-DCSK is performed in the same

fashion as in conventional DCSK. In the second case, the permutation index is erroneously estimated and the modulated bit is despread at the output of the wrong correlator. In this case, the probability of correct detection will be simply equal to $\frac{1}{2}$. Consequently, the total BER of modulated bits would be expressed as Kaddoum *et al.* (2016b)

$$Pr_{\text{mod}} = Pr_{\text{DCSK}}(1 - Pr_{\text{ed}}) + 0.5Pr_{\text{ed}}, \tag{A II-23}$$

where Pr_{DCSK} is the BER for DCSK. Using (A II-21), (A II-22) and (A II-23), the detailed form of Pr_M is revealed as

$$Pr_M = \frac{Pr_{\text{DCSK}}}{\log_2(M)}(1 - Pr_{\text{ed}}) + \frac{2n2^{n-1} + (2^n - 1)}{2\log_2(M)(2^n - 1)} Pr_{\text{ed}}. \tag{A II-24}$$

4.2 Erroneous permutation detection probability Pr_{ed}

In order to estimate the transmitted permutation index, the PI-DCSK detector and decision logic circuits select the maximum absolute value that is obtained at the output of one of the 2^n engaged correlators. For equiprobable transmitted permuted sequences, the error probability conditioned on the k^{th} user transmitted permutation $P_j^{(k)}$ is given by

$$\begin{aligned} Pr_{\text{ed}} &= Pr\left(\left|D_{i,j}^{(k)}\right| < \max\left(\left|D_{i,m}^{(k)}\right|\right) \middle| P_j^{(k)}\right), \\ &\text{for} \quad 1 \leq \underset{m \neq j}{m} \leq 2^n, \end{aligned} \tag{A II-25}$$

where $D_{i,m}^{(k)}$ and $D_{i,j}^{(k)}$ are the decision variables at the m^{th} and j^{th} correlator outputs, respectively. In agreement with (A II-25), an erroneous permutation index estimation will occur if the maximum absolute value of the decision variable $\left|D_{i,m}^{(k)}\right|$ is larger than $\left|D_{i,j}^{(k)}\right|$.

As observed in (A II-10), the i^{th} data block decision variable of the k^{th} user at the output of the m^{th} correlator may follow two different patterns according to two hypotheses. The first hypothesis is when the index of the correlator output M is equal to the transmitted permutation

index j, i.e $j = m$, where $1 \leq m \leq 2^n$, while the second hypothesis is when the index of the correlator output does not match the index of transmitted permutation i.e., $m \neq j$. Subsequently, the decision variable defined in (A II-10) can be rewritten as

$$D_{i,m}^{(k)} = \begin{cases} S_{i,j}^{(k)} + \mathrm{MUI}_{i,j}^{(k)} + N_{i,j}^{(k)}, & \text{for} \quad m = j, \\ I_{i,m}^{(k)} + \mathrm{MUI}_{i,m}^{(k)} + N_{i,m}^{(k)}, & \text{for} \quad m \neq j, \end{cases} \tag{A II-26}$$

where $S_{i,j}^{(k)}$ represents the desired signal, $\mathrm{MUI}_{i,j}^{(k)}$ and $\mathrm{MUI}_{i,m}^{(k)}$ are the multi user interference (MUI) components, $N_{i,m}^{(k)}$ and $N_{i,j}^{(k)}$ are interference components generated by Gaussian noise and $I_{i,m}^{(k)}$ is the interference that models the cross-correlation of different permuted chaotic sequences. As such, the desired signal $S_{i,j}^{(k)}$ can be rewritten from (A II-10) as

$$\begin{aligned} S_{i,j}^{(k)} &= \left(\sum_{l=1}^{L_k} \lambda_{l,k} P_j^{(k)} \left(\mathbf{x}_{i,\beta+\tau_{l,k}}^{(k)} \right) \right) \\ &\quad \times \left(\sum_{l=1}^{L_k} \lambda_{l,k} a_{i,n+1}^{(k)} P_j^{(k)} (\mathbf{x}_{i,\beta+\tau_{l,k}}^{(k)}) \right)^T \\ &= \sum_{l=1}^{L_k} \lambda_{l,k}^2 a_{i,n+1}^{(k)} P_j^{(k)} (\mathbf{x}_{i,\beta+\tau_{l,k}}^{(k)}) P_j^{(k)} (\mathbf{x}_{i,\beta+\tau_{l,k}}^{(k)})^T \\ &\quad + \sum_{l=1}^{L_k} \sum_{\substack{l'=1 \\ l' \neq l}}^{L_k} \lambda_{l,k} \lambda_{l',k} a_{i,n+1}^{(k)} P_j^{(k)} (\mathbf{x}_{i,\beta+\tau_{l',k}}^{(k)}) P_j^{(k)} (\mathbf{x}_{i,\beta+\tau_{l,k}}^{(k)})^T \\ &\approx a_{i,n+1}^{(k)} \sum_{k=1}^{\beta} \sum_{l=1}^{L_k} \lambda_{l,k}^2 \left(x_{i,k-\tau_{l,k}}^{(k)} \right)^2. \end{aligned} \tag{A II-27}$$

The last approximation in (A II-27) occurs as a result of the low auto-correlation property of time-shifted chaotic sequences Kaddoum & Gagnon (2012)

$$\mathbf{x}_{i,\tau_{l,k}}^{(k)} \left(\mathbf{x}_{i,\tau_{l',k}}^{(k)} \right)^T \approx 0, \qquad \text{for} \quad l \neq l'. \tag{A II-28}$$

Therefore, the mean value of the i^{th} data block at the j^{th} correlator output, conditioned on a given $a_{i,n+1}^{(k)}$, is

$$E \left(D_{i,j}^{(k)} | a_{i,n+1}^{(k)} \right) \approx a_{i,n+1}^{(k)} \frac{\log_2(M) E_b}{2} \sum_{l=1}^{L_k} \lambda_{l,k}^2. \tag{A II-29}$$

The approximation in (A II-29) arises from the assumption that $\tau_{max} << \beta T_c$, which means that ISI is negligible.

From (A II-10), $\mathrm{MUI}_{i,j}^{(k)}$ can be restated as

$$\begin{aligned}\mathrm{MUI}_{i,j}^{(k)} &= \sum_{\substack{u=1\\u\neq k}}^{N_u}\sum_{l=1}^{L_u}\lambda_{l,u}P_j^{(k)}\left(\mathbf{R}_{i,\beta+\tau_{l,u}}^{(u)}\right)\\ &\times\left(\sum_{l=1}^{L_k}\lambda_{l,k}a_{i,n+1}^{(k)}P_j^{(k)}(\mathbf{x}_{i,\beta+\tau_{l,k}}^{(k)})+\sum_{\substack{u=1\\u\neq k}}^{N_u}\sum_{l=1}^{L_u}\lambda_{l,u}\mathbf{D}_{i,\tau_{l,u}}^{(u)}\right)^T\\ &+\sum_{l=1}^{L_k}\lambda_{l,k}P_j^{(k)}\left(\mathbf{x}_{i,\beta+\tau_{l,k}}^{(k)}\right)\left(\sum_{\substack{u=1\\u\neq k}}^{N_u}\sum_{l=1}^{L_u}\lambda_{l,u}\mathbf{D}_{i,\tau_{l,u}}^{(u)}\right)^T.\end{aligned} \tag{A II-30}$$

Due to the low cross-correlation between different permuted chaotic sequences, as described in (A II-1) and (A II-2), the multi-user interference $\mathrm{MUI}_{i,j}^{(k)}$ can be modelled as a zero mean Gaussian variable with variance

$$\begin{aligned}&\mathrm{var}\left(\mathrm{MUI}_{i,j}^{(k)}\right)=\\ &\sum_{\substack{u=1\\u\neq k}}^{N_u}\sum_{l=1}^{L_u}\sum_{l'=1}^{L_k}E\left(\left[\lambda_{l,u}\lambda_{l',k}a_{i,n+1}^{(k)}P_j^{(k)}\left(\mathbf{R}_{i,\beta+\tau_{l,u}}^{(u)}\right)\right.\right.\\ &\qquad\left.\left.\times\left(P_j^{(k)}(\mathbf{x}_{i,\beta+\tau_{l',k}}^{(k)})\right)^T\right]^2\right)\\ &+\sum_{\substack{u=1\\u\neq k}}^{N_u}\sum_{\substack{u'=1\\u'\neq k}}^{N_u}\sum_{l=1}^{L_u}\sum_{l'=1}^{L_u}E\left(\left[\lambda_{l,u}\lambda_{l',u'}P_j^{(k)}\left(\mathbf{R}_{i,\beta+\tau_{l,u}}^{(u)}\right)\right.\right.\\ &\qquad\left.\left.\times\left(\mathbf{D}_{i,\tau_{l',u'}}^{(u')}\right)^T\right]^2\right)\\ &+\sum_{l=1}^{L_k}\sum_{\substack{u=1\\u\neq k}}^{N_u}\sum_{l'=1}^{L_u}E\left(\left[\lambda_{l,k}\lambda_{l',u}P_j^{(k)}\left(\mathbf{x}_{i,\beta+\tau_{l,k}}^{(k)}\right)\left(\mathbf{D}_{i,\tau_{l',u}}^{(u)}\right)^T\right]^2\right)\\ &\approx(N_u-1)\frac{\log_2^2(M)E_b^2}{2\beta}\sum_{l=1}^{L_k}\lambda_{l,k}^2+(N_u-1)^2\frac{\log_2^2(M)E_b^2}{4\beta}.\end{aligned} \tag{A II-31}$$

The last approximation in (A II-31) emerges from two standard assumptions. The first assumption is that the expectation of the squared product of two different chaotic sequences is equal

to Kaddoum *et al.* (2015a), Zhou *et al.* (2007)

$$\begin{aligned} &E\left(\left[\mathbf{x}_{i,v}^{(u)} P_j^{(k)}\left(\mathbf{x}_{i,v}^{(k)}\right)\right]^2\right) = E\left(\left[P_z^{(k)}\left(\mathbf{x}_{i,v}^{(u)}\right) P_j^{(k)}\left(\mathbf{x}_{i,v}^{(k)}\right)\right]^2\right) \\ &= \frac{\log_2^2(M) E_b^2}{4\beta}, \qquad \text{for} \quad z \neq j \quad \text{and} \quad u \neq k. \end{aligned} \tag{A II-32}$$

The second assumption is that the overall mean energy of a channel with L_u paths is equal to

$$\sum_{l=1}^{L_u} E\left(\lambda_{l,u}^2\right) = 1. \tag{A II-33}$$

Furthermore, the noise interference component of the i^{th} data block at the j^{th} correlator output can be written as

$$\begin{aligned} N_{i,j}^{(k)} = &\sum_{\substack{u=1 \\ u\neq k}}^{N_u} \sum_{l=1}^{L_u} \lambda_{l,u} P_j^{(k)}\left(\mathbf{R}_{i,\beta+\tau_{l,u}}^{(u)}\right)(\mathbf{n}_{i,0,k}^D)^T \\ &+ P_j^{(k)}\left(\mathbf{n}_{i,\beta,k}^R\right)\left(\sum_{\substack{u=1 \\ u\neq k}}^{N_u} \sum_{l=1}^{L_u} \lambda_{l,u} \mathbf{D}_{i,\tau_{l,u}}^{(u)}\right)^T \\ &+ \left(\sum_{l=1}^{L_k} \lambda_{l,k} P_j^{(k)}\left(\mathbf{x}_{i,\beta+\tau_{l,k}}^{(k)}\right)\right)(\mathbf{n}_{i,0,k}^D)^T \\ &+ P_j^{(k)}(\mathbf{n}_{i,\beta,k}^R)\left(\sum_{l=1}^{L_k} \lambda_{l,k} a_{i,n+1}^{(k)} P_{j^{(i)}}^{(k)}\left(\mathbf{x}_{i,\beta+\tau_{l,k}}^{(k)}\right)\right)^T \\ &+ P_j^{(k)}(\mathbf{n}_{i,\beta,k}^R)(\mathbf{n}_{i,0,k}^D)^T. \end{aligned} \tag{A II-34}$$

In (A II-34), all terms are uncorrelated, while channel coefficients and noise samples are independent. Hence, the variance of $N_{i,j}^{(k)}$ can be easily written as

$$\begin{aligned} \text{var}(N_{i,j}^{(k)}) &= (N_u - 1) N_0 \frac{\log_2(M) E_b}{2} \\ &+ N_0 \frac{\log_2(M) E_b}{2} \sum_{l=1}^{L_k} \lambda_{l,k}^2 + \beta \frac{N_0^2}{4}. \end{aligned} \tag{A II-35}$$

Subsequently, the overall variance of the k^{th} user, j^{th} correlator decision variable is equal to

$$\begin{aligned}
&\text{var}\left(D_{i,j}^{(k)}\right) = \text{var}\left(\text{MUI}_{i,j}^{(k)}\right) + \text{var}\left(N_{i,j}^{(k)}\right) \\
&\approx (N_u-1)\frac{\log_2^2(M)E_b^2}{2\beta}\sum_{l=1}^{L_k}\lambda_{l,k}^2 + (N_u-1)^2\frac{\log_2^2(M)E_b^2}{4\beta} \\
&+(N_u-1)N_0\frac{\log_2(M)E_b}{2} \\
&+N_0\frac{\log_2(M)E_b}{2}\sum_{l=1}^{L_k}\lambda_{l,k}^2 + \beta\frac{N_0^2}{4}.
\end{aligned} \tag{A II-36}$$

Furthermore, by using the properties mentioned in (A II-1) and (A II-2), the disturbance component $I_{i,m}^{(k)}$ in (A II-26) is approximately equal to zero, because of the low cross-correlation between different permuted replicas

$$\begin{aligned}
I_{i,m}^{(k)} = &\left(\sum_{l=1}^{L_k}\lambda_{l,k}P_m^{(k)}(\mathbf{x}_{i,\beta+\tau_{l,k}}^{(k)})\right) \\
&\times\left(\sum_{l=1}^{L_k}\lambda_{l,k}a_{i,n+1}^{(k)}P_j^{(k)}(\mathbf{x}_{i,\beta+\tau_{l,k}}^{(k)})\right)^T \approx 0.
\end{aligned} \tag{A II-37}$$

Using the same techniques as in (A II-31) and (A II-34), it can be easily shown that the variances of $\text{MUI}_{i,m}^{(k)}$ and $N_{i,m}^{(k)}$ are equal to the variances of $\text{MUI}_{i,j}^{(k)}$ and $N_{i,j}^{(k)}$, respectively. Subsequently, the overall variance of the k^{th} user, m^{th} correlator, where $m \neq j$, decision variable would be stated as

$$\begin{aligned}
&\text{var}\left(D_{i,m}^{(k)}\right) = \text{var}\left(\text{MUI}_{i,m}^{(k)}\right) + \text{var}\left(N_{i,m}^{(k)}\right) \\
&\approx (N_u-1)\frac{\log_2^2(M)E_b^2}{2\beta}\sum_{l=1}^{L_k}\lambda_{l,k}^2 + (N_u-1)^2\frac{\log_2^2(M)E_b^2}{4\beta} \\
&+(N_u-1)N_0\frac{\log_2(M)E_b}{2} \\
&+N_0\frac{\log_2(M)E_b}{2}\sum_{l=1}^{L_k}\lambda_{l,k}^2 + \beta\frac{N_0^2}{4}.
\end{aligned} \tag{A II-38}$$

It is important to note that due to the absolute value operator, the mean value of $\left|D_{i,j}^{(k)}\right|$ is independent of the modulated bit value and hence $a_{i,n+1}^{(k)}$ will be omitted in the derivations that shall follow. The absolute values of the 2^n-1 random variables $\left|D_{i,m}^{(k)}\right|$ follow folded normal distribution due to the fact that $D_{i,m}^{(k)}$ is a zero mean Gaussian random variable Papoulis (1991).

Moreover, they are independent and hence, order statistics theory can be applied to compute (A II-25) as Kaddoum *et al.* (2016b)

$$Pr_{\text{ed}} = 1 - \int_0^{\infty} \left(F_{\left|D_{i,m}^{(k)}\right|}(y) \right)^{2^n - 1} f_{\left|D_{i,j}^{(k)}\right|}(y) dy, \tag{A II-39}$$

where $F_{\left|D_{i,m}^{(k)}\right|}(y)$ is the cumulative distribution function (CDF) of $\left|D_{i,m}^{(k)}\right|$ given as

$$F_{\left|D_{i,m}^{(k)}\right|}(y) = \text{erf}\left(\frac{y}{\sqrt{2\text{var}\left(D_{i,m}^{(k)}\right)}} \right), \tag{A II-40}$$

where $\text{erf}(\cdot)$ is error function given as

$$\text{erf}(z) = \int_0^{z} \frac{2}{\sqrt{\pi}} e^{-x^2} dx. \tag{A II-41}$$

More, $f_{\left|D_{i,j}^{(k)}\right|}(y)$ is the probability density function (PDF) of the folded normally distributed random variable $\left|D_{i,j}^{(k)}\right|$ which is given as

$$\begin{aligned} f_{\left|D_{i,j}^{(k)}\right|}(y) = & \frac{1}{\sqrt{2\pi\text{var}\left(D_{i,j}^{(k)}\right)}} \left[\exp\left(-\frac{\left(y - E\left(D_{i,j}^{(k)}\right)\right)^2}{2\text{var}\left(D_{i,j}^{(k)}\right)} \right) \right. \\ & \left. + \exp\left(-\frac{\left(y + E\left(D_{i,j}^{(k)}\right)\right)^2}{2\text{var}\left(D_{i,j}^{(k)}\right))} \right) \right]. \end{aligned} \tag{A II-42}$$

By substituting $\gamma_b = E_b/N_0 \sum_{l=1}^{L_k} \lambda_{l,k}^2$ in the expressions (A II-28), (A II-30) and (A II-33), we may rewrite (A II-37) as

$$\begin{aligned} Pr_{\text{ed}} &= 1 - \tfrac{1}{\sqrt{\pi W}} \int_0^{\infty} \left(\text{erf}\left(\tfrac{y}{\sqrt{W}} \right) \right)^{2^n - 1} \\ &\times \left[\exp\left(- \frac{\left(y - \frac{\log_2(M)}{2} \gamma_b \right)^2}{W} \right) \right. \\ &\left. + \exp\left(- \frac{\left(y + \frac{\log_2(M)}{2} \gamma_b \right)^2}{W} \right) \right] dy, \end{aligned} \tag{A II-43}$$

where

$$\begin{aligned} W &= (N_u - 1) \tfrac{\log_2^2(M)}{\beta} \left(\tfrac{E_b}{N_0} \gamma_b + \tfrac{(N_u - 1)}{2} \left(\tfrac{E_b}{N_0} \right)^2 \right) \\ &+ (N_u - 1) \log_2(M) \tfrac{E_b}{N_0} + \log_2(M) \gamma_b + \tfrac{\beta}{2}. \end{aligned} \tag{A II-44}$$

4.3 BER of modulated bit

In order to estimate the modulated bit, the despreading process is performed as in conventional DCSK, by comparing the decision variable $D_{i,j}^{(k)}$ to a zero threshold. Then, by using (A II-29) and (A II-36), the bit error rate probability Pr_{DCSK} would be scripted as

$$Pr_{\text{DCSK}} = \frac{1}{2} \text{erfc} \left(\frac{E\left(D_{i,j}^{(k)} \right)}{\sqrt{2 \text{var}\left(D_{i,j}^{(k)} \right)}} \right), \tag{A II-45}$$

where $\text{erfc}(x) = 1 - \text{erf}(x)$ is the complementary error function. After some straightforward operations, the instantaneous BER probability of DCSK system would be noted as

$$Pr_{\text{DCSK}} = \frac{1}{2} \text{erfc} \left(\frac{\log_2(M) \gamma_b}{2\sqrt{W}} \right), \tag{A II-46}$$

where W is as mentioned in (A II-45). The bit energy E_b can be assumed to be constant for higher spreading factors β. Therefore, for L_k independent identically distributed (i.i.d.)

Rayleigh-fading channels, the PDF of instantaneous γ_b can be written as Proakis (1995)

$$f(\gamma_b, \bar{\gamma}_c, L_k) = \frac{\gamma_b^{L_k-1}}{(L_k-1)!\,\bar{\gamma}_c^{L_k}} \exp\left(-\frac{\gamma_b}{\bar{\gamma}_c}\right), \tag{A II-47}$$

where $\bar{\gamma}_c$ is equal to

$$\bar{\gamma}_c = \frac{E_b}{N_0} E\left(\lambda_{l,k}^2\right) = \frac{E_b}{N_0} E\left(\lambda_{j,k}^2\right), l \neq j. \tag{A II-48}$$

For dissimilar channels, however, the PDF of γ_b can be written as

$$f(\gamma_b) = \sum_{l=1}^{L_k} \frac{\rho_l}{\bar{\gamma}_l} \exp\left(-\frac{\gamma_b}{\bar{\gamma}_l}\right), \tag{A II-49}$$

where

$$\rho_l = \prod_{\substack{j=1 \\ j \neq l}}^{L_k} \frac{\bar{\gamma}_l}{\bar{\gamma}_l - \bar{\gamma}_j}. \tag{A II-50}$$

Notice that for $L_k = 1$ and $\lambda_{1,k} = 1$ the channel reduces to AWGN. Finally, the averaged BER of the PI-DCSK system over multipath Rayleigh fading channels is given as

$$\bar{P}r_{M\text{fad}} = \int_0^\infty Pr_M f(\gamma_b) d\gamma_b, \tag{A II-51}$$

where the integral in (A II-51) is evaluated numerically.

5. Results and Discussions

In this section, the performance of the proposed PI-DCSK scheme is evaluated. In Monte-Carlo simulation, the Chebyshev polynomial function is used for the generation of chaotic samples. The performance analysis is carried out for AWGN and multipath Rayleigh fading channels. To analyse the performance in multipath Rayleigh fading channels, three different channel profiles are used. In the first channel model named CM1, a two-ray channel is used with an

average power gain of $E\left(\lambda_1^2\right) = E\left(\lambda_2^2\right) = 1/2$. The second channel model named CM2 uses a three-ray channel with the following gains $E\left(\lambda_1^2\right) = 4/7, E\left(\lambda_2^2\right) = 2/7, E\left(\lambda_3^2\right) = 1/7$. Finally, the third channel model named CM3 uses a five-ray channel with equal gains in all five paths, i.e., $E\left(\lambda_i^2\right) = 1/5$, where $i = 1, \cdots, 5$. For all multipath channel profiles, the delay spreads are varying according to the uniform distribution between zero and a, where $a \ll \beta T_c$.

5.1 Performance evaluation

In order to verify our theoretical derivations, the results obtained in (A II-51) are validated by Monte Carlo simulation over AWGN, CM1, CM2 and CM3 channels. First, the averaged

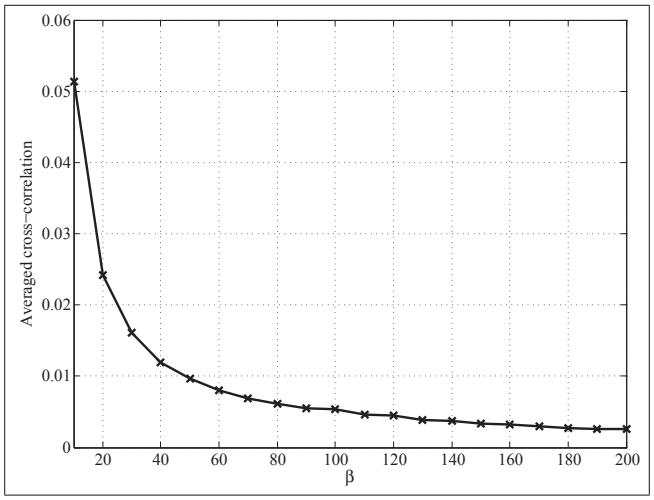

Figure-A II-4 Averaged cross-correlation of two differently permuted sequences for various β

cross-correlations, defined as (A II-2), of two differently permuted sequences chosen as in Lau *et al.* (2003), are shown in Fig. II-4, for different β. The cross-correlations are calculated and averaged for 1000 different permuted sequences. It can be seen that the cross correlation is low and exponentially decreases when the spreading factor increases.

In Figs. II-5-II-6, the influence of different modulation orders M on the PI-DCSK BER performance over AWGN and the multipath Rayleigh fading channels CM1, CM2 and CM3 is shown. As observed in these figures, there is a perfect match between the BER results obtained

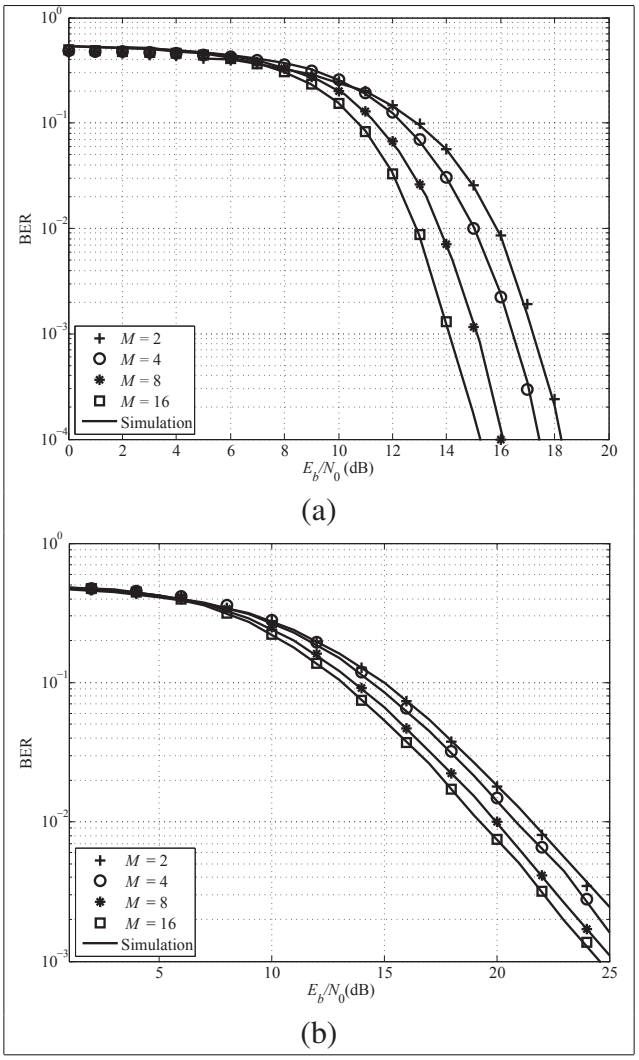

Figure-A II-5 The influence of different modulation orders M on PI-DCSK performance for $\beta = 200$ over (a) AWGN and (b) CM1 channels

by the analytical expressions of (A II-24) and (A II-51), versus Monte-Carlo simulation. Predictably, as M increases the PI-DCSK BER performance improves, which is due to the fact that for higher M, more bits are mapped within a symbol for the same transmitted energy and, hence, the required E_b/N_0 needed to achieve a certain BER performance reduces. Furthermore, it should be noticed that the BER performance of PI-DCSK for $M = 2$ is equal to the conventional DCSK. For example, Fig. II-5 (a) clearly indicates that in order to achieve a BER of 10^{-3}, the required E_b/N_0 level for PI-DCSK must be approximately 3 dB lower for $M = 16$ in comparison to $M = 2$. In other words, when M increases, the number of bits per PI-DCSK

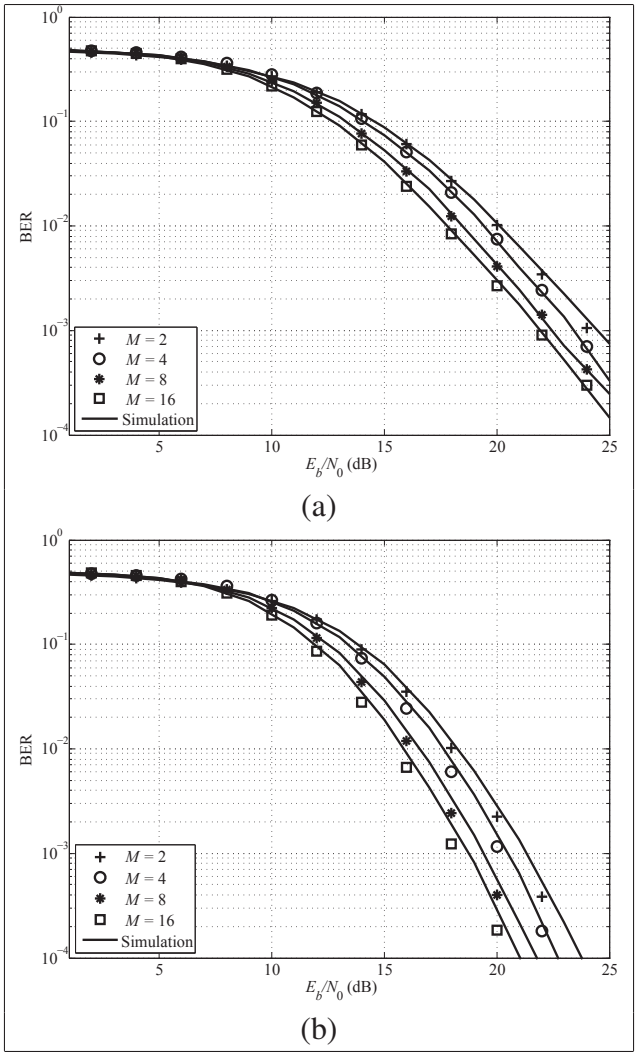

Figure-A II-6 The influence of different modulation orders M on PI-DCSK performance for $\beta = 200$ over (a) CM2 and (b) CM3 channels

frame increases, while the transmitted energy remains constant. This explains the obtained performance behaviour and proves the high energy efficiency of the system. Furthermore, it is evident that there is a perfect match between theoretical and simulation results for all channel models, which validates our analytical approach. In Figs. II-7-II-8 respectively, the influence of different spreading sequence length β on the PI-DCSK BER performance over AWGN and multipath Rayleigh fading channels CM1, CM2 and CM3 is shown. It is obvious that when β increases the PI-DCSK BER performance degrades. This is owing to the fact that for higher values of β, the noise$\times$noise cross correlation terms in (A II-36) and (A II-38) become more

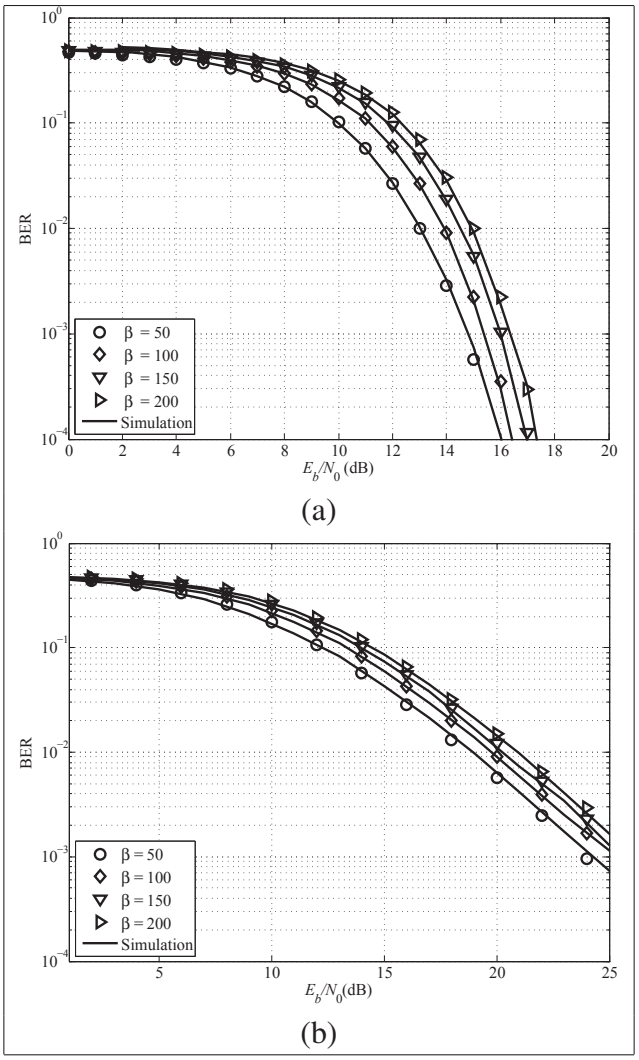

Figure-A II-7 The influence of β on PI-DCSK performance for $M = 4$ over (a) AWGN and (b) CM1 channels

significant, which causes the degradation of PI-DCSK BER performance. To show the validity limit of our assumption, we plotted the BER performance over CM3. Hence, the gap between analytical and simulation results over CM3, which occurs for $\beta = 50, 100$, is caused by the ISI interference that is neglected in the derivation of the analytical expressions. Therefore, to have an idea about the optimal spreading factor values, the BER curves of PI-DCSK versus spreading sequence length β for various modulation orders M, are plotted in Fig. II-9. It is shown that for a given E_b/N_0 ratio, there exists an optimal spreading sequence length β within the range from 5 to 40, which optimizes the BER performance. If we let β_{opt} to indicate the

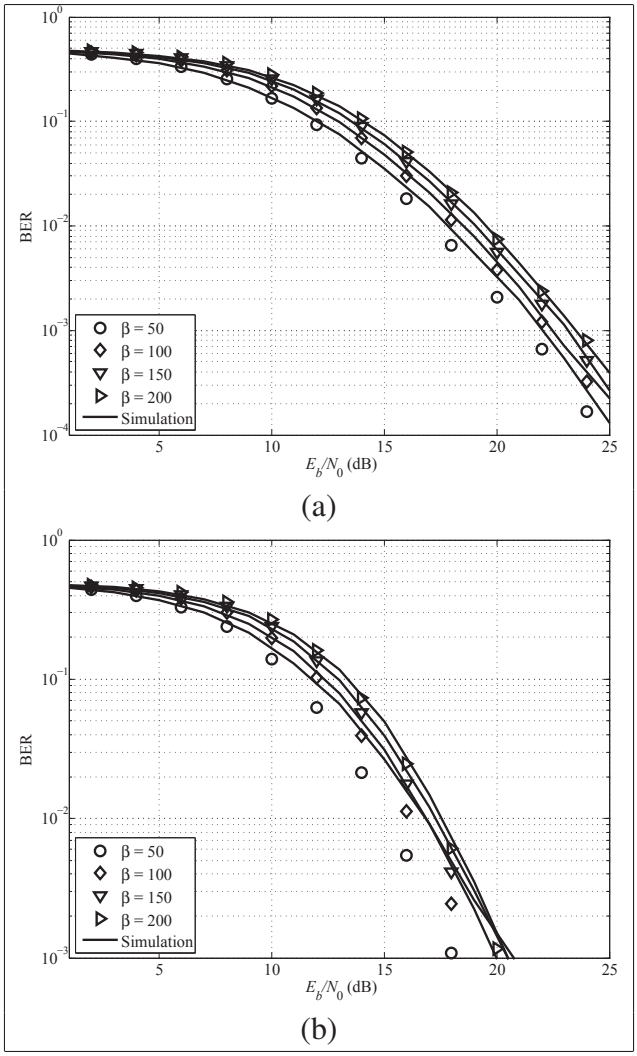

Figure-A II-8 The influence of β on PI-DCSK performance for $M = 4$ over (a) CM2 and (b) CM3 channels

optimal value of β, we observe that β_{opt} is dynamic and keeps an incremental trend as the modulation order M increases. For example, at $E_b/N_0 = 14$ dB, $\beta_{\text{opt}} < 10$ for $M = 2$, while this value is $\beta_{\text{opt}} \approx 50$ for $M = 16$. Furthermore, it can be seen that the BER performance deteriorates as the spreading factor β escalates, despite the increment of quasi-orthogonality between differently permuted replicas of the reference sequence for larger β values. This is because the contribution of the noise-noise cross terms of (A II-36) and (A II-37) is more significant than the increment of quasi-orthogonality between the two permuted sequences, as the spreading sequence grows.

The effect of ISI on BER performance is shown in Fig. II-10. The results are obtained for CM1 channel profile with $E_b/N_0 = 16$ dB and $\beta = 200$. It is clear that ISI can be neglected when the channel delay spread is much lower than the symbol duration, as expected. However, for larger delay spreads the influence of this interference increases significantly, which causes a mismatch between theoretical BER expressions that assume zero ISI and the simulated system performance.

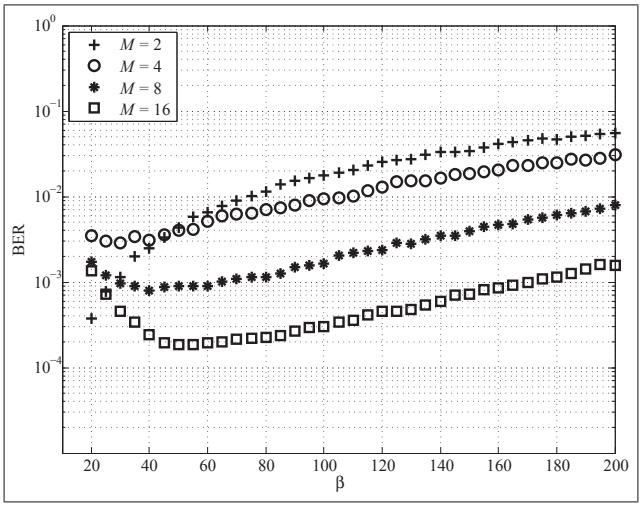

Figure-A II-9 BER performance of PI-DCSK at $E_b/N_0 = 14$ dB for various β and M

5.2 Multiple access performance

To evaluate the effects of the number of users on PI-DCSK, the BER performance for three and six users are examined, over AWGN and fading channels.

In Fig. II-11, PI-DCSK BER performance over CM2 is shown for the modulation orders $M = 2, 16$, a spreading factor of $\beta = 300$ and $N_u = 3$ users. As illustrated, the best performance is obtained when $M = 2$. It arises from the fact that when the number of users rises, the MUI variance expressions in (A II-36) and (A II-38) increase the overall noise level at each correlator output. Subsequently, as the decision logic will have to choose between $M/2$ correlator outputs, there will be a higher possibility that an error will occur in the estimation

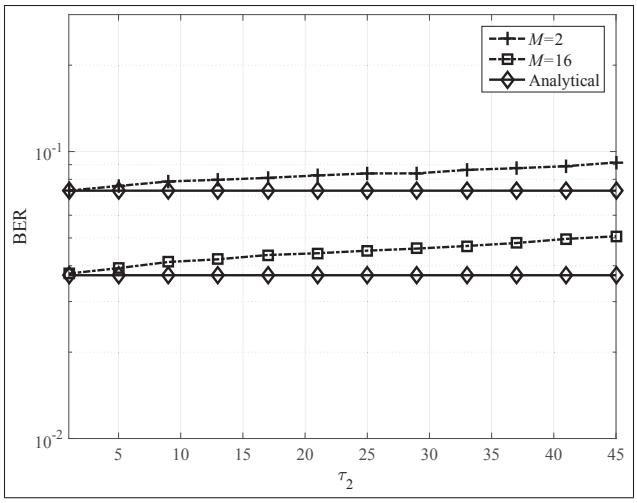

Figure-A II-10 The BER performance of PI-DCSK for CM1 versus τ_2 for $\beta = 200$, $E_b/N_0 = 16$ dB and $M = 2, 16$

of the permutation index (mapped bits), which increases the BER and leads to performance deterioration.

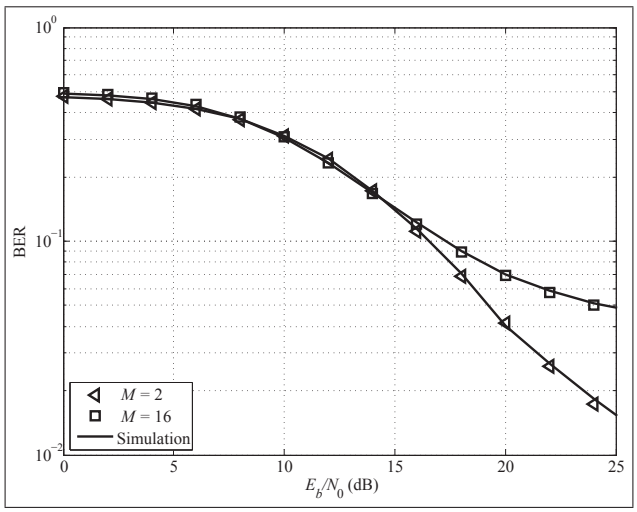

Figure-A II-11 The influence of modulation order on PI-DCSK performance for $M = 2$, 16, $\beta = 300$ and $N_u = 3$ over CM2 channel

In Figs. II-12-II-14 respectively, the influence of the spreading sequence length on MUI interference in a multi-user scenario, over AWGN, CM2 and CM3 channels for $M = 4$, is shown. As

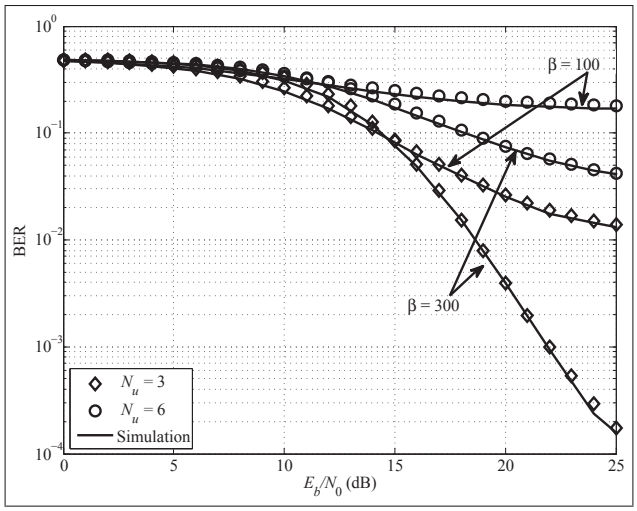

Figure-A II-12 The influence of β on PI-DCSK performance for $M = 4$ and $N_u = 3, 6$ over AWGN channel

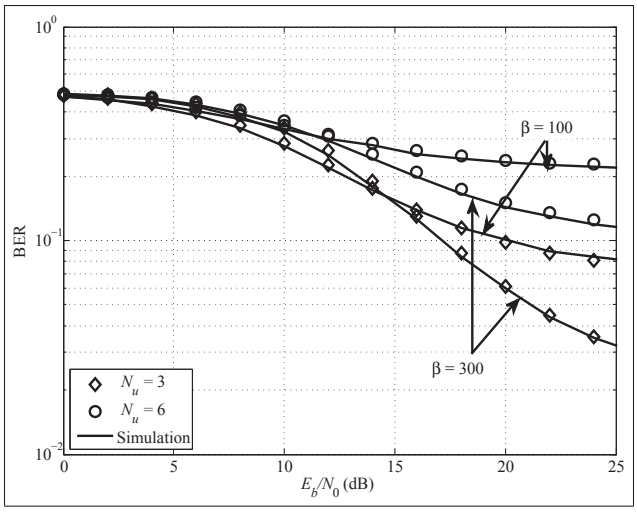

Figure-A II-13 The influence of β on PI-DCSK performance for $M = 4$ and $N_u = 3, 6$ over CM2 channel

highlighted, when the number of users increases from 3 to 6 the BER increases, i.e the performance degrades, for a fixed β value, i.e. $\beta = 100$. However, when β increases to 300, the MUI variance is additionally spread, which decreases the overall BER and enhances performance. To conclude, in order to keep MUI noise at an acceptable level, β should be appropriately

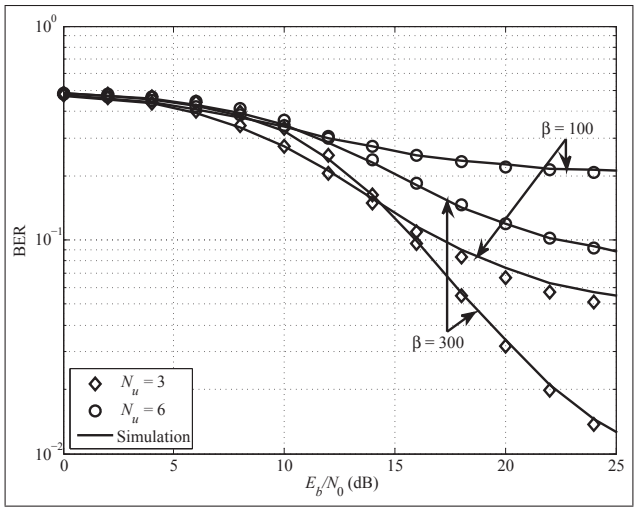

Figure-A II-14 The influence of β on PI-DCSK performance for the cases of $M = 4$ and $N_u = 3, 6$ over CM3 channel

chosen. Furthermore, as viewed in Figs. II-12 and II-13, there is a perfect match between analytical and simulation results for both channel models.

In conclusion, the BER performance of the proposed scheme degrades as the number of users increases due to the increment in MUI. Additionally, for the same number of users, the PI-DCSK BER performance worsens as the modulation level increases. However, by increasing the spreading factor, the BER drops and performance improves because the MUI will stretch over a larger bandwidth.

5.3 Comparison with other non-coherent chaotic modulations

The BER performance of PI-DCSK in comparison with OM-DCSK is evaluated over AWGN, CM1 and CM3 channels. The outcome of this comparison is shown in Fig. II-11. This comparison reveals that the BER performance of PI-DCSK and OM-DCSK are approximately similar for $M > 2$, while PI-DCSK significantly outperforms OM-DCSK for $M = 2$ for all channel models. For instance, PI-DCSK needs 2 dB less at the receiver in order to achieve a BER of $= 10^{-3}$ compared to OM-DCSK over an AWGN channel.

In addition, in comparison with PI-DCSK, the BER performance of OM-DCSK significantly degrades over the timely dispersed channel i.e. CM3. This is a consequence of the higher number of correlators at the receiver for the same modulation level M and a loss of orthogonality between different Walsh codes used to construct the orthogonal signal basis. Furthermore, the proposed PI-DCSK achieves the observed BER improvement while sustaining a reduced complexity in comparison to OM-DCSK, as was stated in Section 2.

In Fig. II-16, the BER performance comparison of PI-DCSK is extended to include DCSK, HE-DCSK and QCSK over AWGN, CM2 and CM3 channels. The PI-DCSK modulation order M is set to 4 and 8. Fig. II-16 reveals that at a BER of $= 10^{-3}$, the DCSK BER performance is about 0.8 dB worse than HE-DCSK, QCSK and 4-ary PI-DCSK, and about 2 dB worse than 8-ary PI-DCSK. However, over CM2, the 4-ary PI-DCSK shows a better performance compared to DCSK while it performs slightly worse in comparison to HE-DCSK and QCSK. Furthermore, for $M = 8$, PI-DCSK performance significantly augments, i.e. BER drops due to the mapping of an extra bit in the permutation index, compared to HE-DCSK and QCSK.

5.4 Discussion

In the proposed PI-DCSK design, multiple quasi-orthogonal sequences are easily generated by virtue of the low auto-correlation properties of the permuted replicas of chaotic sequences.

Therefore, no extra hardware, neither for Hilbert transform nor for the generation of Walsh codes is needed in PI-DCSK in comparison to similar multilevel modulations like OM-DCSK. Moreover, dispensing with the usage of Walsh codes at the receiver, the PI-DCSK scheme enjoys full properties and advantages of non-coherent modulation. Furthermore, by mapping an extra bit into the permutation indices, the PI-DCSK data rate, BER performance, energy and spectral efficiencies are significantly improved compared to other rival modulation schemes.

6. Conclusions

In this paper, a new multi-user multi-level non-coherent PI-DCSK scheme is proposed and analysed for chaos-based communication systems. In the proposed design, time-multiplexing

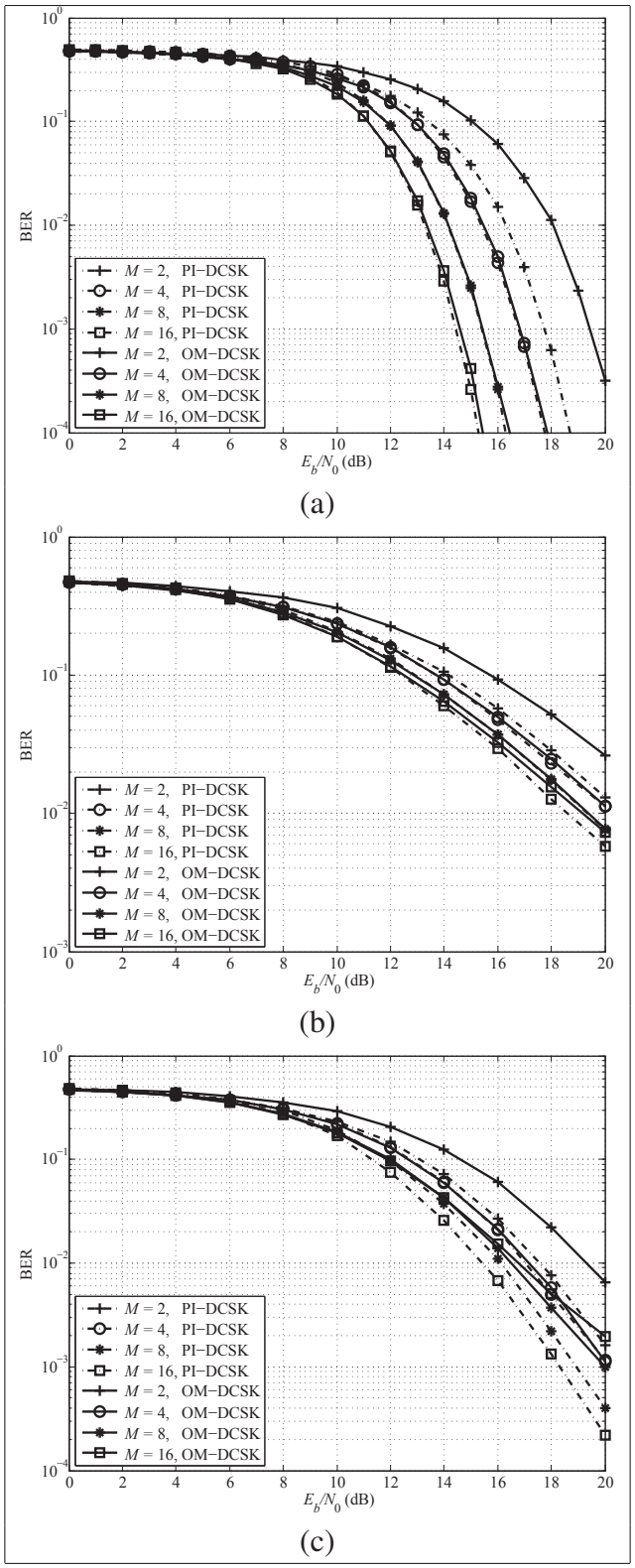

Figure-A II-15 A BER performance comparison of PI-DCSK to OM-DCSK over (a) AWGN channels for $\beta = 256$, (b) CM1 and (c) CM3 channels with $\beta = 128$

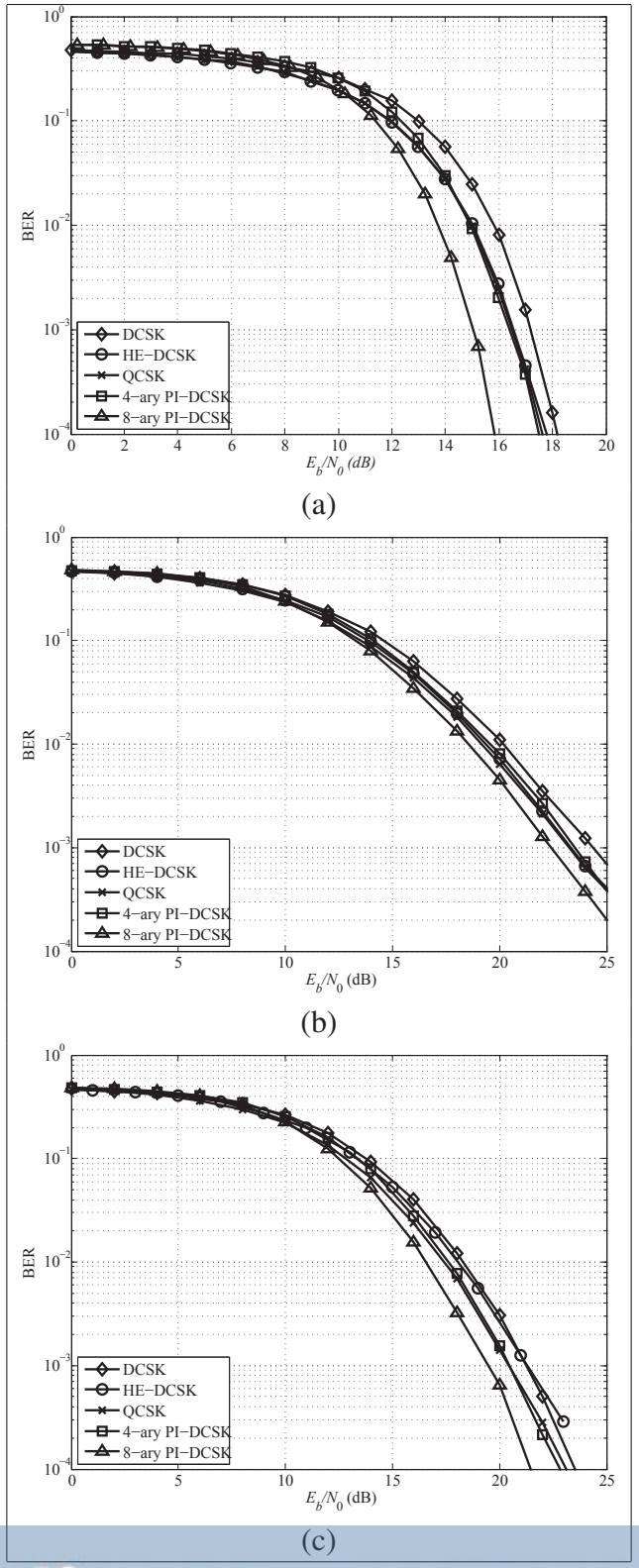

Figure-A II-16 A BER performance comparison of PI-DCSK to DCSK, HE-DCSK and QCSK for $M = 4$, 8 and $\beta = 200$ in (a) AWGN, (b) CM2 and (c) CM3 channels

is used to separate reference and data bearing sequences, as in conventional DCSK. In the PI-DCSK scheme presented here, multiple quasi-orthogonal data sequences are formed as a consequence of permuting the reference sequence. In particular, a block of n bits is mapped in the indices of different permutations, where each of the 2^n possible permutations denotes a distinguishable permutation applied to the reference sequence. In completion, the modulated bit is spread by the *selected* permuted reference signal. As multiple bits per data frame are ferried through the use of indexing, the PI-DCSK energy and spectral efficiencies are significantly boosted compared to its competitors.

In addition, the utilisation of different permutations eradicates the similarity between reference sequences and data bearing sequences, which in turn significantly increases the PI-DCSK transmitted data security. Moreover, an efficient multiple access method is proposed for adoption in the PI-DCSK system, by granting absolute access to a distinct set of $M/2$ permutations out of $\beta! - 1$ possible, for each user.

Furthermore, closed-form theoretical expressions of multi-user PI-DCSK system BER over AWGN and multipath Rayleigh channels are derived. Monte-Carlo simulation is used to validate the theoretical results obtained in this work.

In continuation, the influence of different system parameters like modulation orders and spreading sequence lengths are analysed. At the end, the BER performance comparison with DCSK, HE-DCSK, QCSK and OM-DCSK is shown. In light of the obtained results, the proposed novel PI-DCSK system is expected to be competitive and is promising.

BIBLIOGRAPHY

[Rev. 3.]. (2014, 7). Single-Pole Double-Throw (SPDT) Switch.

[Cel]. (2015, 2). RF Switch Guide; Making your switch selection fast and easy.

Abouei, J., Plataniotis, K. N. & Pasupathy, S. (2010). Green modulation in dense wireless sensor networks. *IEEE Int. Conf. Acoustics, Speech and Signal Process,*, pp. 3382-3385.

Abu-Alhiga, R. & Haas, H. (2009). Subcarrier-index modulation OFDM. *20th IEEE Int. Symp. Personal, Indoor and Mobile Radio Commun.*, pp. 177-181.

An, Z., Wang, J., Wang, J., Huang, S. & Song, J. (2015). Mutual information analysis on spatial modulation multiple antenna system. *IEEE Trans. on Commun.*, 63(3), 826–843.

Andrews, J. G., Buzzi, S., Choi, W., Hanly, S. V., Lozano, A., Soong, A. C. & Zhang, J. C. (2014). What will 5G be? *IEEE Journal on selected areas in communications*, 32(6), 1065–1082.

Bai, L., Choi, J. & Yu, Q. (2014). *Low Complexity MIMO Receivers*. Springer.

Barnaghi, P., Wang, W., Henson, C. & Taylor, K. (2012). Semantics for the Internet of Things: early progress and back to the future. *Int. J. Semantic Web and Information Systems (IJSWIS)*, 8(1), 1-21.

Başar, E. (2015). Multiple-input multiple-output OFDM with index modulation. *IEEE Signal Process. Lett.*, 22(12), 2259–2263.

Basar, E. (2016). Index modulation techniques for 5G wireless networks. *IEEE Communications Magazine*, 54(7), 168–175.

Başar, E., Aygölü, Ü., Panayırcı, E. & Poor, H. V. (2013). Orthogonal frequency division multiplexing with index modulation. *IEEE Trans. on Signal Process.*, 61(22), 5536-5549.

Basar, E., Wen, M., Mesleh, R., Di Renzo, M., Xiao, Y. & Haas, H. (2017). Index modulation techniques for next-generation wireless networks. *IEEE Access*, 5, 16693–16746.

Berger, L. T., Schwager, A., Pagani, P. & Schneider, D. (2014). *MIMO Power Line Communications: Narrow and Broadband Standards, EMC, and Advanced Processing*. CRC Press.

Bonald, T., Elayoubi, S.-E., El Falou, A. & Landre, J.-B. (2011). Radio capacity improvement with HSPA+ dual-cell. *Communications (ICC), 2011 IEEE International Conference on*, pp. 1–6.

Bowick, C. (2011). *RF circuit design*. Newnes.

Chang, H.-C., Liu, Y.-C. & Su, Y. T. (2013). Detection of spatial-modulated signals in the presence of CSI error and time-spatial correlation. *IEEE Globecom Workshops (GC Wkshps)*, pp. 82-86.

Chau, Y., Yu, S.-H. et al. (2001). Space modulation on wireless fading channels. *Vehicular Technology Conference, 2001. VTC 2001 Fall. IEEE VTS 54th*, 3, 1668–1671.

Chen, P., Wang, L. & Lau, F. C. M. (2013). One Analog STBC-DCSK Transmission Scheme not Requiring Channel State Information. *IEEE Trans. Circuits Syst. I, Reg. Papers*, 60(4), 1027-1037. doi: 10.1109/TCSI.2012.2209304.

Chen, P., Fang, Y., Han, G. & Chen, G. (2016). An Efficient Transmission Scheme for DCSK Cooperative Communication Over Multipath Fading Channels. *IEEE Access*, 4, 6364-6373. doi: 10.1109/ACCESS.2016.2613890.

Cheng, G., Wang, L., Xu, W. & Chen, G. (2016). Carrier Index Differential Chaos Shift Keying Modulation. *IEEE Trans. Circuits Syst. II, Exp. Briefs*, PP(99), 1-1. doi: 10.1109/TCSII.2016.2613093.

Cheng, G., Wang, L., Xu, W. & Chen, G. (2017). Carrier index differential chaos shift keying modulation. *IEEE Transactions on Circuits and Systems II: Express Briefs*, 64(8), 907–911.

Chung, W.-G., Lim, E., Yook, J.-G. & Park, H.-K. (2007). Calculation of spectral efficiency for estimating spectrum requirements of IMT-Advanced in Korean mobile communication environments. *ETRI journal*, 29(2), 153–161.

Cimini Jr, L. J. & Sollenberger, N. R. (1997). OFDM with diversity and coding for advanced cellular internet services. *IEEE Global Telecommun. Conf.*, 1, 305-309.

Cimini Jr, L. J., Daneshrad, B. & Sollenberger, N. R. (1996). Clustered OFDM with transmitter diversity and coding. *IEEE Global Telecommun. Conf., GLOBECOM'96*, 1, 703-707.

Daemen, J. & Rijme, V. (2002). *The Design of RijndaeL: AES - The Advanced Encryption Standard (Information Security and Cryptography)*. Springer-Verlag Berlin Heidelberg.

Dahlman, E., Parkvall, S. & Skold, J. (2013). *4G: LTE/LTE-Advanced for Mobile Broadband, 2nd Ed.* Academic press.

Damen, M. O., El Gamal, H. & Caire, G. (2003). On maximum-likelihood detection and the search for the closest lattice point. *Information Theory, IEEE Transactions on*, 49(10), 2389–2402.

David, T. & Pramod, V. (2005). Fundamentals of wireless communication. *New York, Cambridge*.

Dedieu, H. & Kennedy, M. P. (1993). Chaos shift keying: modulation and demodulation of a chaotic carrier using self-synchronization Chua's circuit. 40, 634-642.

Di Renzo, M. & Haas, H. (2010). A general framework for performance analysis of space shift keying (SSK) modulation for MISO correlated Nakagami-m fading channels. *Communications, IEEE Transactions on*, 58(9), 2590–2603.

Di Renzo, M. & Haas, H. (2011). Space Shift Keying (SSK-) MIMO over Correlated Rician Fading Channels: Performance Analysis And a New Method for Transmit-Diversity. *IEEE Trans. on Communications*, 59(1), 116–129.

Di Renzo, M., Narayanan, S., Graziosi, F. & Haas, H. Distributed Spatial Modulation: A Cooperative Diversity Protocol for Half–Duplex Relay–Aided Wireless Networks.

Di Renzo, M., Haas, H. & Grant, P. M. (2011). Spatial modulation for multiple-antenna wireless systems: a survey. *IEEE Communications Magazine*, 49(12), 182–191.

Di Renzo, M., Haas, H., Ghrayeb, A., Sugiura, S. & Hanzo, L. (2014). Spatial modulation for generalized MIMO: Challenges, opportunities, and implementation. *Proceedings of the IEEE*, 102(1), 56–103.

Di Renzo, M., Haas, H., Ghrayeb, A., Hanzo, L. & Sugiura, S. (2016). 'Spatial modulation for multiple-antenna communication. Wiley Encyclopedia of Electrical and Electronics Engineering.

Elavarasan, P. & Nagarajan, G. (2015). A Summarization on PAPR Techniques for OFDM Systems. *Journal of The Institution of Engineers: Series B*, 96(4), 381–389. doi: 10.1007/s40031-014-0156-2.

Erceg, V., Sampath, H. & Catreux-Erceg, S. (2006). Dual-polarization versus single-polarization MIMO channel measurement results and modeling. *IEEE Transactions on Wireless Communications*, 5(1), 28–33.

Escribano, F. J., Kaddoum, G., Wagemakers, A. & Giard, P. (2016). Design of a new differential chaos-shift-keying system for continuous mobility. *IEEE Transactions on Communications*, 64(5), 2066–2078.

European Commission & European ICT Industry. (2014). Fifth Generation Infrastructure Public Private Partnership [Format]. Consulted at https://5g-ppp.eu/.

Fang, Y., Han, G., Chen, P., Lau, F. C. M., Chen, G. & Wang, L. (2016). A Survey on DCSK-Based Communication Systems and Their Application to UWB Scenarios. *IEEE Commun. Surv. Tut.*, 18(3), 1804-1837. doi: 10.1109/COMST.2016.2547458.

Foschini, G. J. (1996). Layered space-time architecture for wireless communication in a fading environment when using multi-element antennas. *Bell labs technical journal*, 1(2), 41–59.

Fu, Y., Wang, C.-X., Yuan, Y., Mesleh, R., Aggoune, H., Alwakeel, M. & Haas, H. (2015). BER Performance of Spatial Modulation Systems Under 3D V2V MIMO Channel Models.

Galias, Z. & Maggio, G. M. (2001). Quadrature chaos-shift keying: theory and performance analysis. *IEEE Trans. Circuits Syst. I: Fundam. Theory Appl.*, 48(12), 1510-1519. doi: 10.1109/TCSI.2001.972858.

Ganesan, S., Mesleh, R., Ho, H., Ahn, C. W. & Yun, S. (2006). On the performance of spatial modulation OFDM. *Signals, Systems and Computers, 2006. ACSSC'06. Fortieth Asilomar Conference on*, pp. 1825–1829.

Golub, G. H. & Van Loan, C. F. (2012). *Matrix computations*. JHU Press.

Haas, H., Costa, E. & Schulz, E. (2002). Increasing spectral efficiency by data multiplexing using antenna arrays. *Personal, Indoor and Mobile Radio Communications, 2002. The 13th IEEE International Symposium on*, 2, 610–613.

Han, S. H. & Lee, J. H. (2005). An overview of peak-to-average power ratio reduction techniques for multicarrier transmission. *IEEE Wireless Commun.*, 12(2), 56-65.

Herceg, M., Miličević, K. & Matić, T. (2016). Frequency-Translated Differential Chaos Shift Keying for Chaos-Based Communications. *J. Franklin Inst.*, 353(13), 2966—2979.

Herceg, M., Kaddoum, G., Vranjes, D. & Soujeri, E. (2017). Permutation Index DCSK modulation technique for secure multi-user high-data-rate communication systems. *IEEE Transactions on Vehicular Technology*.

Hong, Y.-W. P., Huang, W.-J. & Kuo, C.-C. J. (2010). Review of Wireless Communications and MIMO Techniques. In *Cooperative Communications and Networking* (pp. 15–65). Springer.

Hu, W., Wang, L. & Kaddoum, G. (2017). Design and performance analysis of a differentially spatial modulated chaos shift keying modulation system. *IEEE Transactions on Circuits and Systems II: Express Briefs*, 64(11), 1302–1306.

Huang, T., Wang, L., Xu, W. & Lau, F. C. M. (2016). Multilevel code-shifted differential-chaos-shift-keying system. *IET Commun.*, 10(10), 1189-1195. doi: 10.1049/iet-com.2015.1109.

Ishibashi, K. & Sugiura, S. (2014). Effects of antenna switching on band-limited spatial modulation. *IEEE Wireless Communications Letters*, 3(4), 345–348.

Jeganathan, J., Ghrayeb, A. & Szczecinski, L. (2008a). Generalized space shift keying modulation for MIMO channels. *Personal, Indoor and Mobile Radio Communications, 2008. PIMRC 2008. IEEE 19th International Symposium on*, pp. 1–5.

Jeganathan, J., Ghrayeb, A. & Szczecinski, L. (2008b). Spatial modulation: optimal detection and performance analysis. *IEEE Communications Letters*, 12(8), 545–547.

Jeganathan, J., Ghrayeb, A., Szczecinski, L. & Ceron, A. (2009). Space shift keying modulation for MIMO channels. *IEEE Transactions on Wireless Communications*, 8(7), 3692–3703.

Kaddoum, G., Chargé, P., Roviras, D. & Fournier-Prunaret, D. (2009a). A methodology for bit error rate prediction in chaos-based communication systems. *Birkhäuser, Circuits, Syst.Signal Process.*, 28, 925-944.

Kaddoum, G., Richardson, F. & Gagnon, F. (2013a). Design and Analysis of a Multi-Carrier Differential Chaos Shift Keying Communication System. *IEEE Trans. Commun.*, 61(8), 3281-3291.

Kaddoum, G., Soujeri, E., Arcila, C. & Eshteiwi, K. (2015a). I-DCSK: An Improved Non-Coherent Communication System Architecture. *IEEE Trans. Circuits Syst. II, Exp. Briefs*, 62(9), 901-905.

Kaddoum, G., Soujeri, E. & Nijsure, Y. (2016a). Design of a Short Reference Noncoherent Chaos-Based Communication Systems. *IEEE Trans. Commun.*, 64(2), 680-689.

Kaddoum, G. (2016a). Design and Performance Analysis of a Multiuser OFDM Based Differential Chaos Shift Keying Communication System. *IEEE Trans. Commun.*, 64(1), 249–260.

Kaddoum, G. (2016b). Wireless chaos-based communication systems: A comprehensive survey. *IEEE Access*, 4, 2621–2648.

Kaddoum, G. & Gagnon, F. (2012). Design of a high-data-rate differential chaos-shift keying system. *IEEE Trans. Circuits Syst. II, Exp. Briefs*, 59(7), 448–452.

Kaddoum, G. & Gagnon, F. (2013a). Lower bound on the bit error rate of a decode-and-forward relay network under chaos shift keying communication system. *IET Communications*, 8(2), 227–232.

Kaddoum, G. & Gagnon, F. (2013b). Performance analysis of STBC-CSK communication system over slow fading channel. *Signal Processing*, 93(7), 2055–2060.

Kaddoum, G. & Soujeri, E. (2015). On the comparison between code-index modulation and spatial modulation techniques. *Information and Communication Technology Research (ICTRC), 2015 International Conference on*, pp. 24–27.

Kaddoum, G. & Soujeri, E. (2016). NR-DCSK: A noise reduction differential chaos shift keying system. *IEEE Trans. Circuits Syst. II, Exp. Briefs*, 63(7), 648–652.

Kaddoum, G. & Tadayon, N. (2017). Differential chaos shift keying: A robust modulation scheme for power-line communications. *IEEE Transactions on Circuits and Systems II: Express Briefs*, 64(1), 31–35.

Kaddoum, G., Chargé, P., Roviras, D. & Fournier-Prunaret, D. (2007). Comparison of chaotic sequences in a chaos based DS-CDMA system. *Proc. International symposium on nonlinear theory and its applications, Vancouver, Canada*.

Kaddoum, G., Roviras, D., Chargé, P. & Fournier-Prunaret, D. (2009b). Accurate bit error rate calculation for asynchronous chaos-based DS-CDMA over multipath channel. *EURASIP Journal on Advances in Signal Processing*, 2009, 48.

Kaddoum, G., Roviras, D., Chargé, P. & Fournier-Prunaret, D. (2009c). Robust synchronization for asynchronous multi-user chaos-based DS-CDMA. *Signal Processing*, 89(5), 807–818.

Kaddoum, G., Roviras, D., Charg'ey, P. & Fournier-Prunarety, D. (2009d). Performance of multi-user chaos-based DS-CDMA system over multipath channel. *Circuits and Systems, 2009. ISCAS 2009. IEEE International Symposium on*, pp. 2637–2640.

Kaddoum, G., Vu, M. & Gagnon, F. (2011). On the performance of chaos shift keying in MIMO communications systems. *Wireless Communications and Networking Conference (WCNC), 2011 IEEE*, pp. 1432–1437.

Kaddoum, G., Gagnon, F. & Couillard, D. (2012a). An enhanced spectral efficiency chaos-based symbolic dynamics transceiver design. *Signal Processing and Communication Systems (ICSPCS), 2012 6th International Conference on*, pp. 1–6.

Kaddoum, G., Vu, M. & Gagnon, F. (2012b). Chaotic symbolic dynamics modulation in MIMO systems. *Circuits and Systems (ISCAS), 2012 IEEE International Symposium on*, pp. 157–160.

Kaddoum, G., Gagnon, G. & Gagnon, F. (2013b). Spread spectrum communication system with sequence synchronization unit using chaotic symbolic dynamics modulation. *International Journal of Bifurcation and Chaos*, 23(02), 1350019.

Kaddoum, G., Richardson, F.-D. & Gagnon, F. (2013c). Design and analysis of a multi-carrier differential chaos shift keying communication system. *IEEE Transactions on Communications*, 61(8), 3281–3291.

Kaddoum, G., Parzysz, F. & Shokraneh, F. (2014). Low-complexity amplify-and-forward relaying protocol for non-coherent chaos-based communication system. *IET Communications*, 8(13), 2281–2289.

Kaddoum, G., Ahmed, M. F. & Nijsure, Y. (2015b). Code Index Modulation: A High Data Rate and Energy Efficient Communication System. *Communications Letters, IEEE*, 19(2), 175–178.

Kaddoum, G., Nijsure, Y. & Tran, H. (2016b). Generalized code index modulation technique for high-data-rate communication systems. *IEEE Transactions on Vehicular Technology*, 65(9), 7000–7009.

Kaddoum, G., Tran, H.-V., Kong, L. & Atallah, M. (2017). Design of simultaneous wireless information and power transfer scheme for short reference DCSK communication systems. *IEEE Transactions on Communications*, 65(1), 431–443.

Kalis, A., Kanatas, A. G. & Papadias, C. B. (2008). A novel approach to MIMO transmission using a single RF front end. *Selected Areas in Communications, IEEE Journal on*, 26(6), 972–980.

Kalis, A., Kanatas, A. G. & Papadias, C. B. (2014). *Parasitic Antenna Arrays for Wireless MIMO Systems*. Springer.

Kennedy, M. P., Kolumbán, G., Kis, G. & Jákó, Z. (2000). Performance evaluation of FM-DCSK modulation in multipath environments. *IEEE Transactions on Circuits and Systems I: Fundamental Theory and Applications*, 47(12), 1702–1711.

Kolumbán, G., Vizvari, G. K., Schwarz, W. & Abel, A. (1996). Differential chaos shift keying: a robust coding for chaos communication. *Proc. NDES*, pp. 92-97.

Kolumbán, G., Kis, G., Kennedy, M. & Jáko, Z. (1997a). FM-DCSK: A new and robust solution to chaos communications. *Proc. Int. Symp. Nonlinear Theory Appl.*, pp. 117–120.

Kolumbán, G., Kennedy, M. P. & Chua, L. O. (1997b). The role of synchronization in digital communications using chaos. I. Fundamentals of digital communications. *IEEE Transactions on circuits and systems I: Fundamental theory and applications*, 44(10), 927–936.

Kurian, A. P., Puthusserypady, S. & Htut, S. M. (2005). Performance enhancement of DS/CDMA system using chaotic complex spreading sequence. *IEEE Transactions on wireless communications*, 4(3), 984–989.

Lau, F. C. M. & Tse, C. K. (2003). *Chaos-Based Digital communication systems*. Springer-Verlag.

Lau, F. C. M. & Tse, C. K. (2009). Methods and systems for transceiving chaotic signals. *US Patent No. US7593531, 2009*.

Lau, F. C. M., Cheong, K. Y. & Tse, C. K. (2003). Permutation-based DCSK and multiple-access DCSK systems. *IEEE Trans. Circuits Syst. I, Fundam. Theory Appl*, 50(6), 733-742. doi: 10.1109/TCSI.2003.812616.

Lee, N., Simeone, O. & Kang, J. (2012). The effect of imperfect channel knowledge on a MIMO system with interference. *IEEE Transactions on Communications*, 60(8), 2221–2229.

Legnain, R. M., Hafez, R. H., Marsland, I. D. & Legnain, A. M. (2013). A novel spatial modulation using MIMO spatial multiplexing. *Communications, Signal Processing, and their Applications (ICCSPA), 2013 1st International Conference on*, pp. 1–4.

Li, Q., Li, G., Lee, W., Lee, M.-i., Mazzarese, D., Clerckx, B. & Li, Z. (2010). MIMO techniques in WiMAX and LTE: a feature overview. *IEEE Communications Magazine*, 48(5), 86–92.

Liao, H.-H., Jiang, H., Shanjani, P., King, J. & Behzad, A. (2009). A fully integrated 2 2 power amplifier for dual band MIMO 802.11 n WLAN application using SiGe HBT technology. *Solid-State Circuits, IEEE Journal of*, 44(5), 1361–1371.

Lipfert, H. (2007). MIMO-OFDM Space Time Coding–Spatial Multiplexing Increasing Performance and Spectral Efficiency in Wireless Systems. IRT–Broadcast Networks and Servers.

Litsyn, S. (2007). *Peak Power Control in Multicarrier Communications*. Cambridge University Press.

Lynnyk, V. & Čelikovskỳ, S. (2010). On the anti–synchronization detection for the generalized Lorenz system and its applications to secure encryption. *Kybernetika*, 46(1), 1–18.

Mesleh, R., Haas, H., Ahn, C. W. & Yun, S. (2006a). Spatial modulation-a new low complexity spectral efficiency enhancing technique. *Communications and Networking in China, 2006. ChinaCom'06. First International Conference on*, pp. 1–5.

Mesleh, R., Haas, H., Ahn, C. & Yun, S. (2006b). Spatial modulation-OFDM. *Proc. of the International OFDM Workshop*, pp. 30–31.

Mesleh, R. & Ikki, S. S. (2012). On the effect of gaussian imperfect channel estimations on the performance of space modulation techniques. *Vehicular Technology Conference (VTC Spring), 2012 IEEE 75th*, pp. 1–5.

Mesleh, R. & Ikki, S. S. (2015). On the impact of imperfect channel knowledge on the performance of quadrature spatial modulation. *Wireless Communications and Networking Conference (WCNC), 2015 IEEE*, pp. 534–538.

Mesleh, R., Stefan, I., Haas, H. & Grant, P. M. (2009). On the Performance of Trellis Coded Spatial Modulation. *Int. ITG Workshop on Smart Antennas*, pp. 235–241.

Mesleh, R., Badarneh, O. S., Younis, A. & Haas, H. (2015). Performance Analysis of Spatial Modulation and Space-Shift Keying With Imperfect Channel Estimation Over Generalized Fading Channels. *Vehicular Technology, IEEE Transactions on*, 64(1), 88–96.

Mesleh, R. Y., Haas, H., Sinanovic, S., Ahn, C. W. & Yun, S. (2008). Spatial modulation. *IEEE Transactions on Vehicular Technology*, 57(4), 2228–2241.

Organization name. (1999). *Norm title*. Institution and norm number. Location: Organization name.

Papoulis, A. (1991). *Probability, Random Variables, and Stochastic Processes*. McGraw-Hill.

Park, C. S., Wang, Y.-P. E., Jongren, G. & Hammarwall, D. (2011). Evolution of uplink MIMO for LTE-advanced. *IEEE Communications Magazine*, 49(2).

Pirinen, P. (2014). A brief overview of 5G research activities. *1st IEEE Int. Conf. 5G for Ubiquitous Connectivity (5GU)*, pp. 17-22.

Prisecaru, F. A. (2010). *Mutual information and capacity of spatial modulation systems*. Bremen, Germany.

Proakis, J. G. (2001). *Digital Communications*. McGraw-Hill.

Proakis, J. G. (1995). Digital Communications. *McGraw-Hill, New York*.

Rawat, P., Singh, K. D., Chaouchi, H. & Bonnin, J. M. (2014). Wireless sensor networks: a survey on recent developments and potential synergies. *The J. of supercomputing*, 68(1), 1-48.

Rushforth, C. (1964). Transmitted-reference techniques for random or unknown channels. *IEEE Trans. on Inf. Theory*, 10(1), 39–42.

Schellmann, M., Zhao, Z., Lin, H., Siohan, P., Rajatheva, N., Luecken, V. & Ishaque, A. (2014). FBMC-based air interface for 5G mobile: Challenges and proposed solutions. *Cognitive Radio Oriented Wireless Networks and Communications (CROWNCOM), 2014 9th International Conference on*, pp. 102–107.

Serafimovski, N., Younis, A., Mesleh, R., Chambers, P., Di Renzo, M., Wang, C.-X., Grant, P. M., Beach, M. A. & Haas, H. (2013). Practical implementation of spatial modulation. *IEEE Transactions on Vehicular Technology*, 62(9), 4511–4523.

Shoaib, S., Shoaib, I., Shoaib, N., Chen, X. & Parini, C. G. (2015). MIMO Antennas for Mobile Handsets. *IEEE Letters on Antennas and Wireless Propagation*, 14, 799–802.

Soujeri, E. & Kaddoum, G. (2015). Performance of SM Detectors Under Channel Imperfections. *15th IEEE International Conference on Ubiquitous Wireless Broadband (ICUWB'2015)*, pp. 1-5.

Soujeri, E. & Kaddoum, G. (2016). The impact of antenna switching time on spatial modulation. *IEEE Wireless Commun. Lett.*, 5(3), 256–259.

Soujeri, E., Kaddoum, G., Au, M. & Herceg, M. (2017). Frequency index modulation for low complexity low energy communication networks. *IEEE Access*, 5, 23276–23287.

Soujeri, E., Kaddoum, G. & Herceg, M. (2018). Design of an initial condition-index chaos shift keying modulation. *Electronics Letters*.

Stavridis, A., Basnayaka, D., Di Renzo, M. & Haas, H. (2014). Average Bit Error Probability of Receive-Spatial Modulation Using Zero-Forcing Precoding. *Computer Aided Modeling and Design of Communication Links and Networks (CAMAD), 2014 IEEE 19th International Workshop on*, pp. 390–394.

Sushchik, M., Tsimring, L. S. & Volkovskii, A. R. (2000). Performance analysis of correlation-based communication schemes utilizing chaos. *IEEE Trans. Circuits Syst. I, Fundam. Theory Appl.*, 47(12), 1684–1691.

Tang, Q., Xiao, Y., Yang, P., Yu, Q. & Li, S. (2013). A new low-complexity near-ML detection algorithm for spatial modulation. *IEEE Wireless Communications Letters*, 2(1), 90–93.

Tse, D. & Viswanath, P. (2005). *Fundamentals of wireless communication*. Cambridge university press.

Tsonev, D., Sinanovic, S. & Haas, H. (2011). Enhanced subcarrier index modulation (SIM) OFDM. *IEEE GLOBECOM Workshops (GC Wkshps)*, pp. 728-732.

Veronesi, D., Riva, R., Bisaglia, P., Osnato, F., Afkhamie, K., Nayagam, A., Rende, D. & Yonge, L. (2011). Characterization of in-home MIMO power line channels. *Power Line Communications and Its Applications (ISPLC), 2011 IEEE International Symposium on*, pp. 42–47.

Vitali, S., Rovatti, R. & Setti, G. (2006). Improving PA efficiency by chaos-based spreading in multicarrier DS-CDMA systems. *Circuits and Systems, 2006. ISCAS 2006. Proceedings. 2006 IEEE International Symposium on*, pp. 4–pp.

Wang, C.-X., Haider, F., Gao, X., You, X.-H., Yang, Y., Yuan, D., Aggoune, H., Haas, H., Fletcher, S. & Hepsaydir, E. (2014). Cellular architecture and key technologies for 5G wireless communication networks. *IEEE Communications Magazine*, 52(2), 122–130.

Weber, R. H. & Weber, R. (2010). *Internet of things*. Springer.

Wu, X., Di Renzo, M. & Haas, H. (2014a). Spatially-Averaging Channel Estimation for Spatial Modulation. *Vehicular Technology Conference (VTC Fall), 2014 IEEE 80th*, pp. 1–5.

Wu, X., Di Renzoy, M. & Haas, H. (2014b). A novel multiple access scheme based on spatial modulation MIMO. *Computer Aided Modeling and Design of Communication Links and Networks (CAMAD), 2014 IEEE 19th International Workshop on*, pp. 285–289.

Wunder, G., Kasparick, M., Wild, T., Schaich, F., Chen, Y., Dryjanski, M., Buczkowski, M., Pietrzyk, S., Michailow, N., Matthé, M. et al. (2014). 5GNOW: Intermediate frame structure and transceiver concepts. *Globecom Workshops (GC Wkshps), 2014*, pp. 565–570.

Xia, Y., Tse, C. & Lau, F. C. (2004). Performance of differential chaos-shift-keying digital communication systems over a multipath fading channel with delay spread. *IEEE Trans. Circuits Syst. II, Exp. Briefs*, 51(12), 680–684.

Xu, W., Huang, T. & Wang, L. (2017). Code-Shifted Differential Chaos Shift Keying With Code Index Modulation for High Data Rate Transmission. *IEEE Transactions on Communications*, 65(10), 4285–4294.

Xu, W., Wang, L. & Kolumbán, G. (2011). A novel differential chaos shift keying modulation scheme. *Int. J. Bifurcation Chaos*, 21(03), 799–814.

Xu, W., Wang, L. & Kolumbán, G. (2012). A new data rate adaption communications scheme for code-shifted differential chaos shift keying modulation. *Int. J. Bifurcation Chaos*, 22(08), 1–8.

Yang, H. & Jiang, G.-P. (2012). High-Efficiency Differential-Chaos-Shift-Keying Scheme for Chaos-Based Noncoherent Communication. *IEEE Trans. Circuits and Systems II,*, 59(5), 312 - 316. doi: 10.1109/TCSII.2012.2190859.

Yang, H. & Jiang, G.-P. (2013). Reference-modulated DCSK: a novel chaotic communication scheme. *IEEE Trans. Circuits Syst. II, Exp. Briefs*, 60(4), 232–236.

Yang, H., Tang, W. K., Chen, G. & Jiang, G.-P. (2016). System design and performance analysis of orthogonal multi-level differential chaos shift keying modulation scheme. *IEEE Trans. Circuits Syst. I, Reg. Papers*, 63(1), 146–156.

Younis, A., Serafimovski, N., Mesleh, R. & Haas, H. (2010). Generalised spatial modulation. *Signals, Systems and Computers (ASILOMAR), 2010 Conference Record of the Forty Fourth Asilomar Conference on*, pp. 1498–1502.

Younis, A., Mesleh, R., Di Renzo, M. & Haas, H. (2014). Generalised spatial modulation for large-scale MIMO. *Signal Processing Conference (EUSIPCO), 2014 Proceedings of the 22nd European*, pp. 346–350.

Younis, A., Mesleh, R. & Haas, H. (2015). Quadrature Spatial Modulation Performance overNakagami–m Fading Channels.

Yu, C.-M., Hsieh, S.-H., Liang, H.-W., Lu, C.-S., Chung, W.-H., Kuo, S.-Y. & Pei, S.-C. (2012). Compressed sensing detector design for space shift keying in MIMO systems. *IEEE Communications Letters*, 16(10), 1556–1559.

Zhou, Z., Zhou, T. & Wang, J. (2007, May). Performance of Multi-User DCSK Communication System Over Multipath Fading Channels. *2007 IEEE International Symposium on Circuits and Systems*, pp. 2478-2481. doi: 10.1109/ISCAS.2007.378741.